Politecnico di Torino

A.a 2023/2024

20/03/2024

Master's Degree in Environmental and Land Engineering

Track: Climate Change

Preserving Trout Spawning Habitat for Sustainable Hydropower Development

Supervisors:

Prof. Paolo Vezza

PhD Alessandro Gueglielmetto

Candidate:

Sara Viale

302809

Acknowledgments

I would like to express my sincere gratitude to my thesis supervisor, Professor Paolo Vezza, for his invaluable guidance and support throughout my research journey, and his encouragement during the challenging moments of my thesis work.

I am particularly grateful for the opportunity to participate in field surveys that allowed me to gain hands-on experience with data collection and analysis. These experiences not only enhanced my technical skills but also fostered a deeper understanding of the research topic.

I would like to extend my sincere gratitude to PhD Alessandro Guglielmetto for his constant support and guidance throughout my research. His willingness to answer my questions and provide assistance whenever needed was truly appreciated. His expertise and patience were invaluable in helping me learn new techniques and troubleshoot problems.

I would also like to acknowledge and thank everyone who collaborated with me on this journey. This thesis is a culmination of collective effort and shared insights, and I am deeply appreciative of the support from each individual who contributed to this academic endeavour.

Contents

List of Figures

List of Tables

List of Abbreviations

IRENA - International Renewable Energy Agency

CVA - Compagnia Valdostana delle Acque

HMU- Hydromorphological Monitoring Units

PHABSIM - Physical HABitat SImulation Model

IFIM - Instream Flow Incremental Methodology

HI - Habitat Integrity Index

HMU_NUM - number of the hydromorphological unit analysed

HMU_TYPE - type such as pool, cascade, riffle, stap, rapid...

Abstract

Estimating habitat availability for fish is important to quantitatively assess the impacts of environmental stressors on natural systems and it's essential for an effective legislation, protection and restoration of ecosystems. This study aimed to establish a biunivocal relationship between trout spawning habitat and flow rate in three rivers of the Aosta Valley, using trout as a bioindicator.

Building on the literature analysis conducted by PhD Giovanni Negro, it was possible to define approximate baseline conditions for a model capable of predicting suitable areas for trout spawning, based on the characteristics of the riverbed.

In October 2023, field surveys were conducted to characterize hydromorphological monitoring units (HMUs) using the MesoHABSIM method. Additionally, the presence and maturity of trout individuals were also recorded. In December 2023, the presence of trout spawning site was verified and both the spawning site and the HMUs in which they were identified were characterized.

The study resulted in the development of an innovative model that integrates the literature analysis conducted by PhD Giovanni Negro with the collected field data. This model serves a dual purpose: to identify potentially suitable areas for trout spawning and, consequently, to define the relationship between available habitat and flow rate.

The developed model has a sensitivity value of 1, a crucial aspect to minimize the oversight of potentially suitable spawning zones, whilst the habitat flow rating curves highlight a positive correlation between habitat availability and flow rate within the studied rivers. The three curves exhibit a similar trend, all characterized by an initial peak followed by a steady decrease.

The model has proven successful in identifying suitable areas for trout spawning and quantifying the available habitat based on flow rate. These results are of significant value for trout conservation and the sustainable management of rivers.

The model provides a foundation for future research aimed at demonstrating that strategically regulating discharges from hydroelectric plants can enhance the habitat for trout and other river organisms, or simply maintain and improve the reproductive habitat of these

organisms during low-flow periods, without having a significant impact on hydroelectric power generation.

Ultimately, this study represents a significant step forward in understanding the interaction between trout and the river environment, offering valuable tools for the conservation and sustainable management not only of the trout species, but of the entire river ecosystem.

Chapter 1 – Introduction - Background

1.1 Sustainability and Efficiency in Hydropower

Green energy sources make an important contribution to the fight against climate change, as they avoid the use of fossil fuels and reduce emissions of carbon dioxide and particulate matter, essential in combating pollution and the greenhouse effect. Moreover, as performance and efficiency continue to improve, the utilization of recycled materials increases, costs are optimized, and the environmental impact decreases, the benefits derived from the use of green energy grow over time (Enel Green Power, n.d.).

Among the various sources of sustainable energy, hydropower, born in the 19th century, is the oldest and, still today, by far the most important quantitatively speaking as the International Renewable Energy Agency (IRENA) indicates, its installed capacity is equal to that of all others added together (Enel Green Power, n.d.).

This type of energy production has several advantages, starting from the fact that it is a clean source, given the absence of emissions of greenhouse gases or other pollutants; in addition to being sustainable, since, thanks to the natural cycle of water, there is a continuous renewal of its sources. It is also extremely flexible given the variability of the water supply, in fact, the production systems require a very small amount of energy to start up and can reach full power within minutes (Enel Green Power, n.d.).

A hydroelectric power plant does not just generate electricity but interacts with the territory in which it is located, contributing to its development. Since it is possible to precisely control the amount of water that is released (after generating electricity) over time, the risk of flooding can be greatly reduced, also benefiting crops in irrigated areas downstream. Although the initial investment in setting up a plant is challenging and costly, overall, waterpower is the cheapest energy in the medium / long term. Moreover, the potential of hydropower is enormous. The massive bodies of water at high altitudes possess significant gravitational potential energy, and harnessing even a fraction of it, provides an abundant and sustainable energy source (Enel Green Power, n.d.).

1.2 Hydropower Development in Alps

The source with the largest contribution to electricity production from RES-E in 2020 is hydro (41% of total production - normalised figure), followed by solar (21%), wind (17%), bioenergy (17%) and geothermal (5%) (GSE, 2020) as showed in *Figure 1* (GSE, 2021).

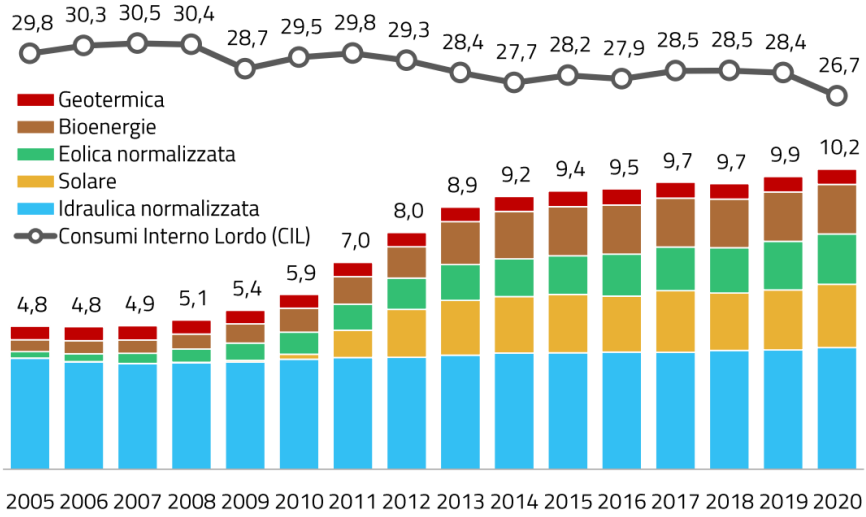

Figure 1: Renewable Electric Energy Sources by Source and Gross Domestic Consumption (Mtoe) (GSE, 2020)

As of the end of 2021, Italy had 4,646 operational hydroelectric plants, excluding pure pumped-storage facilities. In the majority of cases, these were small-scale plants, each with a total capacity of less than 1 MW (GSE, 2021).

Most hydroelectric plants are located in the northern regions (81.2%) of the country and in particular in Piedmont (1,018 plants), Trentino-Alto Adige (587 plants in the province of Bolzano, 280 in the province of Trento) and Lombardy (721). Consequently, as showed in *Figure 2* (GSE, 2021), the hydroelectric production in Italy is concentrated in the northern regions. This is mainly due to the presence of the Alps, which are characterised by a high-altitude difference, numerous watercourses, and Alpine lakes.

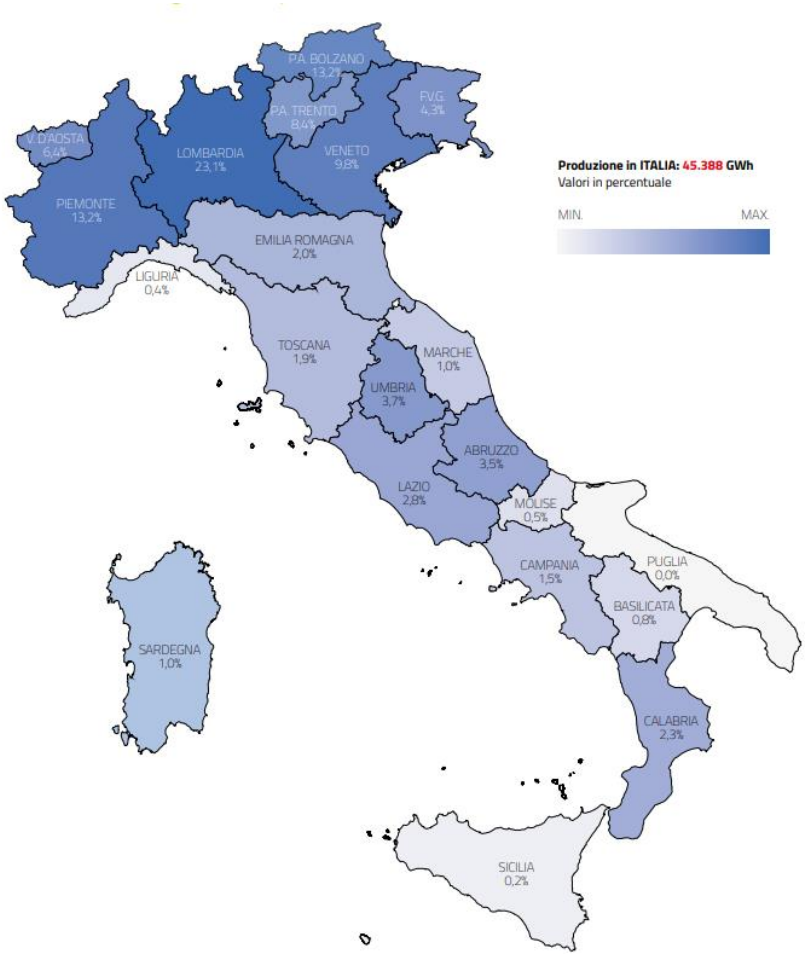

Figure 2: Regional Distribution of Hydroelectric Production (Gwh) in 2021 (GSE, 2021)

These geographical features create an optimal setting for the establishment of reservoirs and the construction of dams. The variations in elevation enable the effective harnessing of gravitational potential energy from water, facilitating energy production.

The use of Alpine hydroelectric resources has, therefore, contributed significantly to the production of renewable energy in Italy, collaborating to the diversification of energy sources and the reduction of greenhouse gas emissions (GSE, 2021).

The management of hydroelectric plants in Italy involves several companies and entities operating in the field of electricity production from renewable sources, among them there is CVA group (Compagnia Valdostana delle Acque).

The CVA Group is an Italian company specialized in water resource management in the Aosta Valley region. Established in 1957, CVA is involved in the integrated management of

water resources, including the production and distribution of drinking water, hydroelectric power generation, and the management of water facilities (CVA, n.d.-d).

The company operates several dams and hydroelectric power plants in the Alpine region, harnessing the hydroelectric potential of the surrounding mountains. Hydroelectric power generation is a significant aspect of CVA's activities, contributing to the supply of renewable energy. In this sector of CVA, there are 32 plants of various types, most of which are run-of-river plants (CVA, n.d.-d).

1.3 Impact on River and Bioindicators

In a study conducted in 2010 by N. Leroy Poff and Julie K. H. Zimmerman on the ecological response to flow alteration, it was found that as flow changes, ecological consequences occur, for example on the presence of habitats and the response of communities in rivers.

The change in flow may be due to several factors, including the presence of hydropower plants for energy production, furthermore, the results of their research suggest that larger changes in flow modification are associated with a greater risk of ecological change with respect to under pre-management conditions (N. LEROY POFF AND JULIE K. H. ZIMMERMAN, 2010).

For this reason, it is critical to understand the interaction between ecosystems and local hydromorphological environment, to quantitatively assess the available habitats and their effects on specific species. Hence, it is crucial to accurately detect, monitor, and assess the impacts of environmental stressors on natural systems. This is essential for an effective legislation, protection, and restoration of ecosystems (Nikolai Friberg, 2011).

There are, however, factors that can exacerbate impacts on river habitats, for example, low-flow periods. During these phases, the volume of water decreases, leading to an alteration of the available habitat as different portions of the riverbed become exposed, whereas they are typically submerged during the rest of the year. This affects the presence of covers, crucial for the survival and spawning of river species, which can vary significantly during these periods.

Low flow can also lead to increased water temperatures due to decreased mixing; this thermal variation affects the availability of habitat for species with specific temperature preferences. Another factor, related to limited water mixing, is the concentration of oxygen in the water, which can decrease, especially in areas with low water flow, such as pools or isolated sections of the river.

From the analysis conducted by N. Leroy Poff and Julie K. H. Zimmerman it was possible to extract quantitative relationships between flow alteration and the ecological response of macro-invertebrates, fish, and riparian vegetation.

Fish were the only taxonomic group to consistently respond negatively to changes in stream magnitude, regardless of whether flows increased or decreased. These findings collectively suggest that fish serve as sensitive indicators of changes in flux, at least based on the measurements and reports provided by this study (N. LEROY POFF AND JULIE K. H. ZIMMERMAN, 2010).

While no clear patterns emerged in the responses of macro-invertebrate insects or riparian species to changes in flux magnitude, responses for riparian species were recorded only in case of decreased magnitude (measured as decreases in peak flow). These responses showed both increases and decreases; however, increases in riparian responses mainly reflected increased cover of non-woody vegetation on the floodplain or an increase in species in elevated areas (N. LEROY POFF AND JULIE K. H. ZIMMERMAN, 2010).

1.4 Importance of Fish and Fish Habitats as Impact Indicators

It is crucial that the impacts of environmental stressors on natural systems are detected, monitored, and assessed accurately to legislate effectively and to protect and restore ecosystems (Nikolai Friberg, 2011).

The temporal and spatial variations in physical characteristics signify the presence of habitat resources. It is feasible to quantify and measure this deviation from reference conditions.

Models are subsequently developed to quantify the variation in habitats based on different types of impacts. Biomonitoring emerges as a crucial tool for monitoring and quantifying these effects (Carter and Resh, 2001, Niemi and McDonald, 2004).

Biomonitoring can be broadly defined as the utilization of biota to assess and monitor changes in the environment (Gerhardt, 2000; Wright et al., 1993, 2000). In the context of aquatic ecosystems, fish are most considered in biomonitoring efforts.

Fish populations and communities serve as indicators in assessing environmental degradation, as they integrate the effects of environmental disturbances on other components of the aquatic ecosystem. This integration is due to their dependence on these factors for survival, growth, or reproduction. Moreover, given the relatively long lifespan of many species, studying populations and communities provides long-term documentation of environmental stress (Lorenzo Tancioni and Michele Scardi, 2005).

The study of fish populations and communities in a river plays a crucial role in evaluating the ecological integrity of lotic systems. They represent sensitive biotic components susceptible to both water pollution and degradation of morphological, hydraulic, and hydrodynamic features. Differences or "dissimilarities" observed in the characteristics of populations and communities (e.g., number and frequency of species, demographic structure) at specific sampling sites compared to expected conditions (reference conditions) can be interpreted as responses to environmental disturbances (Lorenzo Tancioni and Michele Scardi, 2005).

Alteration in site conditions resulting from environmental disturbances, could lead to changes in fish habitat, with direct consequences on fish populations.

This thesis focuses on utilizing fish habitats as impact indicators, recognizing their pivotal role in the reproductive ecology of fish populations. Suitable spawning habitats exert a substantial influence on the survival, growth, and reproduction of fish species.

1.5 Spawning Site as Bio-Indicator

Spawning sites of trout are used as a bioindicator in this study, as they are a predominant species in the considered rivers, as observed during the conducted field analyses.

There are two different species of trout in these rivers: Brown Trout and Marble Trout, some information on which is given below, taken from the *Nature Conservation Notebooks* (Zerunian & De Ruosi, n.d.).

Brown Trout

The brown trout (Salmo trutta) is a species of freshwater fish that inhabits various types of environments within its range, requiring clear, cold water (with temperatures below 15 °C) and high oxygen levels.

In inland waters, the brown trout adapts to two distinct habitats: the upper sections of rivers, characterised by strong currents and gravelly bottoms, where it completes its entire biological cycle, and medium to large lake environments, mainly used for feeding and spawning, during which it ascends tributary streams.

Morphologically, brown trout are medium-sized, displaying variable colour patterns depending on their habitat. Young individuals display a distinctive pattern of large greyish spots along their flanks as showed in *Figure* 3 (Marco Fortunato, 2016).

Figure 3: Brown Trout (Marco Fortunato, 2016)

It is a carnivorous predator that feeds on invertebrates, crustaceans, worms, small fish and occasionally amphibians. Its growth depends on the available trophic resources and the thermal conditions of its environment.

However, brown trout populations are often subject to artificial introductions for recreational fishing purposes, leading to instability in their dynamics. These introductions frequently involve individuals of Atlantic origin, resulting in the genetic contamination of native populations of brown trout, marble trout and grayling in the Adriatic; a phenomenon that poses a significant threat to indigenous populations (Zerunian & De Ruosi, n.d.).

Marble Trout

The Marbled Trout, Salmo marmoratus, inhabits the portions of watercourses at medium and high altitudes, preferring clear, cool waters with gravelly and pebbly bottoms.

This species is a large predator whose diet evolves with age. In its early years it feeds on insects and crustaceans, but as it grows up it prefers other species of fish.

Figure 4: Marble Trout (Pesca Fiume, n.d.)

The Marbled Trout (showed in *Figure 4* (Pesca Fiume, n.d.)) grows at a faster rate than the Brown Trout and can live more than 10 years. However, it is subject to various anthropogenic threats, including intensive fishing and water pollution. In addition, hybridisation with other trout species, such as the Brown Trout, poses a significant threat to its genetic diversity.

Currently, this species is classified as 'endangered' in the Red List of Autochthonous Freshwater Fish in Italy and is included among the 'species of Community interest' according to Directive 92/43/EEC (Zerunian & De Ruosi, n.d.).

Spawning

Spawning in trout, for both species, takes place in the winter period, between November and January; the Marble trout initiates spawning a month earlier than the Brown trout, between November and December, while the Brown trout, mainly between December and January.

During this period, sexually mature individuals move to the upstream stretches of rivers and smaller tributaries, in search of suitable areas to lay their gametes. The females arrive first and, after intense competition, conquer suitable sites, which are generally located in shallow water with moderate flow velocity and a gravelly bottom. Here, with rapid movements of the tail they clean a small area of debris, preparing a sort of oval nest where they lay their eggs, fertilised immediately afterwards by the males; the eggs are then covered by the gravel moved with strong tail strokes by the females, thus being protected from predators (Zerunian & De Ruosi, n.d.).

Each female lays about 1500-2500 eggs per kilogram of body weight; embryonic development is long and takes about 450-degree days (this means, for example, that 45 days are needed at a temperature of 10 °C).

After hatching, juveniles remain close to the spawning site for an extended period, moving downstream only after about a year (Zerunian & De Ruosi, n.d.).

Spawning sites

As mentioned above, since trout's spawning sites are used as bioindicators, in this Chapter are reported the characteristics of trout spawning zones taken from the literature.

Drawing inspiration from Ph.D. Giovanni Negro's meticulous study, *'Habitat Preferences of Italian Freshwater Fish: A Systematic Review of Data Availability for Applications of the MesoHABSIM Model*' which examined 250 publications encompassing the literature on

Italian Freshwater Fish, the findings pertinent to the Brown Trout and Marble Trout species are presented.

Negro's extensive analysis considers as target physical habitat descriptors:

- Water depth.
- Current velocity.
- Biotic/abiotic substrates.
- Covers/shelters.

Specifically, water depth and flow velocity values were processed according to their frequency distribution and split in nine categories, respectively in 15 and 15 cm/s increments (range 0–120 cm, or cm/s, and above), while data on biotic/abiotic substrates were regrouped into 12 categories, both subdivisions follow the classification proposed by Hauer et al. (2006), as reported in the MesoHABSIM standards (Negro et al., 2021).

A systematic review was carried out for physical habitat preferences for 31 freshwater fish species and three freshwater lampreys, summarized for two critical life stages (adult and juvenile) and two bioperiods (rearing/growth and spawning) (Negro et al., 2021).

However, in this thesis' study, the only species under consideration are Brown Trout and Marble Trout, and the life stage examinate is spawning. For this reason, these are the only information adopted from Negro's study.

Moreover, given that this analysis covers literature until 2021, Alessandro Guglielmetto, Ph.D. student at the Polytechnic University of Turin in the Department of Environment, Land and Infrastructure Engineering (DIATI), is currently integrating data from Negro's study to enhance the comprehensiveness of the analysis.

Below are reported the showing ranges of depth, flow velocity, abiotic substrates, and temperature considered suitable by the literature analysis conducted by Negro and implemented by Guglielmetto.

In *Figure 5, 6 and 7* (for brown trout) and *Figure 8, 9, and 10* (for marble trout) on the y-axis, the classes of flow velocity, depth, or substrate (depending on the graph) are

represented, whereas the x-axis indicates the number of scientific articles in which a specific class was identified as suitable for spawning.

Physical benchmarks from literature (Brown trout):

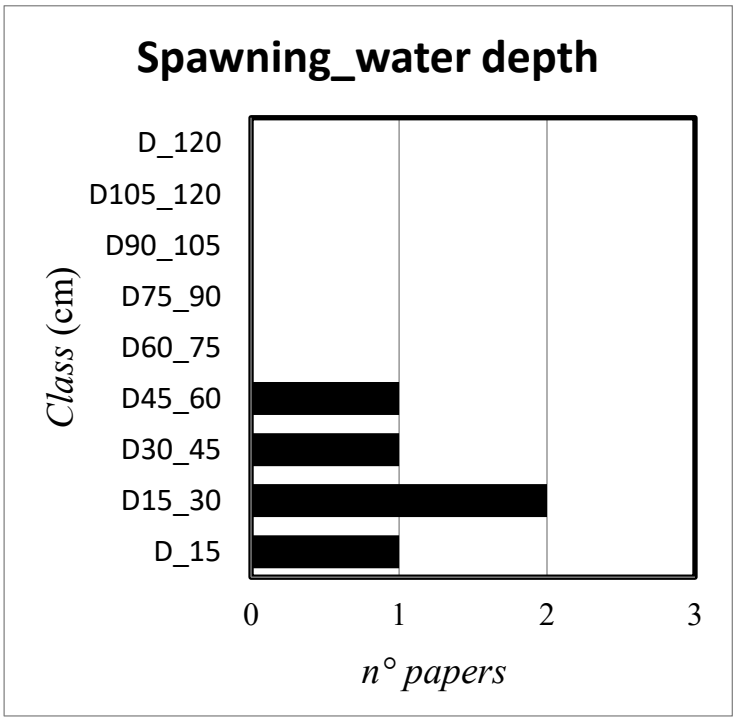

Figure 5: Brown Trout - Spawning Suitable Water Depth Ranges

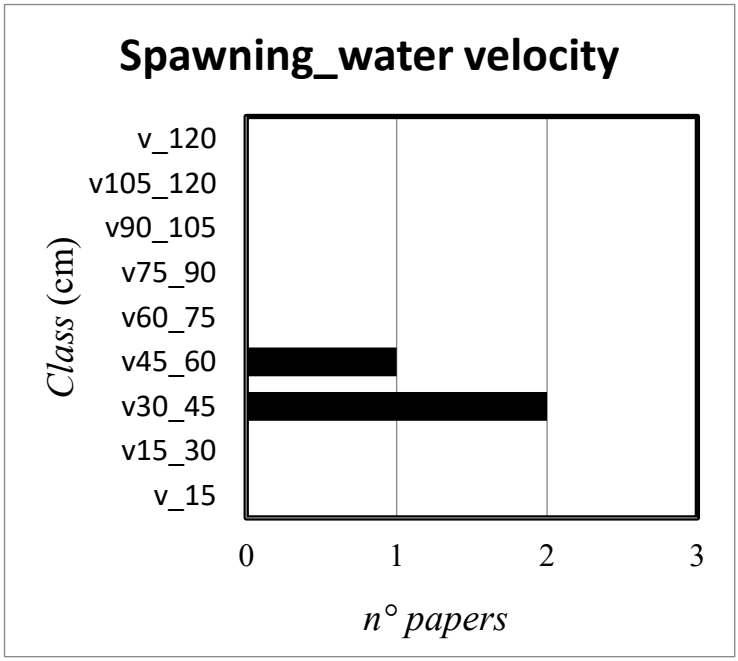

Figure 6: Brown Trout - Spawning Suitable Water Velocity Ranges

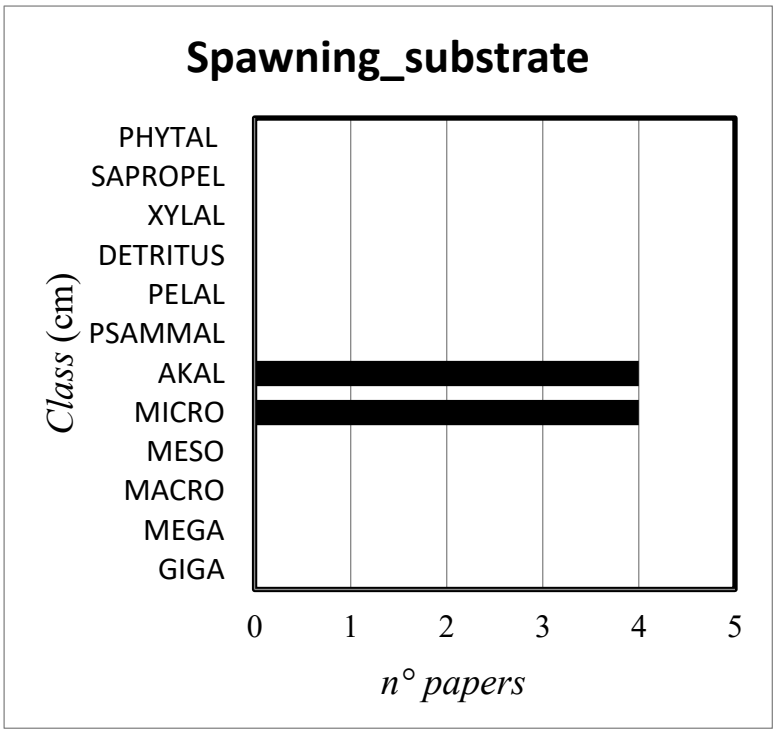

Figure 7: Brown Trout - Spawning Suitable Substrate Classes

Table 1: Brown Trout - Microhabitat Classes

Microhabitat Classes	
Depth	<60 cm
Flow velocity	0.3-0.6 m/s
Substrate	1-6 cm
Covers	None

Table 1 shows the classes considered suitable for Brown Trout's spawning derived by this analysis.

Physical benchmarks from literature (Marble trout)

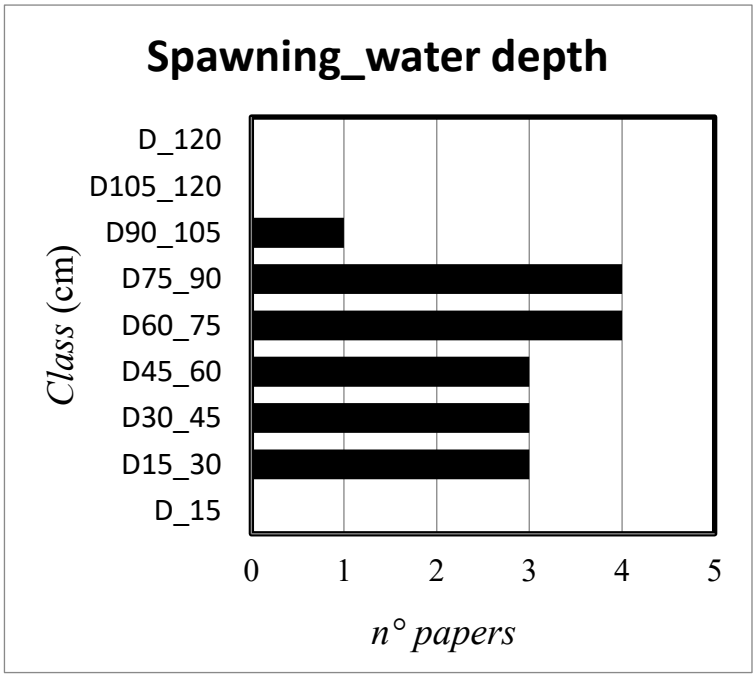

Figure 8: Marble Trout - Spawning Suitable Water Depth Ranges

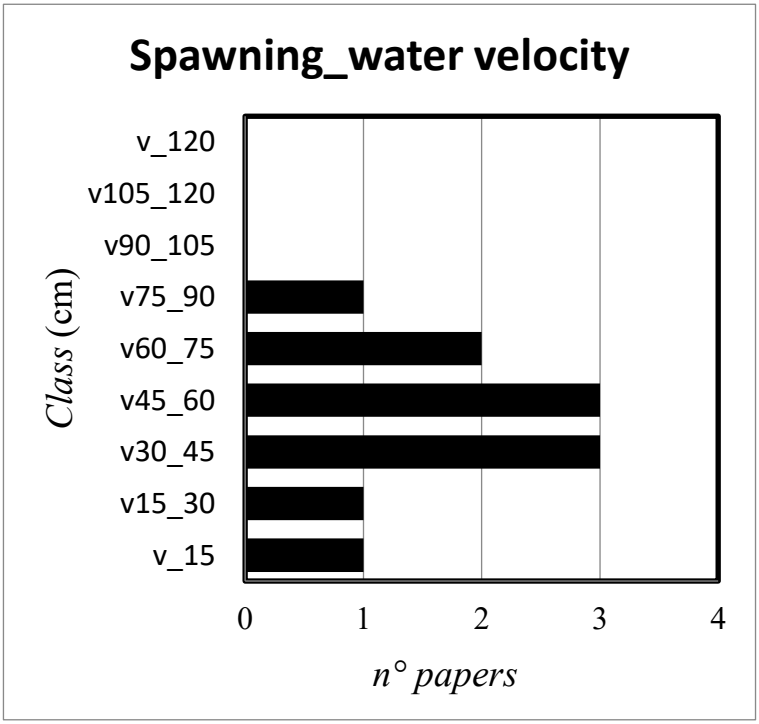

Figure 9: Marble Trout - Spawning Suitable Water Velocity Ranges

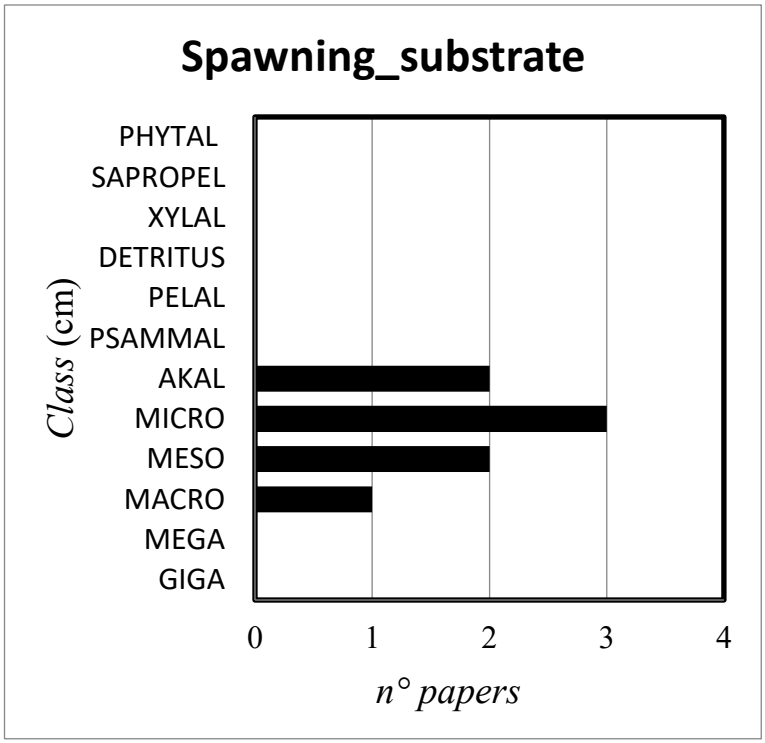

Figure 10: Marble Trout - Spawning Suitable Substrate Classes

Table 2: Marble Trout - Microhabitat Classes

Microhabitat Classes	
Depth	15-105 cm
Flow velocity	< 0.9 m/s
Substrate	1-25 cm
Covers	None

Table 2 shows the classes considered suitable for Marble Trout's spawning derived by this analysis.

1.6 Purpose and Objectives of The Thesis

This study aims to experimentally establish a biunivocal relationship between trout spawning habitat and flow rate in mountain rivers. This information could be helpful for future research and management strategies aimed at balancing hydroelectric power generation with the conservation of trout and river ecosystem.

To comprehensively understand the relationship between trout spawning habitat and flow rate, this study focusses on three rivers in Aosta Valley (Graines, Ayasse, and Savara) with hydroelectric power stations but minimal other anthropogenic impacts. Trout serve as bio-indicators, and their spawning during low-flow periods is used to evaluate changes in spawning habitat under varying flow rates.

In order to pursuit this objective, a model is developed to predict suitable areas for trout spawning based on specific riverbed characteristics. This model facilitates the establishment of a biunivocal relationship between habitat and flow rate.

Furthermore, the study seeks to assess the impact of increased flow during low-flow periods. It investigates whether increasing flow in such periods can create new areas suitable for trout spawning, consequently enhancing the habitat.

This study aims to provide a foundation for future research aimed at demonstrating that strategically regulating discharges from hydroelectric plants can enhance the habitat for trout and other river organisms, or simply maintain and improve the reproductive habitat of these organisms during low-flow periods, without having a significant impact on hydroelectric power generation.

Ultimately, this study represents a significant step forward in understanding the interaction between bedload sediment transport and trout spawning habitat, offering valuable insights for fish conservation and sustainable management of sediment fluxes.

Chapter 2 – Materials and Methods

2.1 Study Area

The watercourses considered for this analysis are Ayasse River, Graines River and Savara River. The choice of these rivers is based on the fact that these streams are relatively untouched; in fact, the only factor influencing their environmental status is the presence of hydroelectric power plants, and no other external factors such as agriculture.

Since the pressures exerted are relatively low, these rivers become ideal for this research and thus for comparing the effects of hydropower plants on river habitats.

Furthermore, these selected river stretches contain a substantial volume of data, including various flow rates in extended periods, which have been utilised in the development of the model. Additionally, these sites are easily accessible and suitable for on-site analyses, further ensuring the accuracy and reliability of the models.

Figure 11 represents an aerial photograph taken from Google Earth, indicating the three points where field surveys were conducted on the three rivers under consideration.

Figure 11: Aosta Valley Map (Google Earth)

2.1.1 Ayasse River

The Ayasse river (showed in *Figure 12*), located in the Valle d'Aosta region of Italy, originates on the southern slope of Mont Collon in the Graian Alps, and flows through the valley of the same name. It is a tributary of the Dora Baltea River, the main watercourse of the Aosta Valley (Regional consortium for protection, n.d.).

Hydrologically, the Ayasse River is sensitive to climatic and seasonal variations, with water flows fluctuating according to rainfall and snowmelt. These fluctuations can affect the river's ecosystem and the fauna that inhabit it.

From an ecological point of view, the Ayasse supports a variety of fauna and flora typical of mountain regions; it is known for its crystal-clear waters during all year and for the presence of wild populations of trout (Regional consortium for protection, n.d.).

Figure 12: Part of the Analysed Section of Ayasse River

Hône, Pontboset and Champorcher are the only significant towns on the torrent, and in this first municipality is located the Hône 2 hydroelectric plant. Characterised by its 12,830-metre-long diversion canal, built halfway up the mountainside following the contour lines of the steep sides of the Ayasse torrent valley (CVA, n.d.-c).

In summer, the plant utilises the energy of water from the torrents in the catchment area, while in winter, water from the Miserin and Vercoce lake basins is added. The hydroelectric plant is equipped with three Pelton-type turbines with a capacity per second of 2 m^3. This equipment gives the plant a total capacity of 11 MW (CVA, n.d.).

In *Figure 13*, the diversion of the Ayasse River for the Hône 2 power plant can be observed; the river section analysed in this thesis study is located downstream of this diversion.

Figure 13: Diversion of the Ayasse River for the Hone Power Plant

2.1.2 Graines River

The Graines River (*Figure 14*) is a watercourse located in the Valle d'Aosta region of Italy, flowing through the Val Graines in a north-westerly direction. The Graines River is a tributary of the Dora Baltea River, the main watercourse in the Aosta Valley.

Ecologically, the Graines River supports a variety of fauna and flora typical of mountain regions. The clear waters of the river are essential for various species of fish and other aquatic organisms that inhabit the river ecosystem.

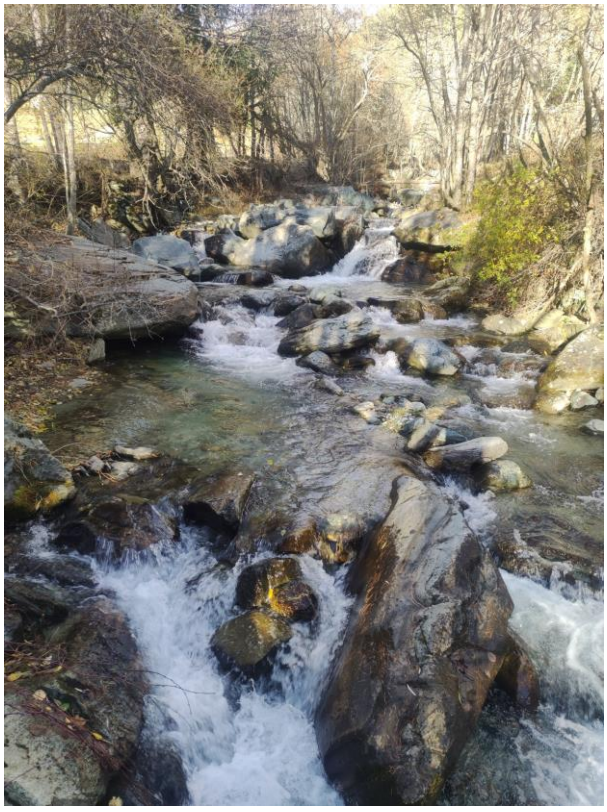

Figure 14: Part of the Analysed Section of Graines River

The water of the Graines stream is collected and transformed into hydroelectric energy by the hydroelectric power station in the municipality of Challad- Saint Vicotr, the Isollaz power station, built in 1928.

This reservoir plant carries out variable load production between full load with 83 m/s and standstill. The power station house has two Pelton-type turbines with a total capacity of 32 MW (CVA, n.d.-b).

In *Figure 15*, the diversion of the Graines River of the Isollaz power plant can be observed; the river section analysed in this thesis study is located downstream of this diversion.

Figure 15: Diversion of the Graines River for the Isollaz Power Plant

2.1.3 Savara River

The Savara River (*Figure 16*) flows through Valsavarenche in the Aosta Valley as a right-hand tributary of the Dora Baltea River.

Glacial activity modelled numerous basins, some of which were filled by meltwater forming mountain lakes such as Lac Noir, Lacs Trebecchi and Lacs du Nivolet. Sarava's origins can be traced back to the foot of the Gran Paradiso massif, taking its life from these lakes (VdA Region, n.d.).

During its course in Valsavarenche, the river is fed by significant tributaries such as Côte Savolère, Lévionaz and Dora di Rhêmes, and further downstream, at Villeneuve, it joins the Dora Baltea. The Savara River basin stands out with an average altitude of 2,513 m above sea level, making it one of the highest inland basins in Valle d'Aosta (VdA Region, n.d.).

Figure 16: Part of the Analysed Section of the Savara River

The Chavonne run-of-river hydroelectric power station came into operation in 1922 and derives the water of Savara River, Grand Eyvua and Nomenon. Contrary to what expected, it is not located close to the riverbed, but halfway up the river in order to discharge the turbined water into the Grand Eyvia power station's bypass channel, to benefit it and the Aymavilles plant.

The Chavonne plant produces renewable hydroelectric energy and can deliver 7 m^3 every second to the five installed Pelton turbines, which together reach a total capacity of 27 MW (CVA, n.d.-a).

In *Figure 17*, the diversion of the Savara River for the Chavonne power plant can be observed; the river section analysed in this thesis study is located downstream of this diversion.

Figure 17: Diversion of the Savara River for the Chavonne Power Plant

2.2 MesoHABSIM: Structure and Application

All the information reported in this section are entirely referred to the Technical Operational Manual for Modelling and Assessment of River Habitat Integrity (ISPRA, 2017a).

River habitat modelling is used to assess the spatial variation of habitat parameters over time in relation to water discharge.

Habitat models can isolate the effect of the hydromorphological component on communities, making them useful in impact assessments and simulations of river management scenarios. There are two types of habitat models, microhabitat models (such as PHABSIM and CAsiMiR), and meso-scale habitat suitability models, such as MesoHABSIM, which describe the use of larger spatial units (mesohabitats).

The MesoHABSIM methodology has proven to be sufficiently flexible and structurally suitable to represent the high morphological variability of Italian watercourses, allowing the analysis of both spatial and temporal variations in available habitat for aquatic ecosystems in cases of both hydrological and morphological alterations.

MesoHABSIM procedure methodology consists of habitat description by hydromorphological survey for different runoff conditions; application of biological models of habitat suitability; and concludes with the analysis of spatial-temporal changes in river habitat.

Mapping HMU (or mesohabitats) is done through the following key steps:

- *Background image acquisition and georeferencing*: high-resolution aerial and satellite images are displayed and can be used as background during the hydromorphological survey on the acquisition tool.
- *Positioning and orientation of the starting station point*: on the first starting point of the polygon, it is necessary to materialize the station point on the ground and orient with respect to geographic north by acquiring the coordinates of the first station point and some Ground Control Points (GCPs)

- *Acquisition of the polygons' outlines representing the HMUs*: This operation consists of describing the wet area perimeter of each individual morphological unit or sub-unit. It is necessary to record enough points such that the perimeter of the surveyed unit is defined in a simplified way, but as close to reality as possible.
- *Collection of environmental descriptors for each HMU*: The environmental descriptors used by the MesoHABSIM methodology are as follows:
  - Date of the survey and the name of the watercourse.
  - Flow rate at the time of the survey (m^3 /s or l/s).
  - Code or name of the unit to be surveyed.
  - Average slope of the free surface (%).
  - Longitudinal connectivity for fish fauna passage (presence/absence).
  - Presence of physical stress or predator covers areas (cover) for fish fauna, such as the presence of large boulders, shading by tree vegetation; overhanging, i.e., the presence of overhanging terrestrial vegetation in contact with the water, accumulations of woody debris, submerged or emergent vegetation (presence/absence).
  - Distribution of substrate classes [12 classes: gigalithal (rocky substrate); megalithal (> 40 cm); macrolithal (20-40 cm); mesolithal (6-20 cm); microlithal (2-6 cm); akal (gravel); psammal (sand); pelal (silt, clay); detritus (organic material); xylal (wood debris, roots); sapropel (dark-colored anoxic mud); phytal (submerged plants)].
  - Frequency distribution of water depth [9 classes: 15 cm intervals to ≥ 120 cm]
    D_15, D15_30, D30_45, D45_60, D60_75, D75_90, D90_105, D105_120 and D_120
  - The frequency distribution of current velocity [9 classes: intervals of 15 cm s -1 to ≥ 120 cm /s]
    CV_15, CV15_30, CV30_45, CV45_60, CV60_75, CV75_90, CV90_105, CV105_120 and CV_120
  - Froude's Number (average value per unit or sub-unit).

The choice of the number of measurement points and their location within the same HMU should be such as to ensure a homogeneous and complete characterization of the HMU; it is usually recommended to collect the required information by random placement in at least 15 measurement points per unit.

In general, point measurements of depth, flow velocity, and substrate representative of each HMU should be of the "stratified random" type for hydraulic sub-units that are homogeneous in terms of hydraulic/sediment conditions; for each hydraulic sub-unit, the number of points collected should be proportional and homogeneous to its area with respect to the area of the entire morphological unit.

To quantify habitat within the studied sub-reach, it is essential to consider various discharge conditions typical of the watercourse's hydrological patterns, including low-flow and near-average to above-average flow scenarios.

Describing HMUs under three different discharge conditions is the minimum recommended to capture spatiotemporal habitat variations. However, in most cases, it is strongly advisable to conduct more surveys (ideally 4 or 5) (ISPRA, 2017b).

2.3 Hydromorphological Data

2.3.1 Field Data Used in Development of the Model

The habitat available for a given organism or target community changes in a watercourse as the flow rate varies. For an assigned morphological configuration, in fact, the areal extent and spatial distribution of HMU is different for different flow values (ISPRA, 2017a).

To be able to construct a model capable of defining suitable spawning areas, it was therefore necessary to use at least three surveys under different flow conditions, so that it was possible to describe the spatial-temporal changes in habitat. The data used for this purpose came from samplings carried out in 2010, 2011 and 2012 on the rivers under investigation, at different flow rates. These samplings made it possible to create a Habitat-Flow rating Curve relating to suitable spawning areas.

The data collected include several variables related to the hydromorphological units examined. Such as HMU_NUM (number of the hydromorphological unit analysed), HMU_TYPE (such as pool, cascade, riffle, stap, rapid...), area, slope, connectivity (with a value of 1 in the presence of connectivity with near hydromorphological units), presence of covers (roots, boulder, overhanging vegetation...), flow velocity, depth, and substrate type.

Regarding Ayasse River sub-tract, sampling was carried out at:

- Flow rate 0.39 m^3 / s on 22-11-2010 (*Figure 18)*
- Flow rate 0.56 m^3 / s on 04-12-2011 (*Figure 19*)
- Flow rate 3.75 m^3 / s on 03-06-2012 (*Figure 20*)

Below are reported satellite images of the river stretch with the subdivision into HMUs at different flow rates taken during the above-mentioned surveys (*Figure 18, Figure 19, Figure 20*).

Figure 18: HMU Representation of the Ayasse River at 390 l/s 22.11.2010

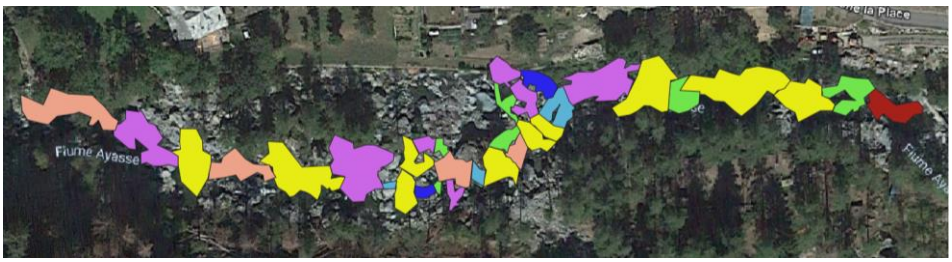

Figure 19: HMU Representation of the Ayasse River at 560 l/s 04.12.2011

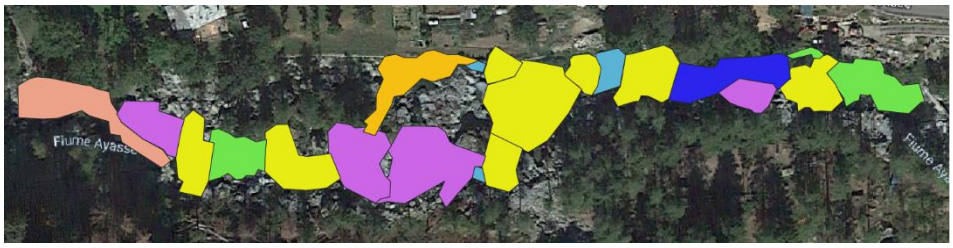

Figure 20: HMU Representation of the Ayasse River at 3750 l/s 03.06.2012

Regarding Graines River sub-tract, sampling was carried out at:

- Flow rate 0.04 m^3 / s on 28-11-2011 (*Figure 21*)
- Flow rate 0.57 m^3 / s on 26-11-2010 (*Figure 22*)
- Flow rate 1,053 m^3 / s on 25-05-2012 (*Figure 23*)

Below are reported satellite images of the river stretch with the subdivision into HMUs at different flow rates taken during the above-mentioned surveys (*Figure 21, Figure 22 and Figure 23*).

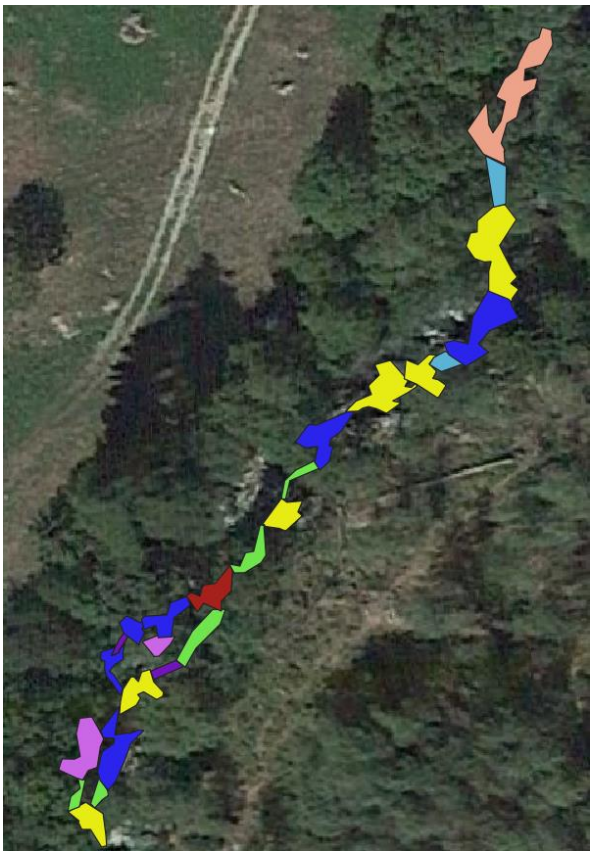

Figure 22: HMU Representation of the Graines River at 40 l/s 28.11.2011

Figure 21: HMU Representation of the Graines River at 5700 l/s 26.11.2010

Figure 23: HMU Representation of the Graines River at 1053 l/s 25.05.2012

Regarding the Savara River sub-tract, sampling was carried out at:

- Flow rate 0.30 m^3 / s on 21-12-2010 (*Figure 24*)
- Flow rate 1.30 m^3 / s on 24-11-2011 (*Figure 25*)
- Flow rate 2.70 m^3 / s on 17-05-2012 (*Figure 26*)
- Flow rate 10.40 m^3 / s on 28-05-2012 (*Figure 27*)

Below are reported satellite images of the river stretch with the subdivision into HMUs at different flow rates taken during the above-mentioned surveys (*Figure 24, Figure 25, Figure 26 and Figure 27*).

Figure 24: HMU Representation of the Savara River at 300 l/s 21.12.2010

Figure 25: HMU Representation of the Savara River at 1300 l/s 24.11.2011

Figure 26: HMU Representation of the Savara River at 2700 l/s 15.05.2012

Figure 27: HMU Representation of the Savara River at 10400 l/s 28.05.2012

2.3.2 Field Data Collection: Definition of HMU Using MesoHABSIM

In October, field activities were carried out to collect data on the identified subtracts of the rivers, Ayasse, Graine and Savara.

During these activities, various data were collected both for the characterisation of hydromorphological units HMU and for the presence / abundance of trout in that specific stretch of river.

For the characterisation of the morphological units HMU, the MesoHABSIM methodology described in *Chapter 2.2 MesoHABSIM: Structure and application*, was used. According to which the description of a surface watercourse must take place within a subtract, which is representative in terms of spatial distribution and relative proportions of typical morphological units (ISPRA, 2017a).

In the case of this analysis, the sub-sections had already been selected during the collected analyses in 2012, 2011 and 2012, so there was no need to define the river sections to be analysed.

The acquisition of the data characterizing the HMUs was carried out using the MapStream software, a QGIS' plugin.

The software allows the hydro-morphological data collection for the application of the MesoHABSIM methodology in perennial and temporary rivers. MapStream converts the signal received from a laser rangefinder in georeferenced points and polygons and allows the collection of physical habitat attributes of each Hydro-Morphological Units (HMUs). The recorded data are organized and formatted to be correctly uploaded in the SimStream-Web service (User Manual, 2021).

In the operation session, the user can choose the type of points to be collected, by flagging the desired point-type shapefile:

- Shapefile STATION: the collected point is assigned to the station position shapefile.
- Shapefile VERTEX: the collected point is assigned to the shapefile containing the polygon's vertices, which are used to draw the polygons of the Hydro-Morphological Units (HMUs).

- Shapefile MEAS: the collected point is assigned to the shapefile containing the measurements of water depth, flow velocity and substrate (User Manual, 2021).

The mapping of the mosaic of HMUs (or mesohabitats) proceeded directly through the following key steps:

- Background image acquisition and georeferencing.
- Positioning and orientation of the station point.
- Acquisition of polygon contours representing HMUs.
- Collection of environmental descriptors for each HMU.

Background image acquisition and georeferencing → First, using a handheld field computer, it was possible to display the high-resolution aerial and satellite images of the survey site within QGIS,

These images were used as a background during the hydromorphological survey, for the periodic quality control of the acquired data. On the image it is, in fact, possible to identify the operator's position and that of the HMUs being surveyed thanks to the GPS positioning integrated in the tablet (ISPRA, 2017a).

Positioning and orientation of the station point → In the context of the MesoHABSIM methodology, HMUs are also described through the delineation of perimeter areas. To do this, it was necessary to acquire, using a GNSS receiver, the coordinates of the stations, i.e. the points from which the description of the HMUs' perimeter wetted area was carried out.

The GNSS (global navigation satellite system) is a geo-radiolocation system that uses a network of orbiting artificial satellites. This system provides a geo-spatial positioning service that allows small, dedicated electronic receivers, such as the topographic GNSS receiver to determine their geographical coordinates (Laterza Enzo, 2021).

In *Figure 28* (NESTLE, n.d.) the type of topographic receiver used in the field during the conducted analyses is shown: GEOMAX zenith 60.

Figure 28: Topographic GNSS Receiver GEOMAX zenith 60 (NESTLE, n.d.)

Acquisition of the contours of the polygons representing the HMUs → The acquisition of the points describing the wetted area of the perimeter of each HMUs was conducted with the use of a rangefinder.

The laser rangefinder is used to measure distances and height differences. By emitting an invisible pulsed energy of infrared laser, it is able to calculate, with a high-precision watch, the time it takes for the laser to hit the target chosen by the operator and return to its source. Knowing the flow velocity of the laser in the atmosphere, the distance D is automatically calculated as (ISPRA, 2017a):

$$D = laser\ speed \times time/2$$

Since this instrument is connected via Bluetooth to the computer, it is possible to see the position of the acquired points on the georeferenced image uploaded to the QGIS platform in real time.

The number of points acquired must be sufficient to describe the perimeter of the wetted area of the HMU in a simplified but as realistic manner as possible.

In *Figure 29* (Cody Corporation, n.d.) the type of laser rangefinder used in the field during the conducted analyses is shown: 360r Trupulse.

Figure 29: Laser Rangefinder Trupulse 360r (Cody Corporation, n.d.)

Once the HMU perimeter mapping is completed, the polygon is registered within the GIS platform.

Collection of environmental descriptors for each HMU → There are several environmental descriptors to be collected to characterize the HMUs:

- Distribution of substrate classes.
- Frequency distribution of water depth.
- Frequency distribution of flow velocity.
- Flow Rate.
- Presence of covers from physical stress or predators.
- Longitudinal connectivity for the passage of fish fauna.

The distribution of substrate classes and longitudinal connectivity for fauna passage were defined by expert judgement by observing the HMU area.

Connectivity with adjacent units was simply described by its presence or absence. The presence of covers was also defined by the presence or absence of possible features, including large boulders, shading by tree vegetation; overhanging, i.e. the presence of overhanging terrestrial vegetation in contact with the water; the presence of undermined banks at the base, accumulations of woody debris, submerged or emergent vegetation (ISPRA, 2017a).

The first three environmental descriptors (substrate, flow velocity and depth) required approximately 10-to-20-point measurements within the same HMU in order to describe the entire unit as homogeneously as possible.

Flow velocity and water depth were acquired through the use of an electromagnetic current meter, which relies on Faraday's law of electromagnetic induction to estimate current velocity.

When a conductor moves within a magnetic field, a voltage is generated that is directly proportional to the flow velocity at which the conductor is moving. The flow of water hitting the instrument sensor perpendicularly, which is the generator of the magnetic field, produces a voltage that the instrument transforms, by means of a linear relationship, into a velocity measurement (ISPRA, 2017a).

In *Figure 30* (Hoskin Scientific, n.d.) the type of electromagnetic current meter used in the field during the conducted analyses is shown: OTT MF PRO.

Figure 30: Electromagnetic Current Meter OTT MF PRO

Again, using the current meter, the flow rate was calculated at the end of the survey. An area was chosen, with a cross section as regular as possible, without considerable bottom slope and with the most rectilinear motion possible (ISPRA, 2017a).

The section was subdivided according to the length of the riverbed into segments, usually 20 cm long, then, for each identified segment, the depth and flow velocity measurement was

performed on a vertical plane. By coupling, in this way, the geometric survey (depth) with the acquisition of flow velocity, the current meter is able to calculate the flow rate in transit.

2.3.3 Field Data Collection: Verification of Trout's Presence

During the month of October, field activities were carried out to collect data on the rivers under consideration, Ayasse, Graines and Savara. During this initial phase of data collection, assistance was provided by an ichthyologist, Michele Spairani, to verify the presence of trout.

Electric fishing was used during the study of the presence and abundance of fish fauna.

Figure 31: Electric Fishing Instrument (Trasmanian Government, 2018)

As showed in *Figure 31* (Trasmanian Government, 2018), this instrument consists of an electric current generator to which a cable is attached to feed the anode, in this case formed by a rod with a flat net at the tip. The cathode, represented by a cable with an uncovered end, that must always remain in the water to close the electric field, is plugged into another connector.

If a fish is subjected to this electric field, it will respond with alternating involuntary and voluntary contractions that induce its motion towards the anode (Marco Angelo Riva (Marple), 2013).

Captured individuals were then placed in different containers, divided according to the hydromorphological unit HMU from which they were taken. To minimise the stress caused, an anaesthetic was used during the operation.

Figure 32: Captured Trout in Container Divided Based on HMU

Within these containers, individuals were restrained to facilitate the measurement of their length and weight. Additionally, these checks allowed for sex verification and identification of mature specimens.

For weighing, a scale was used, while for measuring the length of the specimen, a fish measuring gauge was used, as illustrated in *Figure 33*, consisting of a curved metal ruler specially designed to fit the shape of the fish.

Figure 33: Fish Measuring Gauge

Recovery from electro stunning took a couple of minutes and afterwards, the caught fish were released in the same unit where they had been taken.

The mortality of fish fauna induced by electrofishing, if sampling is conducted properly, is negligible *(of the order of 1-2%)*, although much depends on the species present, the size of the fish, and climatic and water chemistry factors, among which temperature plays an important part. In the context of sampling in an upland area, specifically focused on the prevalent presence of salmonids, it is possible to conduct the operation with virtually no mortality, as pointed out by Marco Angelo Riva (Marple) in 2013.

In the image depicted in *Figure 34*, the two operators in the upper part are conducting HMU definition analysis using MesoHABSIM, while the operators in the foreground are conducting trout presence analysis using an electro-stunner.

Figure 34: Field Survey in Ayasse River

2.3.4 Field Data Collection: Trout Spawning

In December, further sampling was conducted to verify spawning sites. Once again, collaboration occurred with an experienced ichthyologist to identify the presence or absence of trout spawning sites.

Figure 35: Trout Individual on Spawning Site on Ayasse River

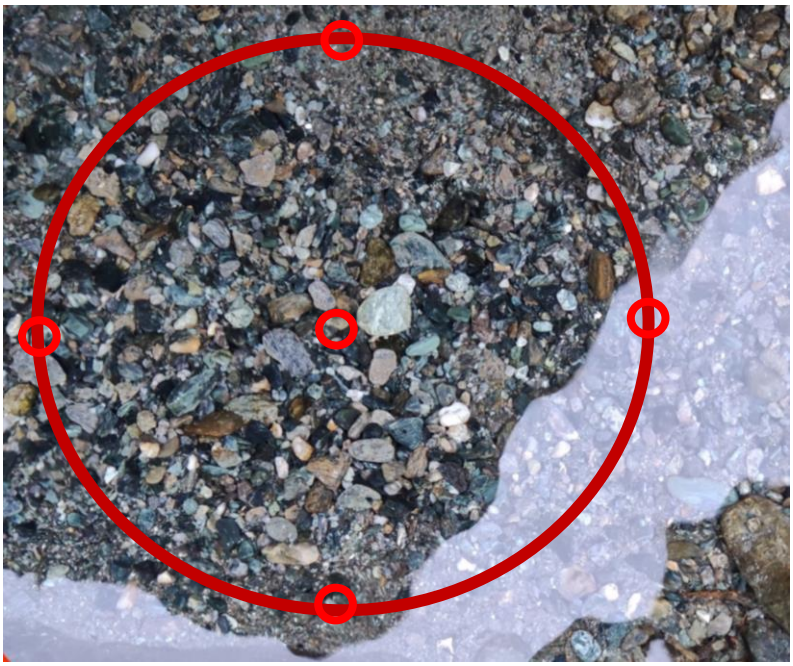

Figure 36: Spawning Area in Ayasse River

In the section above, images of two identified spawning areas in the Ayasse River are presented. In the first one (*Figure 35*), a male brown trout can also be seen defending the spawning site from possible predators after the fertilisation phase.

As mentioned in *Chapter 1.5 Spawning Site as Bio-Indicator*, during spawning, adult specimens with rapid movements of the tail clean a small area of debris, preparing a sort of oval spawning site where they lay their eggs; the eggs are then covered by the gravel moved with strong tail strokes by the females. These areas are in fact often recognisable due to the cleanliness and distribution of the substrate due to the movement of debris by the adults after laying their eggs.

After identifying the spawning area, an analysis was carried out using an acoustic current meter. This instrument allowed the measurement of depth, bottom flow velocity, and flow velocity at 60% of depth.

These measurements were carried out at different points of the spawning site in order to be able to fully characterise this area, as illustrated in *Figure 36*:

- Central point of the spawning site,
- Upstream of the central point,
- Downstream of the central point,

- Right of the central point,
- Left of the central point.

Furthermore, the amount of dissolved oxygen, conductivity, and temperature were assessed using a portable multiparameter probe at the central point of each spawning area. Specifically, for temperature, continuous monitoring was carried out using the HOBO MX2201 probe, as illustrated in *Figure 37*.

Figure 37: Temperature Parameter HOBO MX2201

Subsequently, employing a 500µm mesh macroinvertebrate sampling net, a substrate sample was collected to be as representative as possible of the spawning site for further laboratory analysis. To enhance representativeness, a 5 cm depth was sampled, and all surface matter was included in the collection process.

Finally, the hydromorphological units (HMUs) considered suitable for spawning, given the presence of spawning sites, were defined, and measured using the MesoHABSIM method.

2.3.5 Granulometric Curves

As mentioned in the previous chapter (*2.3.4 Field data Collected: Trout Spawning*), during fieldwork, sediment samples were collected in the spawning area using a 500 μm mesh macroinvertebrate sampling net.

Subsequently, a granulometric analysis was carried out on field samples, representative of the spawning sites.

The analysis carried out led to the creation of several granulometric curves, which were later used to better characterise the properties of a suitable spawning area.

The representation of the granulometric curve of a soil is the most usual classification that can be performed on any type of soil. It makes it possible to identify in what percentage clay, silt, sand, gravel and pebbles are present, and thus to describe a soil on the basis of the size of its grains and their quantity (Civil Protection - Autonomous Province of Trento, n.d.).

The purpose of particle size analysis is to group the constituent particles of soil into different size classes and determine the weight percentages of each particle size class (Gloria Campilongo, 2021).

According to the Italian Geotechnical Association, the main classes are:

- Gravel (between 2 mm and 60 mm),
- Sand (between 2 mm and 75 μm),
- Silt (between 75 μm and 2 μm)
- Clay (below 2 μm).

To create the Granulometric Curve, sieves with different mesh sizes, decreasing downwards, were used. The sieves were stacked on a mechanical sieve shaker which, by vibrating and tilting, promoted the passage of the granules, as showed in *Figure* 38 (Protezione Civile - Provincia Autonoma di Trento, n.d.). At the end, each aliquot was weighed, together with any fraction present in the collection container (Magno et al., n.d.).

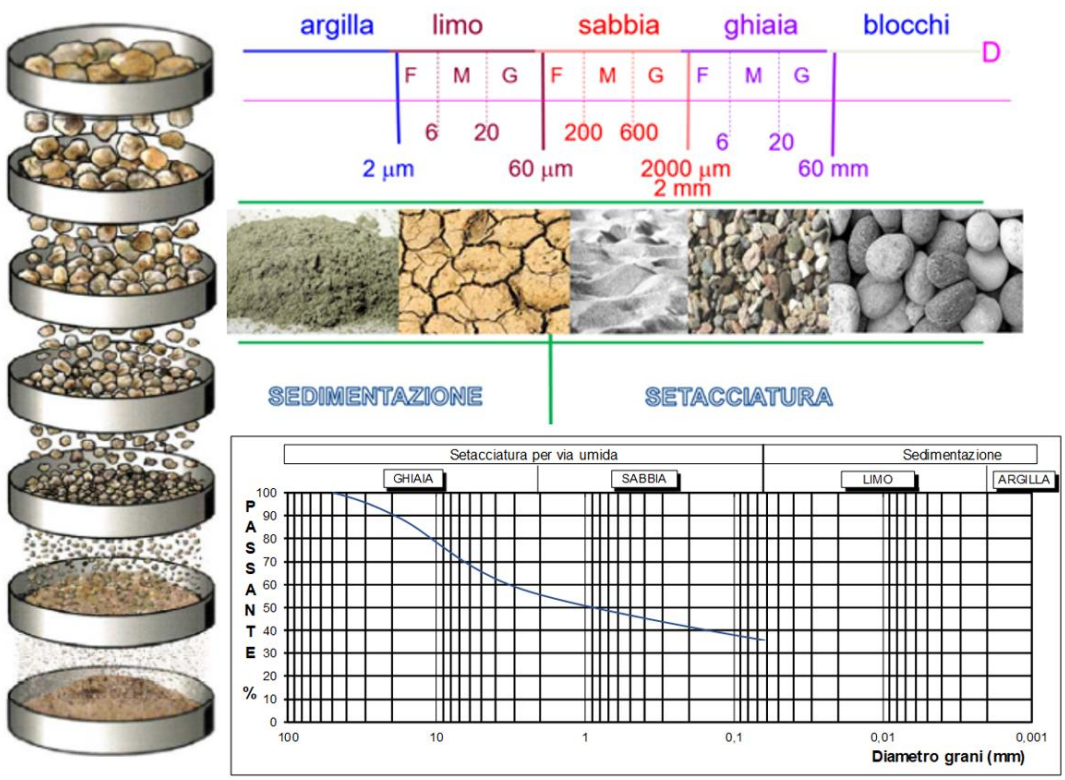

Figure 38: Granulometric Analysis (Protezione Civile – Provincia Autonoma di Trento, n.d.)

In the analysis performed, sieves with the following dimensions were used:

- 75 mm
- 63 mm
- 50 mm
- 38.1 mm
- 25.4 mm
- 19 mm
- 13.2 mm
- 9.5 mm
- 5.6 mm
- 3.3 mm

It was decided to stop the particle size classification at the sand class, as the tool used to collect the samples, having a mesh size of 500µm, was not able of taking classes smaller than that size.

2.4 Theoretical Data

2.4.1 Data Consistency

Through the use of the model, constructed with the conditions derived from literature research, it was possible to create the Habitat Flow rating Curve based on data obtained from samplings conducted in the years 2010, 2011, and 2012 at various flow rates. This approach allowed to observe how the distribution of suitable habitats for trout spawning varied with different flow rates and, consequently, channel characteristics.

Before utilizing these samples, however, it was necessary to examine the presence of any inconsistencies. To achieve this, an analysis was conducted involving seven distinct checks, all of which are integral components of the conventional data verification routine recommended by the methodology developers.

Increase in wetted area with the increment of the flow rate → for each river, it was possible to observe an increase in the flooded area with the increase in flow rate. This increase was attributed to the emergence of new flooded areas, as supported by *Table 3* provided below.

Table 3: Wetted Area's Variation with Increasing Flow

Ayasse		*Graines*		*Savara*	
390 l/s	1739 m^2	**40 l/s**	247 m^2	**300 l/s**	1814 m^2
560 l/s	2191 m^2	**570 l/s**	420 m^2	**1300 l/s**	2353 m^2
3750 l/s	3372 m^2	**1053 l/s**	503 m^2	**2700 l/s**	2388 m^2
				10400 l/s	3522 m^2

Consistency in the classification of HMUs for different flow rate conditions → It was verified that, despite the increase in flow rate and the different period in which the data were collected, there was consistency in the HMU classification. During this analysis, different hydromorphological units HMUs were compared within the same river subtract at different flow rates.

The goal was to verify the consistency, namely if the same area would be classified in a roughly similar manner despite fluctuations in the flow rate.

However, it should not be forgotten that with an increase in flow rate, areas previously categorized in different HMUs as distinct classes may be grouped into a single HMU. In such cases, it was crucial to ensure that the HMU at higher flow rates was consistently classified in comparison to the HMUs at lower flow rates.

Due to space limitations, it is not practical to report the entire comparison analysis down below.

Reasonable increase in depth and flow velocity as flow rate increases → As the flow rate increases, a consequent increase in depth and flow velocity is expected. For this point, it was necessary to calculate the cumulative depth and flow velocity curve for each river's flow rate. The frequency distribution of depth and flow velocity values measured during the surveys was expected to shift to the right as the flow rate increases.

Ayasse

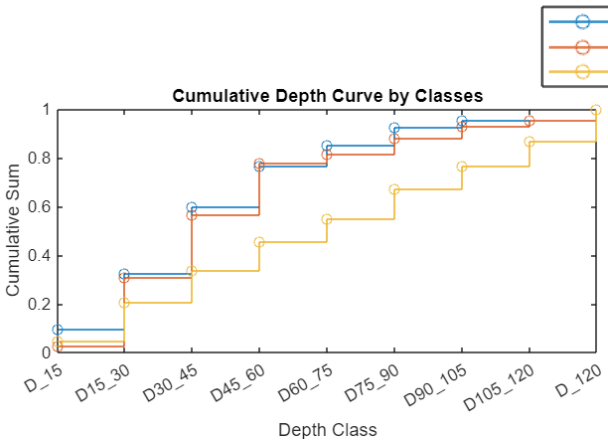

Figure 40: Ayasse - Cumulative Depth Curve

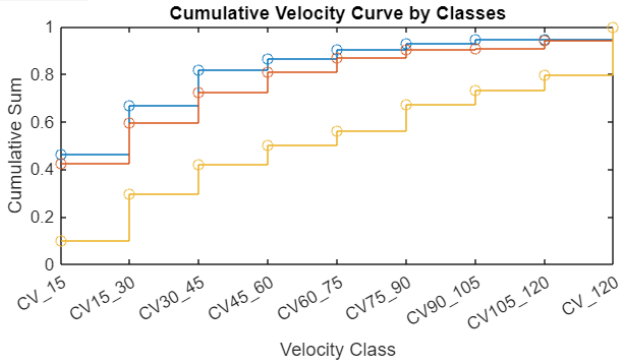

Figure 39: Ayasse - Cumulative Flow Velocity Curve

Regarding Ayasse River, the analysis of the graphs shows that, as the flow rate increases, the cumulative curve shifts on the right, as expected. This phenomenon is consistent with the expectation that at higher flow rates correspond greater water depths and velocities.

There is just one intersection of the cumulative depth curves between the 390 l/s and 560 l/s flow rates. However, this detail does not rise any significant concerns since the overall trend is essentially correct.

Graines

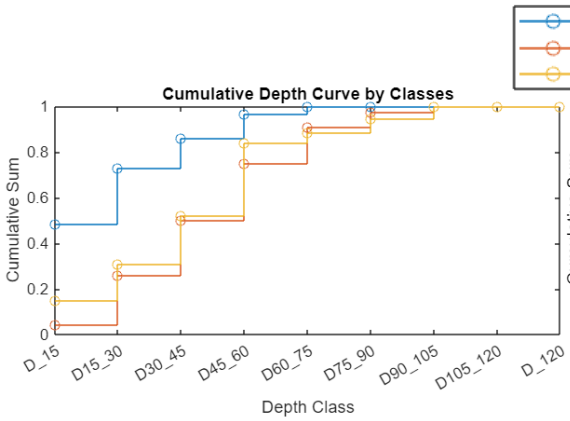

Figure 41: Graines - Cumulative Depth Curve

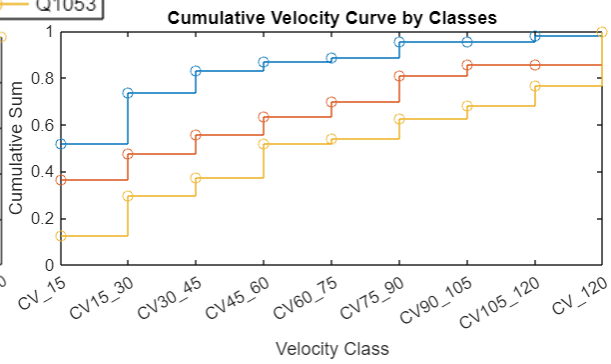

Figure 42: Graines - Cumulative Flow Velocity Curve

The cumulative flow velocity curves (*Figure 42*) for different flow rates follow the expected trend. However, in the cumulative depth curves (*Figure 41*) some intersections emerge between the curves at flow rates of 570 l/s and 1053 l/s.

The observed discrepancies may be attributed to potential measurement errors. These errors could have been subsequently propagated into the following classes, amplifying the discrepancies.

For this reason, an analysis was carried out considering the HMUs at higher flow rates, primarily characterized by depth classes within the ranges where the cumulative curves intersected. From the analysis, it appeared that the classification at 570 l/s was less reliable concerning the number of calculated points to represent the unit. In fact, in the characterization of the HMUs there should be at least from 10 to 20 points, to represent correctly the HMU. However, in these data, there are less than 10 points per HMU.

Savara

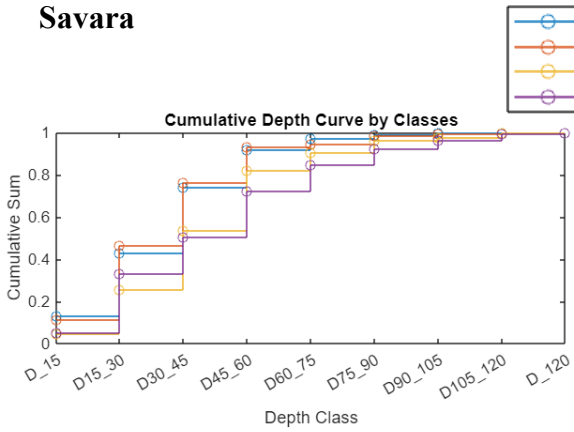

Figure 43: Savara - Cumulative Depth Curve

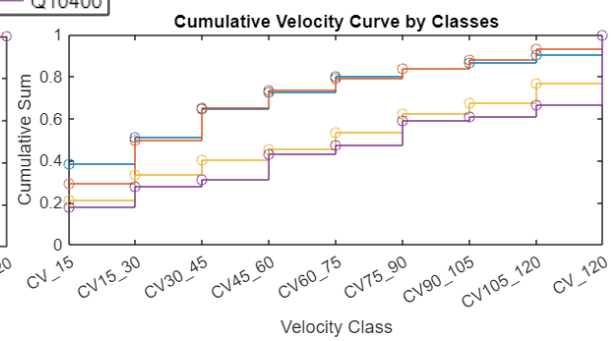

Figure 44: Savara - Cumulative FLow Velocity Curve

Both the cumulative depth and velocity curves (*Figure 43* and *44*) show intersections mainly between the 300 l/s and 1300 l/s flow curves.

For this reason, the same type of analysis used for Graines River was employed, revealing that the Hydromorphological Monitoring Units (HMUs) exhibiting an opposite behaviour in the flow velocity analysis also pose issues in the depth analysis. It is, then, likely that those units have been characterized erroneously. Furthermore, for the Savara River case, the points used to describe the units are insufficient, as for the other two rivers.

Distribution of depth and flow velocity values consistent with the flow value at the time of the survey → It was expected that by using an average of flow velocity, depth and width calculated for each HMU, it was possible to estimate a flow rate that should be consistent with the flow value measured at the time of field data collection. To calculate the average velocity and depth, the arithmetic mean formula was used with the data collected in the field (10 to 20 points are calculated for each hydromorphological unit in a homogeneous manner to best characterise the unit):

$$\bar{X} = \frac{\sum_{i=1}^{n} x_i}{n}$$

To calculate the average width, the QGIS platform was used, with which it is possible to measure the distances between different points. It was therefore possible to calculate an average of measured widths for each HMU.

Most of these calculations returned a flow rate value that effectively approximates the flow rate calculated in the field. However, it was important to consider that the use of this calculation often led to an overestimation of the flow rate, as the average flow velocity and depth were calculated over the entire HMU area, rather than the section as happen in the field measurement.

Consistency in classification and distribution of substrates between surveys with similar flow rates (and wetted areas) → Below are reported two inconsistencies that may occur and should be checked between different survey:

- Occurrence/Disappearance of a substrate class.
- Oscillation of the relative frequencies of each class by more than 10-15%.

Down below are reported different graphs showing the substrate's distribution at different flow rates of all the three rivers.

Ayasse

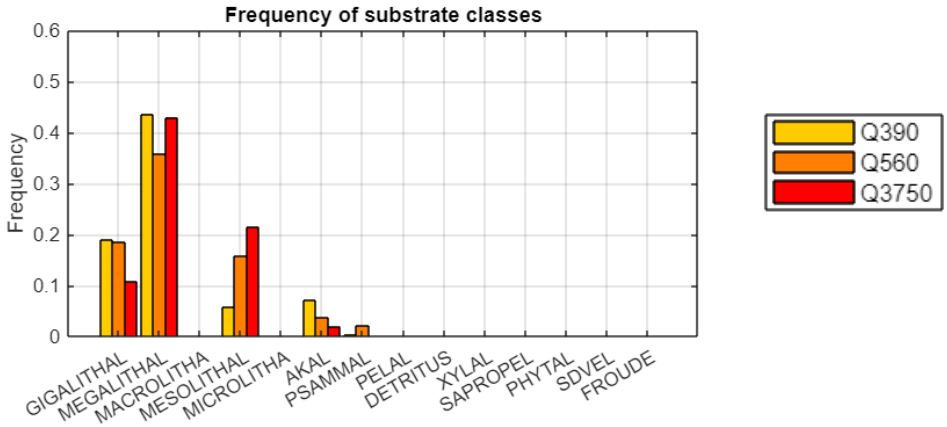

Figure 45: Ayasse - Substrate Frequency

Graines

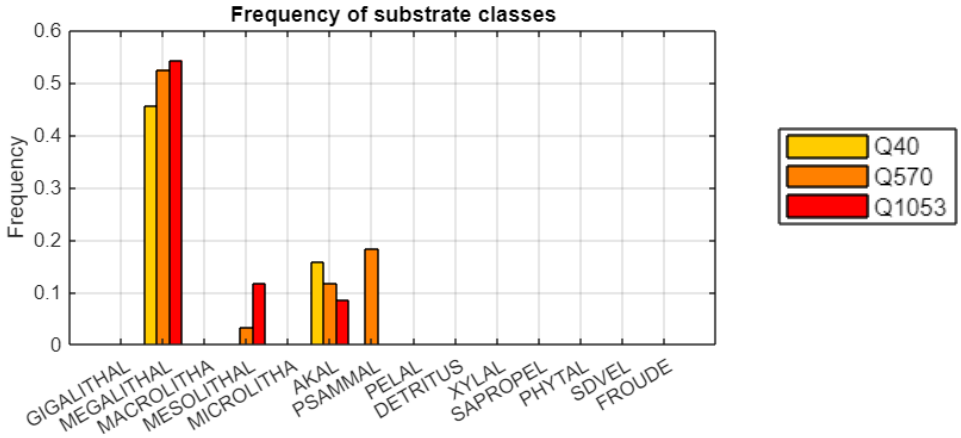

Figure 46: Graines - Substrate Frequency

Savara

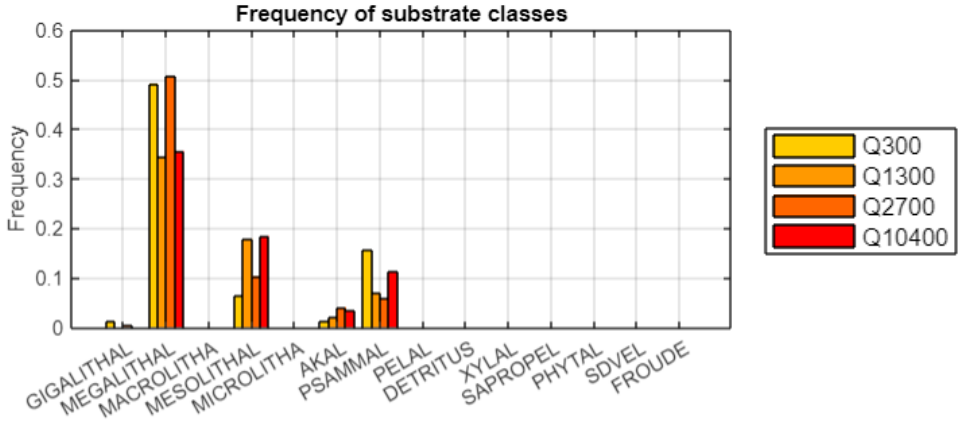

Figure 47: Savara - Substrate Frequency

From the graphs presented, it is possible to observe fluctuations in the frequency of various substrates with changing flow rates. However, these oscillations consistently fall below the 10-15% range and were therefore not deemed as inconsistencies.

Additionally, there are cases in which the presence of certain classes, such as PSAMMAL, may be noticed at some flow rates while absent at others. Nevertheless, this discrepancy was not regarded as an inconsistency due to the notably low frequency of this class. In fact, the more predominant classes consistently appear across all flow rates, and variations between similar flow rates remain within the acceptable range of 10-15%.

As a result, no inconsistencies were considered based on these observations.

Consistency in the maximum and minimum elevation values of the HMU for the slope's calculation → QGIS platform was used to classify various HMUs based on their slope. This approach facilitated the comparison of different slopes, as HMUs within the same class are generally expected to exhibit similar slope characteristics.

Most units classified as Pool had a slope ranging from 10 cm to 30 cm, with a few exceptions up to 50 cm. This slope value was consistent with the classification of the units; in fact, pools are characterised by a very low slope.

There are some classes whose gradient range can vary greatly, not only between different streams, but also at different flow rates, such as Step or Cascade, which can vary from a few tens of centimetres to over a metre.

Inconsistency on hydromorphological data collected using SimStream Web → this check is performed with SimStream Web, in fact, warnings may appear during data upload, automatic checks on the input data conducted by SimStream on the gradient value for each HMU compared to the maximum common value of 1.0%.

However, many of these warnings were negligible, as the maximum gradient value (of 1.0 %) was only slightly exceeded, with gradient values such as 1.26 % or 1.8 %.

2.4.2 Model for Identifying Suitable Spawning Sites

Starting from the literature analysis conducted by PhD Giovanni Negro, an initial model was created, able to indicate suitable spawning areas, the model is unique, as the spawning characteristics of Marble Trout and Brown Trout are similar.

To create this model, a crucial challenge had to be addressed: the scale transition from a spawning area to a Hydromorphological Monitoring Unit (HMU), significantly larger. The model's conditions were derived from the description of spawning sites, which, though occupying only a few cm^2, were compared with the features of the entire HMU, much larger than individual spawning areas.

For this reason, the conditions related to flow velocity, depth, and substrate that characterize spawning areas do not need to be satisfied for the entire HMU but only for a specific percentage. Below are reported the requirements:

- Regarding flow velocity, suitable conditions for spawning must be met for at least 60% of the entire HMU.
- Concerning depth, suitable conditions for spawning must be met for at least 50% of the entire HMU.
- As for substrate, suitable conditions for spawning must be met for at least 5% of the entire HMU, with the additional specification that this area must be at least 0.25 m^2.

The chosen percentage thresholds aim to achieve an overlap in flow velocity, depth, and substrate conditions. By applying these percentage limits, the goal is to enhance the probability that a given point satisfies all three conditions necessary for spawning.

Moreover, the inclusion of a lower limit of 0.25 m^2 for substrate area is used to ensure an area sufficiently large to allow fish spawning.

Under these circumstances, the specific Hydromorphological Unit (HMU) can be considered suitable for spawning, given that the other conditions related to covers and connectivity are also met.

Figure 48 shows the decision tree representing the conditional model for adult trout spawning on which the model was based.

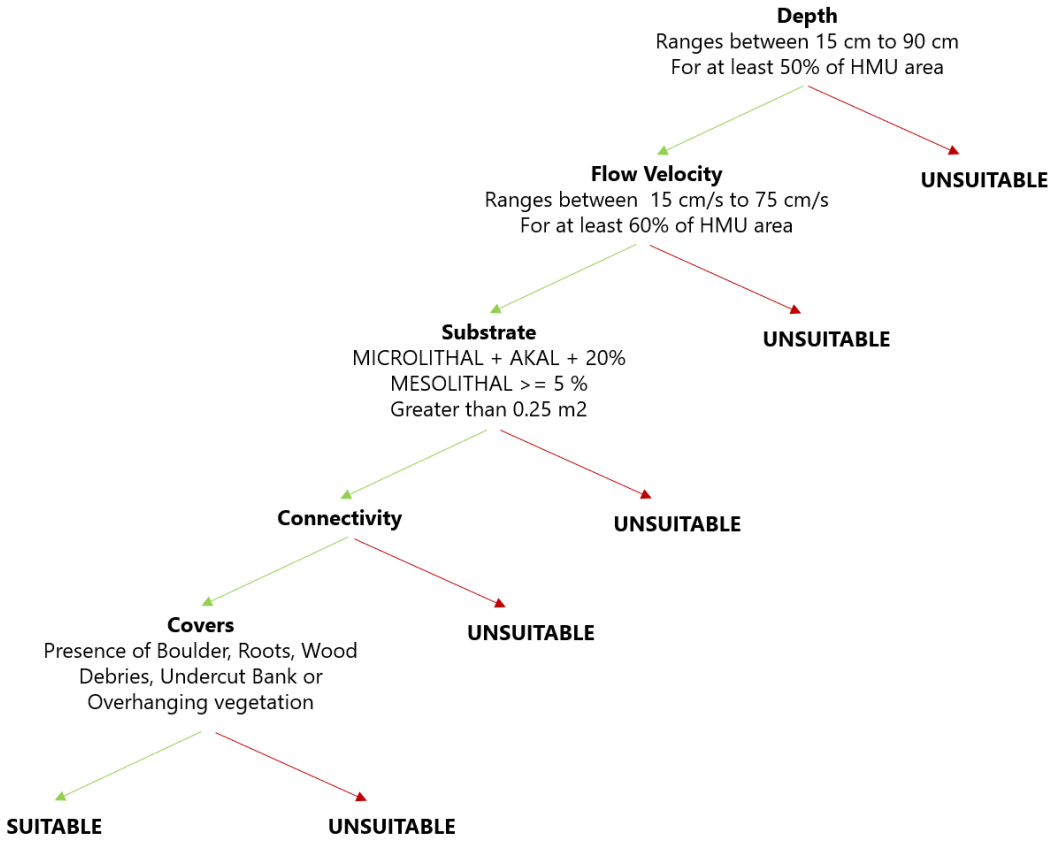

Figure 48: Decision Tree Representing the Conditional Model for Adult Trout Spawning

The conditions verified within the same HMU are reported below:

- Optimal flow velocity was assessed to be in the range of 15 to 75 cm/s, so the MesoHABSIM classes considered are *CV15_30, CV30_45, CV45_60 and CV60_75*. Moreover, this condition has to be verified in at least 60 per cent of the unit area.
- Depth suitable for spawning was estimated to be in the range of 15 cm to 90 cm, so the MesoHABSIM classes considered are *D15_30, D30_45, D45_60, D60_75 and D75_90.* Moreover, this condition must be verified in at least 50 per cent of the unit area.
- Optimal substrate must contain the presence of microlithal, akal and mesolithal, and must be present for at least 5% of the unit area, furthermore, the area satisfying this condition must be at least 0.25 m^2.

- The presence of at least one cover within the HMU is necessary to allow trout to hide in case predators are present. The covers considered are boulders, overhanging vegetation, wood debris and undercut bank.
- Longitudinal connectivity with the previous and next unit is necessary so that the trout can move after depositing and fertilising the eggs.

If all these conditions are satisfied, then the hydromorphological unit HMU can be considered suitable for spawning.

After outlining the conditions to be tested, a model was developed using the PyCharm programming language. The choice of this language was based on the model's future use. Indeed, it will be employed in SimStream Web, where all models from the literature have been written using this programming language and share the same structure outlined below.

This model can assess the suitability of a HMU for spawning by analysing the characteristics of the unit within the input files uploaded (data containing field measurements such as flow velocity, depth, covers, substrate, etc.).

The model is showed below:

```
From import build_var, all_sum, all_zero, any_one

# PRESENCE BOUNDARY
def presence_header (as_unique=True):
c1 = ( "D15_D30", "D30_45", "D45_60", "D60_75", "D75_90" )
c2 = ( "CV15_30", "CV30_45", "CV45_60", "CV60_75" )
c3 = ( "MICROLITHAL", "AKAL" , “MESOLITHAL" )
c4 = ( "ROOTS", "BOULDERS", "WOODY_DEBR", "OVERHA_VEG", “UNDERC_BAN" )
c5 = ( "CONNECTIV" )
c6 = ( "AREA" )
if as_unique:
    return build_var(c1, c2, c3, c4, c5, c6)
else:
     return c1, c2, c3, c4, c5, c6


 def presence(header, row):
c1, c2, c3, c4, c5, c6 = header
```

```
return all_sum(row, c1) > .49 and all_sum(row, c2) > .59 and (row[c3.index("MICROLITHAL")] +
row[c3.index("AKAL")] + .2 *row[c3.index("MESOLITHAL")]) > .049 and any_one(row,c4) and
any_one(row, c5) and (row[c3.index("MICROLITHAL")] + row[c3.index("AKAL")] + .2 *
row[c3.index("MESOLITHAL")]) * row[c6.index("AREA")] > .25
```

After constructing the initial model, its conditions were compared to the characteristics observed during field analyses conducted in the winter period.

This comparison allowed for adjustments to the model, creating different versions capable of more accurately identifying areas suitable for spawning.

Subsequently, the effectiveness of the different models was assessed using data from December 2023 concerning spawning area characteristics.

2.4.3 Validation of the Model Using Field Collected Data

Following the development of Habitat- Flow Rate models for trout spawning, a validation process was executed. Field data collected in December 2023 and February 2024 served as model inputs. This data described characteristics of both HMUs containing observed trout spawning sites and those lacking such observations.

To assess the goodness of the models, a quantitative assessment of model performance was implemented.

This procedure assists in determining the suitability of the model for specific applications and may help to identify those aspects of the model that need improvement (Vaughan & Ormerod 2005; Barry & Elith 2006; Guisan et al. 2006). An assessment of model performance can also provide a basis for comparing alternative modelling techniques (Loiselle et al. 2003; Segurado & Araujo 2004; Pearson et al. 2006) or different models.

Models generating presence–absence predictions, as in the case of this analysis, are usually evaluated by comparing the predictions with a set of validation sites and constructing a confusion matrix that records the number of true positive, false positive, false negative and true negative cases predicted by the model (Allouche et al., 2006).

One simple measure of accuracy that can be derived from the confusion matrix is the proportion of correctly predicted sites (overall accuracy). However, this measure was criticized for ascribing high accuracies for rare species (Fielding & Bell 1997; Manel, Dias & Ormerod 1999).

Two alternative measures that are often derived from the confusion matrix are sensitivity and specificity. Sensitivity is the proportion of observed presences that are predicted as such, and therefore quantifies omission errors. Specificity is the proportion of observed absences that are predicted as such, and therefore quantifies commission errors (Allouche et al., 2006).

Within this analysis, sensitivity played a primary role, reflecting the model's capacity to accurately identify areas suitable for trout spawning.

Conversely, specificity assumed a less critical role, measuring the model's ability to correctly exclude unsuitable areas. However, sensitivity remained crucial due to the potential for false negatives since suitable habitat may remain unused.

Chapter 3 – Results

3.1. Field Collected HMU Results

In October 2023, field activities were carried out to collect data on the rivers under consideration, Ayasse, Graines and Savara.

During these surveys, various data were collected for the characterisation of hydromorphological units HMU, and the river's subsections analysed using the MesoHABSIM method are reported below.

The lengths of the analysed subsections are shorter than those analysed in 2010, 2011 and 2012. This is because in the case of the previous surveys, there were more days available to carry out measurements on individual streams, which led to an excess of redundant data.

Furthermore, in the context of this specific analysis, the evaluation focused on the population status, the identification of possible areas of interest to be analysed during the winter period and the validation of the model. Therefore, it was sufficient to ensure good heterogeneity in the Hydromorphological Monitoring Units (HMU), considering the presence or absence of certain parameters. It was not necessary to sample the entire tract, but rather have more than 15/20 HMUs to obtain meaningful results.

The number of HMUs collected in October 2023 for each river is shown in *Table 4* below:

Table 4: HMU Data Collected Summary

River	Date of survey	Flow Rate	NUM_HMU
Ayasse	16 October 2023	350 l/s	23
Graines	23 October 2023	171 l/s	32
Savara	24 October 2023	1 253 l/s	23

Below are reported photos showing the position and size of the calculated hydromorphological units HMUs during field activities:

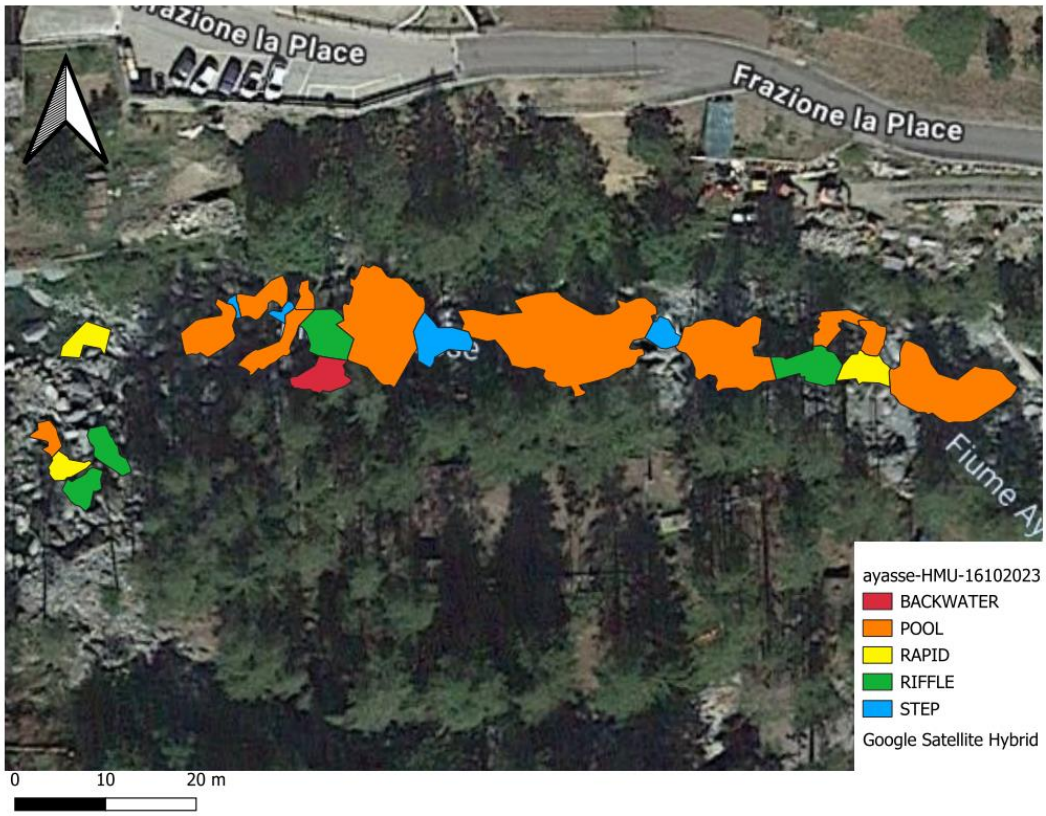

Figure 49: HMU Ayasse - 16 October 2023

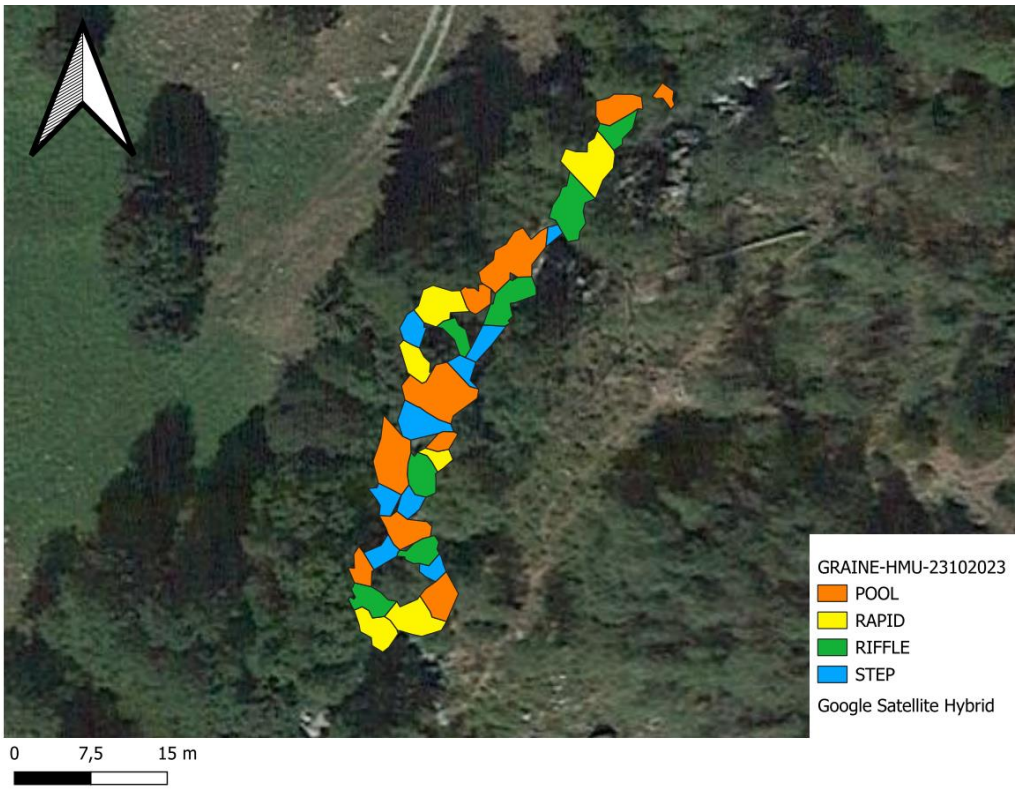

Figure 50: HMU Graines - 23 October 2023

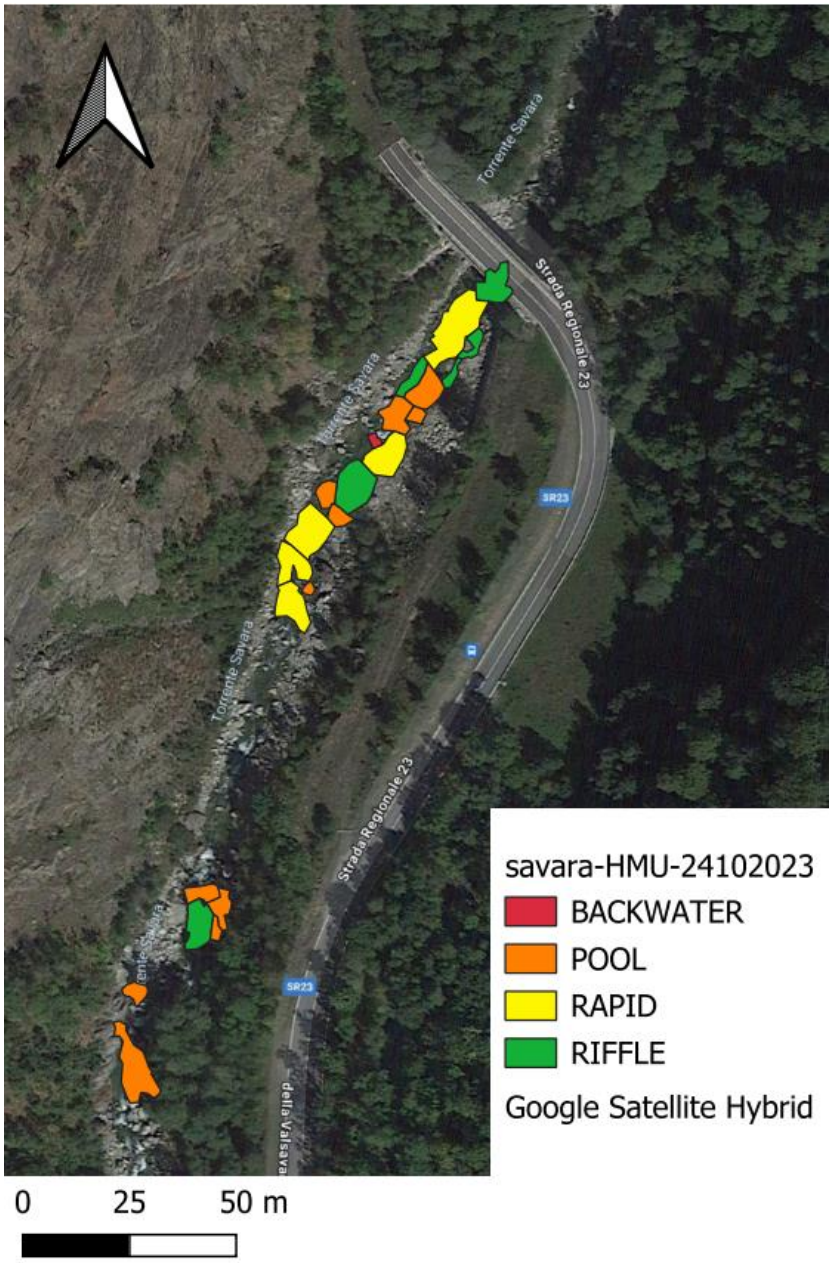

Figure 51: HMU Savara - 24 October 2023

As described in *Chapter 2.3.2, Field Data Collection: Definition of HMU using MesoHABSIM*, after acquiring polygon contours representing HMUs, environmental descriptors were collected for each HMU, such as substrate classes, depth, flow velocity, covers...

Below, is reported an example of the data collected in the field (*Table 5*), which includes parameters such as flow velocity, depth, and substrate, used to characterise the hydromorphological units HMU (not all tables are provided for reasons of length).

Table 5: Graines – HMU Data Collection - 23 October 23

HMU_NUM	HMU_TYPE	PNTNUM	DEPTH (m)	VELOCITY (m/s)	SUBSTRATE
1	RAPID	1	0,08	0,5	MESO
1	RAPID	2	0,2	0,9	MACRO
1	RAPID	3	0,02	1,2	MEGA
1	RAPID	4	0,25	1,1	PSAMMAL
1	RAPID	5	0,13	0,01	MESO
1	RAPID	6	0,48	0,17	MEGA
1	RAPID	7	0,26	0,14	MACRO
1	RAPID	8	0,14	1,6	MACRO
1	RAPID	9	0,08	1,3	MESO
1	RAPID	10	0,12	0	MEGA
1	RAPID	11	0,12	1,4	MEGA
1	RAPID	12	0,11	1,1	MACRO
1	RAPID	13	0,06	0,35	MESO
2	RAPID	1	0,23	0,32	MACRO
2	RAPID	2	0,28	0,18	MESO
2	RAPID	3	0,13	1,01	MEGA
2	RAPID	4	0,12	0,7	MEGA
2	RAPID	5	0,23	0,01	AKAL
2	RAPID	6	0,15	0,73	MACRO
2	RAPID	7	0,14	1,21	PSAMMAL
2	RAPID	8	0,13	0,58	MICRO
2	RAPID	9	0,09	0,34	AKAL
3	RIFFLE	1	0,15	0	PSAMMAL
3	RIFFLE	2	0,14	0,38	MACRO
3	RIFFLE	3	0,11	0,73	MESO
3	RIFFLE	4	0,17	0,85	MESO
3	RIFFLE	5	0,11	0,3	MACRO

3.2 Spawning Sites Observation and Description

During data collection in October, thanks to the support of an ichthyologist, it was possible to verify the presence of trout within the hydromorphological units characterised and reported in the previous *Paragraph 3.1 Field Collected HMU results*.

During this analysis, it was possible to verify not only the presence of trout but also to identify mature individuals, adults in which the presence of reproductive organs and/or the presence of eggs in female specimens were found.

Table 6 shows the number of trout that have been identified, as well as the number of individuals suitable for spawning that have been identified:

Table 6: Summary Data Collected Trout Presence

Summary Trout Presence		
River	*N° Trout*	*N° Mature Trout*
Ayasse	343	54
Graines	108	10
Savara	79	21

In December 2023, further samplings were conducted to verify spawning areas. Once again it was possible to verify the presence of trout spawning sites.

During these surveys, comprehensive data on depth, flow velocity, substrate, dissolved oxygen, temperature, and conductivity were gathered. Below, summarized graphs depicting depth and flow velocity are provided, while the analysis of substrate is presented in *Chapter 3.3 Granulometric Curve Result*.

Table 7: Flow Rates During December Survey

River	Date of survey	Flow Rate
Ayasse	7 December 2023	163 l/s
Graines	19 December 2023	106 l/s
Savara	18 December 2023	555 l/s

Ayasse

Table 8: Ayasse - Informative Chart on Spawning Data

No. of total points	100
Sampled HMU	4
Temperature	1-4 °C
OD	101-105 %
Conductivity	171-191 µS/cm

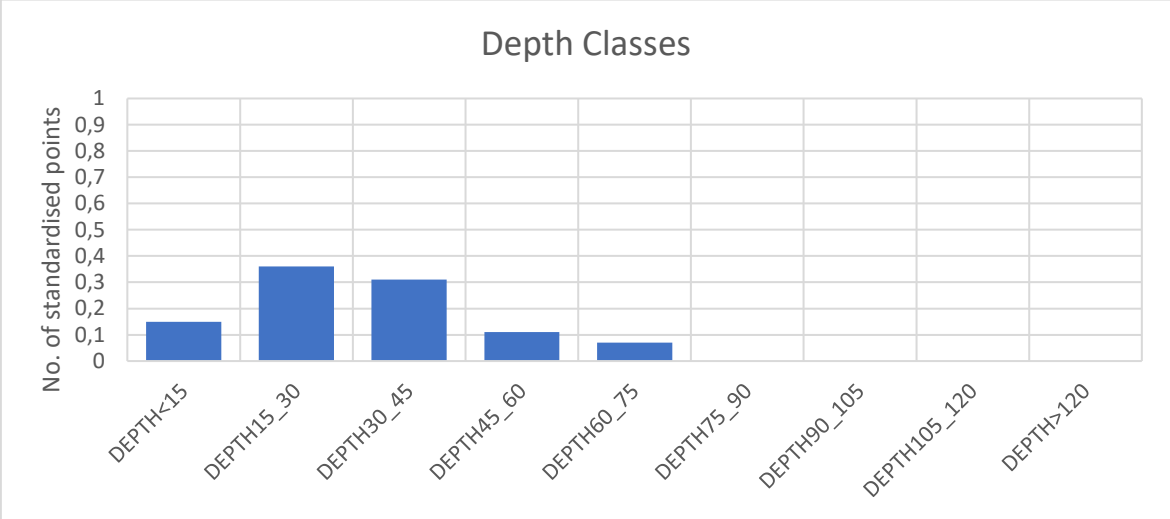

Figure 52: Ayasse -Depth Classes

Figure 52 shows the depth classes that emerged from the field analyses. The optimal depths for trout spawning derived from the analysis of the spawning sites on the Ayasse River are in the range of 0 cm to 75 cm.

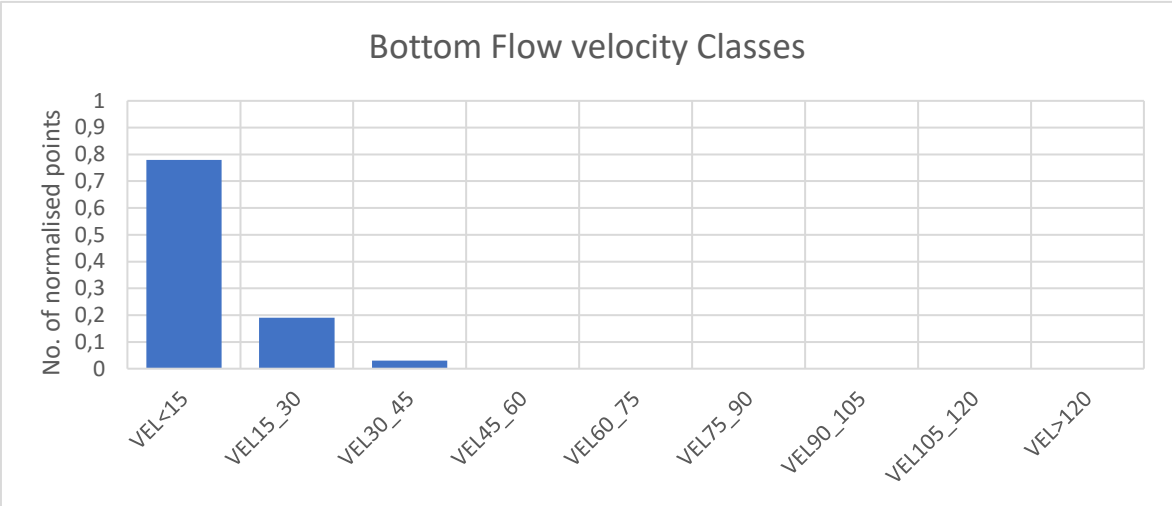

Figure 54: Ayasse - Bottom Flow Velocity Classes

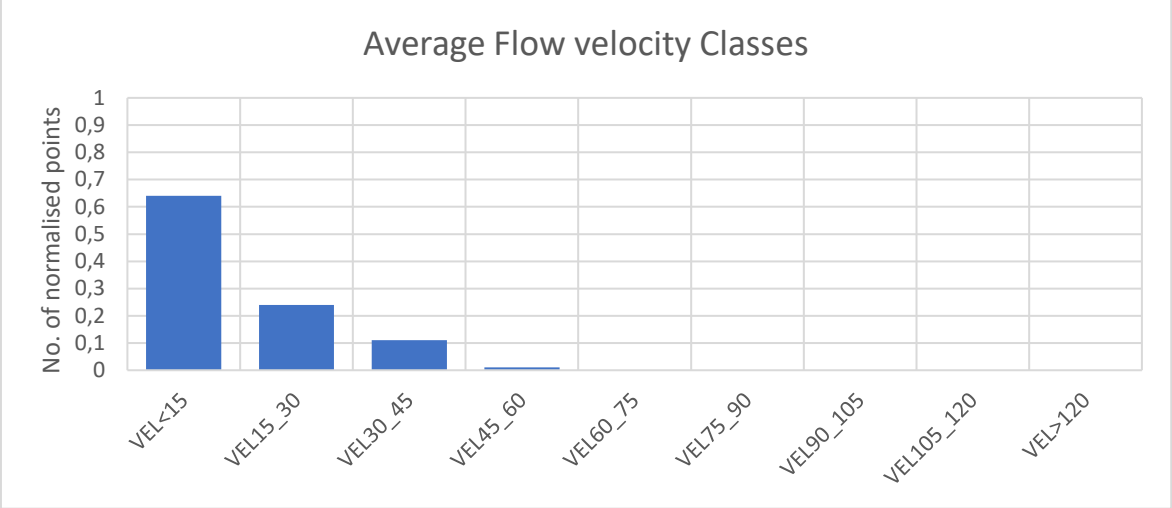

Figure 53: Ayasse - Average Flow Velocity Classes

Figure 53 shows the flow velocity classes that emerged from the field analysis. The optimal trout spawning velocities derived from the analysis of the spawning sites on the Ayasse River are in the range between 0 cm and 60 cm.

Graines

Table 9: Graines - Informative Chart on Spawning Data

No. of total points	22
Sampled HMU	5
Temperature	2,8 °C
OD	102-104 %
Conductivity	113-115 µS/cm

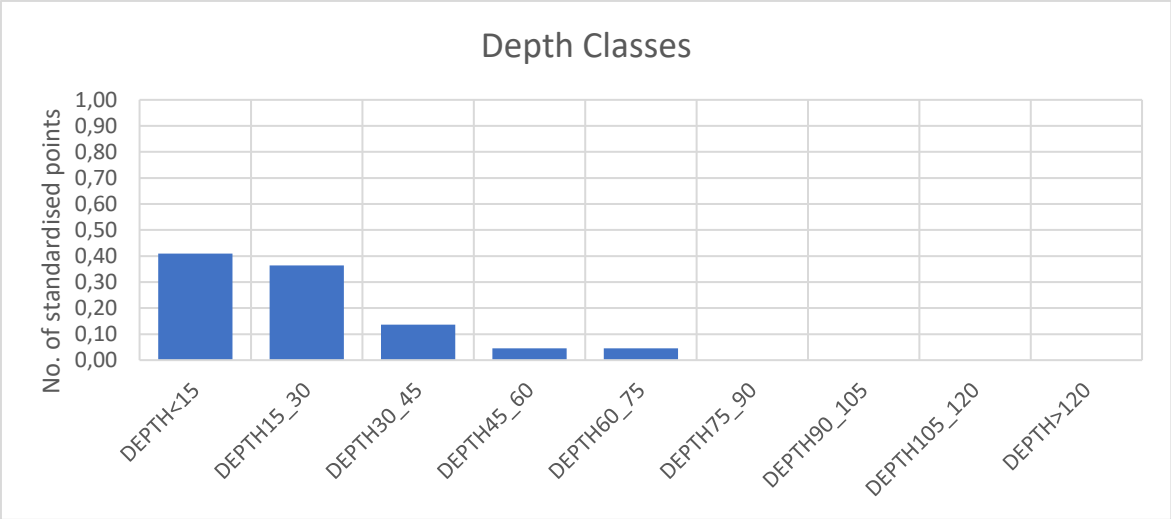

Figure 55: Graines - Depth Classes

Figure 55 shows the depth classes that emerged from the field analysis. The optimal depths for trout spawning derived from the analysis of spawning sites on the Graines River are in the range of 0 cm to 75 cm.

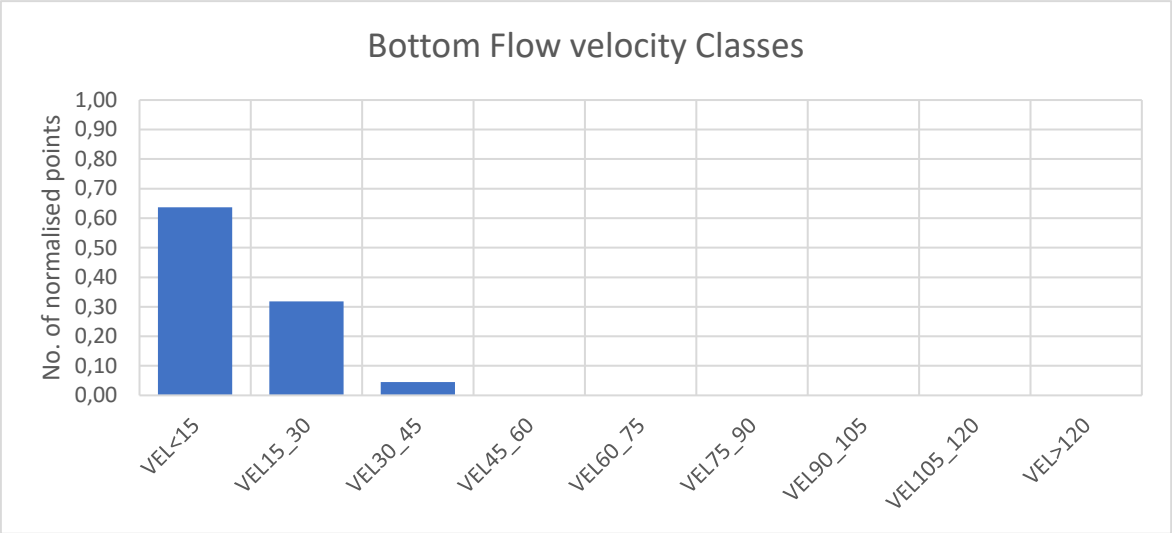

Figure 56: Graines - Bottom Flow Velocity Classes

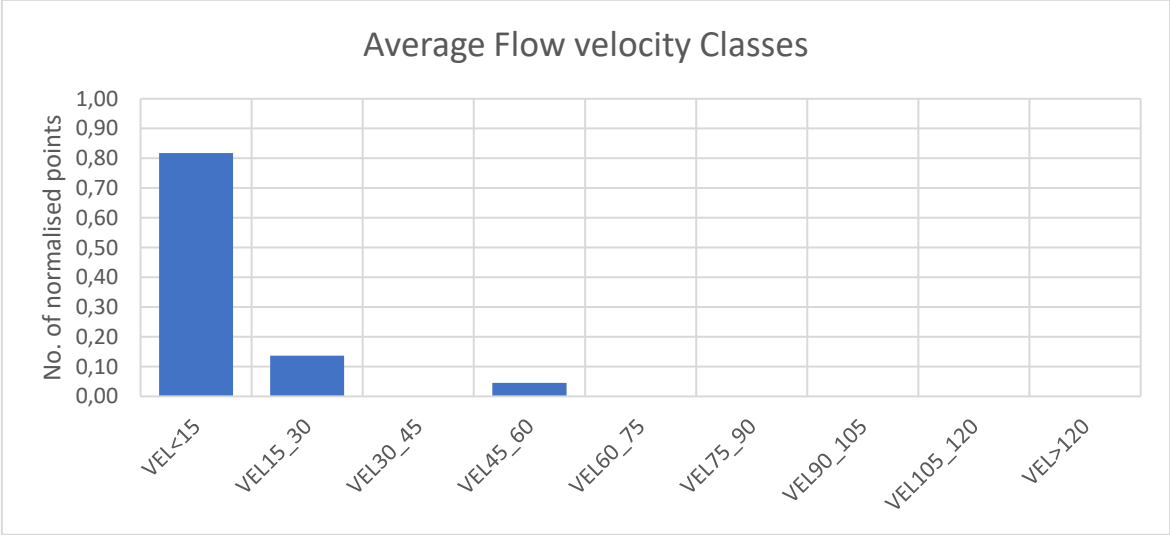

Figure 57: Graines - Average Flow Velocity Classes

From *Figure 57, it* is possible to observe the presence of the flow velocity classes that emerged from the field analysis. The optimal trout spawning velocities derived from the analysis of spawning sites on the Graines River are in the range of 0 cm to 60 cm.

Savara

Table 10: Savara - Informative Chart on Spawning Data

No. of total points	34
Sampled HMU	5
Temperature	3-4 °C
OD	101-103 %
Conductivity	190-212 µS/cm

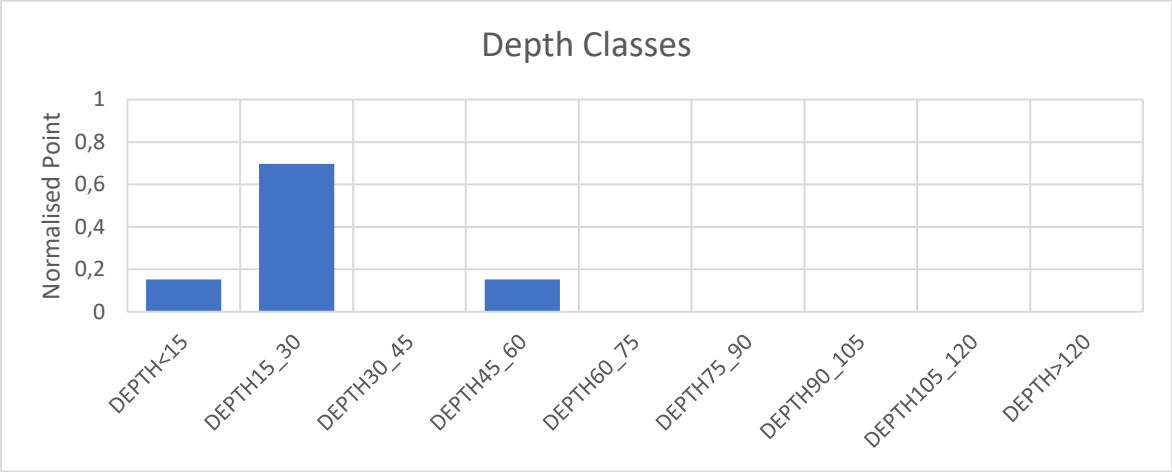

Figure 58: Savara - Depth Classes

Figure 58 shows the depth classes that emerged from the field analyses. The optimal depths for trout spawning obtained from the analysis of spawning sites on the Savara River are in the range between 0 cm and 60 cm.

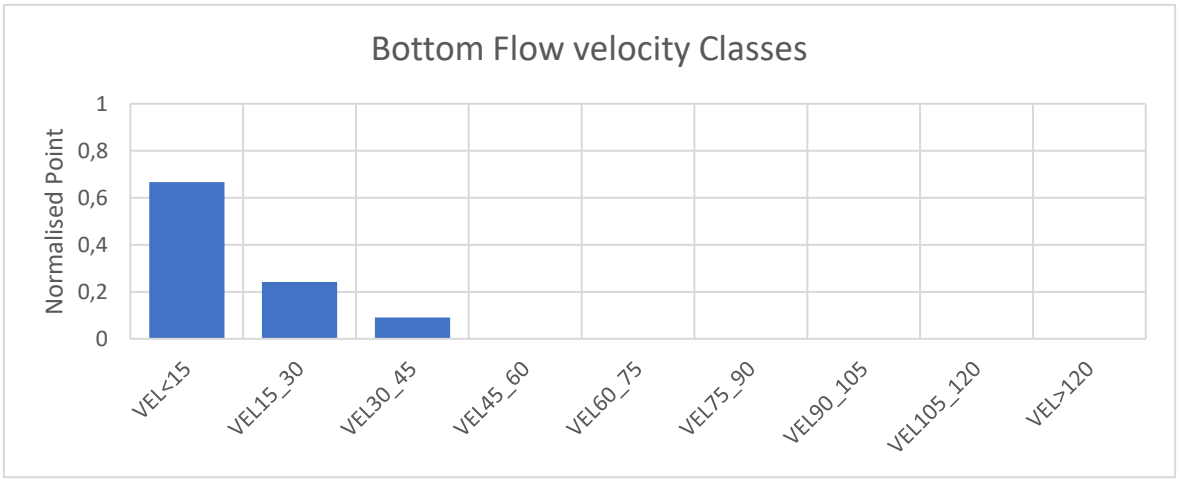

Figure 59: Savara - Bottom Flow Velocity Classes

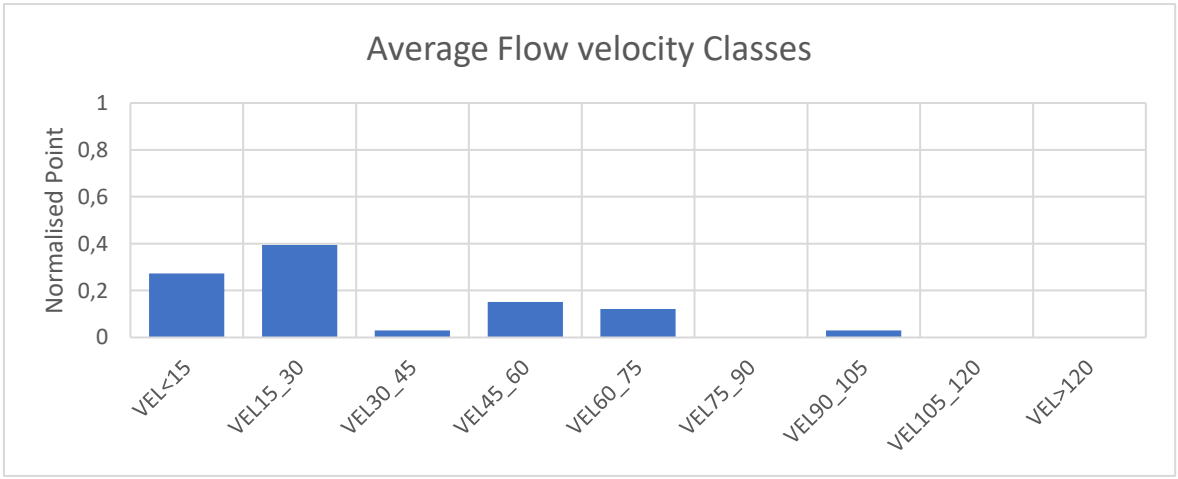

Figure 60: Savara - Average Flow Velocity Classes

Figure 60 shows the flow velocity classes that emerged from the field analyses. The optimal trout spawning velocities derived from the analysis of spawning sites on the Savara River are in the range between 0 cm and 105 cm.

3.3 Grain Size Distribution

Ayasse

Due to space constraints, the results of the data from the particle size analysis are given in Appendix A, while the grain size curve for each spawning site is shown below.

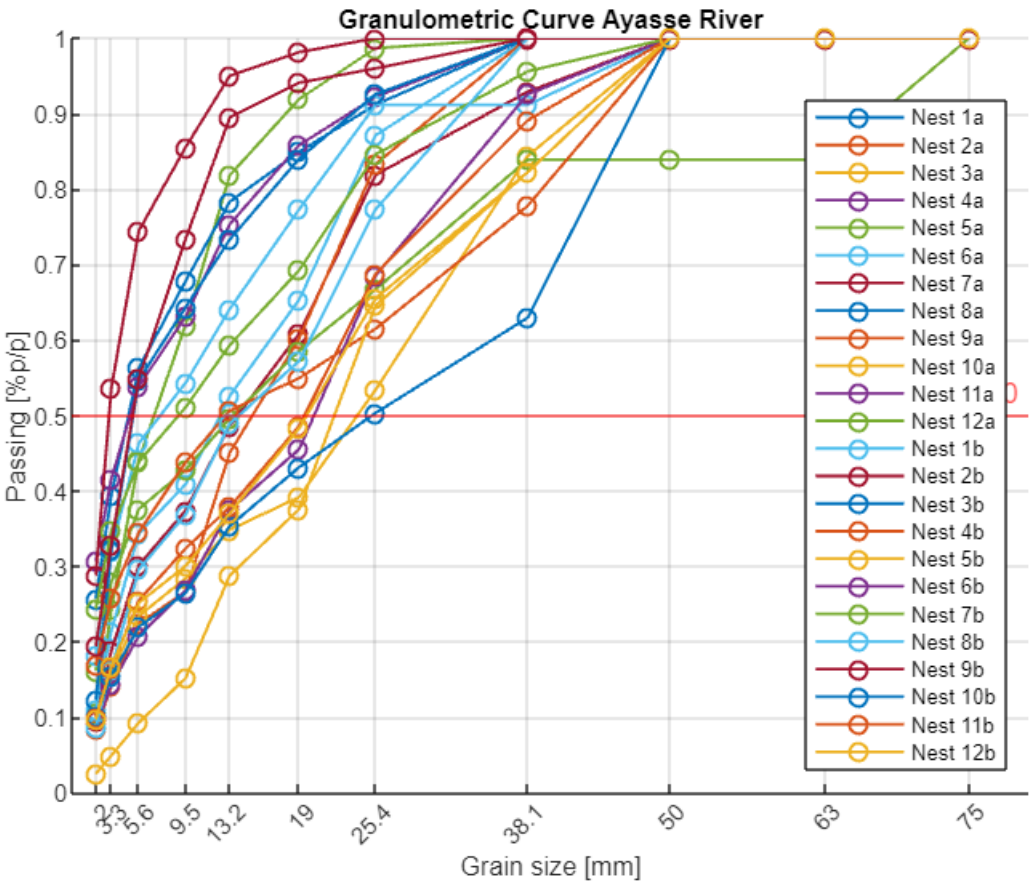

Figure 61: Ayasse - Granulometric Curve

From the granulometric curve (*Figure 61*) obtained by analysing the substrate in the spawning sites of the Ayasse River, it can be observed that the curves for each analysed spawning site exhibit the same trend.

The grain size curves show the percentage of passage (on the y-axis) as a function of grain size in mm (x-axis).

Table 11: Ayasse – Grain Size at Certain Percentages

NEST N°	D16	D50	D84
1 A	<3.3	7	14,5
2 A	<3.3	7	14,5
3 A	<3.3	7	14,5
4 A	<3.3	7	14,5
5 A	<3.3	7	14,5
6 A	<3.3	12,5	24,5
7 A	<3.3	14	27,5
8 A	<3.3	5	18,5
9 A	4	15	25,5
10 A	3,3	24	38,1
11 A	<3.3	5	18
12 A	<3.3	13,5	38,1
1 B	<3.3	7,5	22
2 B	<3.3	3	9
3 B	<3.3	5	19
4 B	<3.3	13	41
5 B	1	24	39
6 B	0,4	20,5	33,5
7 B	<3.3	9	25,4
8 B	3,3	14	29
9 B	<3.3	5	12
10 B	3,5	25	45
11 B	3,3	19,5	35
12 B	3,3	19,5	39

Table 11 shows the grain sizes in mm corresponding to specific percentage of passage 16% (D16), 50% (D50) and 84% (D84) for each grain size curve.

In doing so, it was possible to represent the distribution of the data obtained from the particle size analysis by means of a box plot, shown in *Figure 62*.

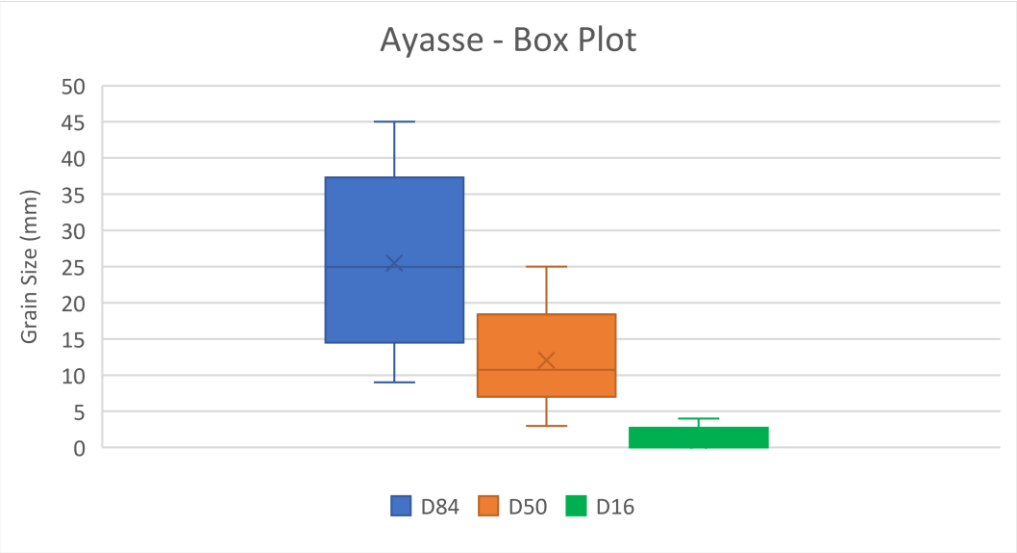

Figure 62: Ayasse - Box Plot Transition at 84%, 50%, and 16%

The box plot represents a statistical analysis of the data where, the minimum and maximum (outer lines of the rectangle) indicate the full range of the data from the minimum to the maximum value, while the shaded area represents 25% (first quantile) to 75% (third quantile).

Below is reported a classification of the substrate, considering that a macro-invertebrate sampling net with a mesh size of 500 µm was used for sediment collection in the field. The classification starts with sand since anything smaller than its mesh size could not be detected:

- Sand: 6 µ -2 mm
- Gravel (Akal): 2-20 cm
- Microlithal: 20- 60 mm
- Mesolithal: 60-200 mm
- Macrolithal: 200-400 mm
- Megalithal: > 400 mm

Taking into consideration the graph in *Figure 61,* the box plot representing the distribution of the data (*Figure 62)* and the substrate classification reported above, most of the grain size present in the spawning areas is distributed in a range between 15 mm and 35 mm.

Consequently, most of the sediments present belong to the akal and microlithal classes.

Graines

Due to space constraints, the results of the data from the particle size analysis are given in Appendix A, while the particle size curve for each spawning site is shown below.

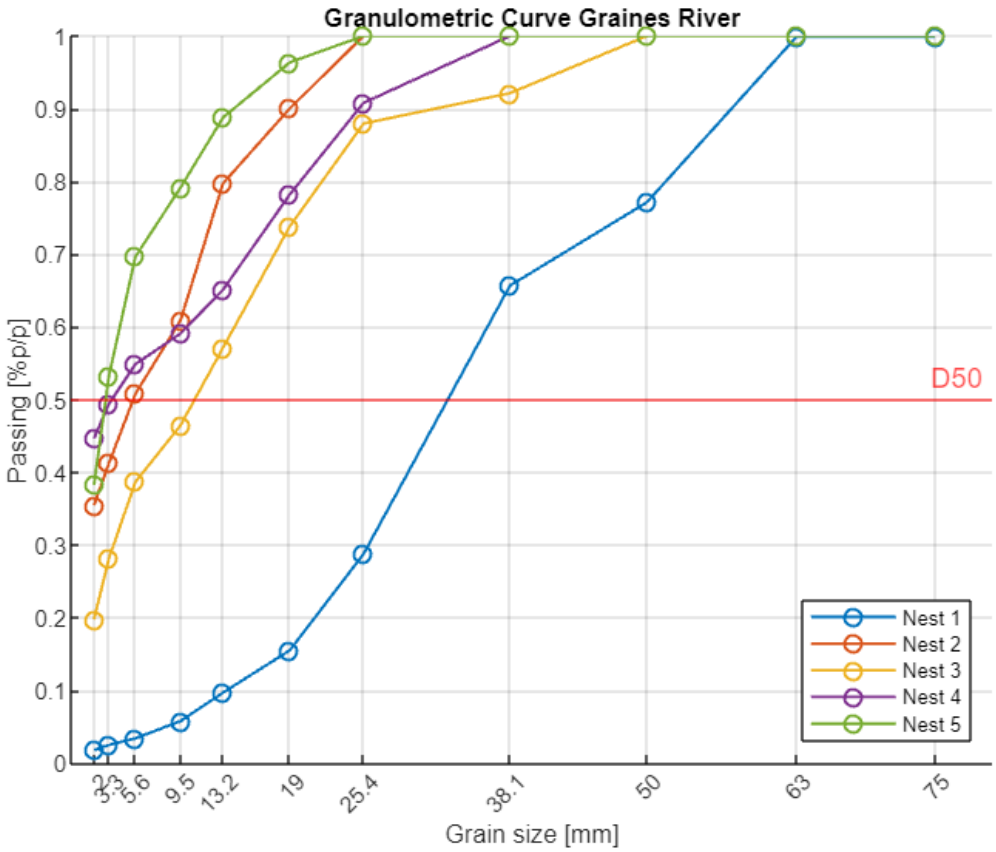

Figure 63: Graines - Granulometric Curve

From the granulometric curve (*Figure 63*) obtained by analysing the substrate in the spawning sites of the Graines River, it can be observed that the curves for each analysed spawning site exhibit the same trend, except for Nest 1.

Table 12: Graines – Grain Size at Certain Percentages

NEST N°	D16	D50	D84
1	19	32	54
2	<3.3	5,6	15
3	<3.3	11	23
4	<3.3	3,3	21
5	<3.3	<3.3	11

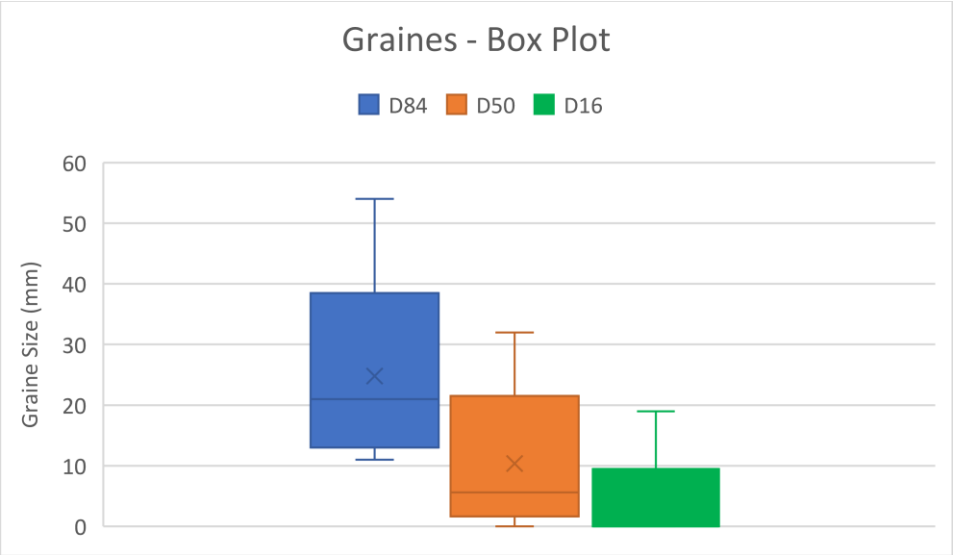

Figure 64: Graines - Box Plot Transition at 84%, 50%, and 16%

Despite the different course of the curve represented by *Nest 1*, taking into consideration the graph in *Figure 63,* the box plot representing the distribution of the data (*Figure 64)* and the substrate classification, most of the grain size present in the spawning areas is distributed in a range between 12 mm and 38 mm.

Consequently, most of the sediments present belong to the akal and microlithal classes.

Savara

Due to space constraints, the results of the data from the particle size analysis are given in Appendix A, while the particle size curve for each spawning sites is shown below.

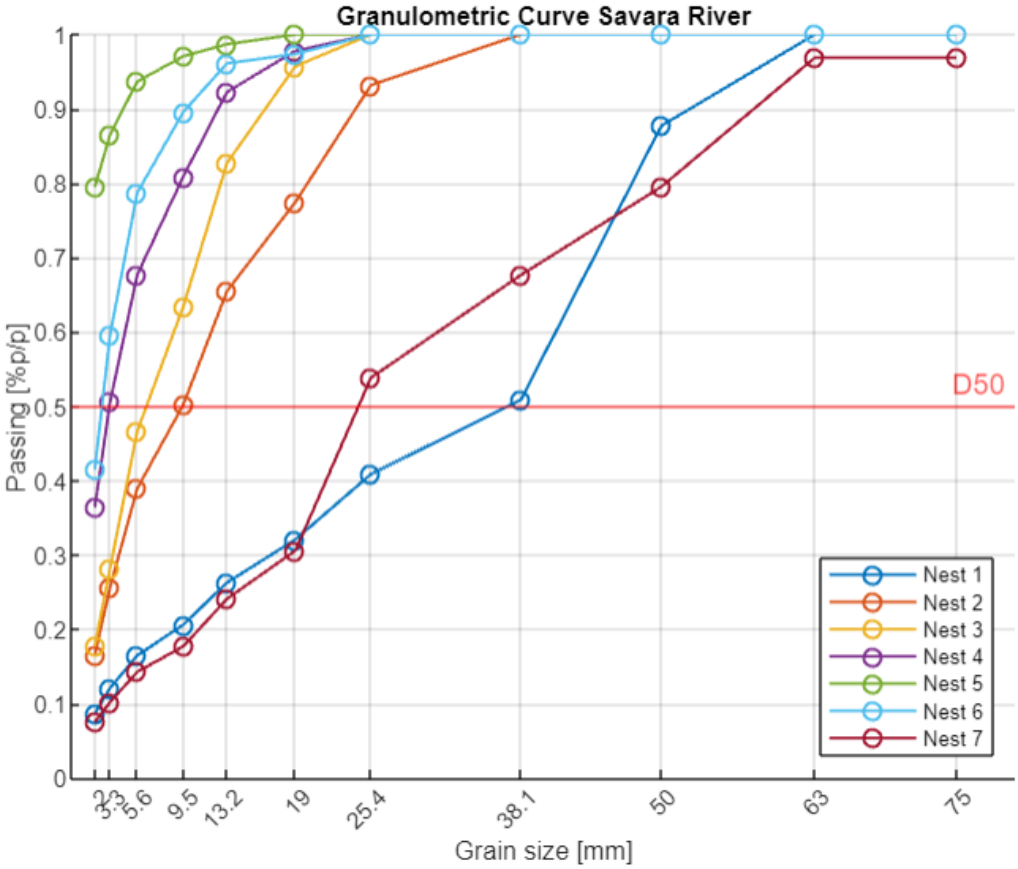

Figure 65: Savara - Granulometric Curve

From the granulometric curve (*Figure 65*) obtained by analysing the substrate in the spawning sites of the Savara River, it can be observed that the curves for each analysed spawning site exhibit the same trend, except for two curves Nest 1 and Nest 7).

Table 13: Savara – Grain Size at Certain Percentages

NEST N°	D16	D50	D84
1	5,6	38,1	49
2	<3.3	9,5	11,5
3	<3.3	6,5	14,5
4	<3.3	3,3	11,2
5	<3.3	<3.3	3,3
6	<3.3	<3.3	9,2
7	7	24,5	55

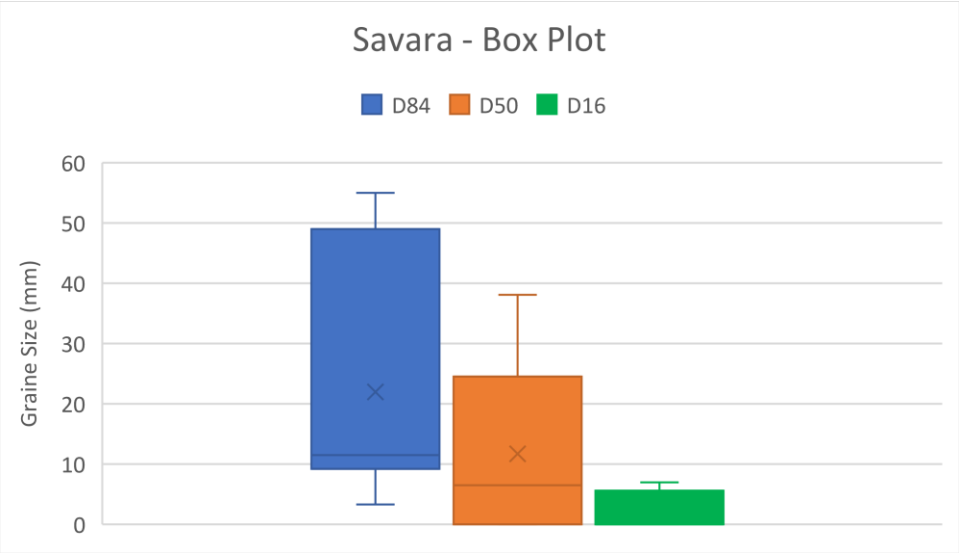

Figure 66: Savara - Box Plot Transition at 84%, 50%, and 16%

Despite these slightly different trends of some spawning sites, taking into consideration the graph in *Figure 65,* the box plot representing the distribution of the data (*Figure 66)* and the substrate classification, most of the grain size present in the spawning areas is distributed in a range between 8 mm and 49 mm.

Consequently, most of the sediments present belong to the akal and microlithal classes.

This result aligns with the findings documented in the literature study on the subject, as referenced in *Chapter 2.4 Spawning Area Description*.

3.4 Spawning Areas Description

To obtain an overall view of the characteristics of the spawning sites, the data collected on each river were combined.

In this section, the summary graphs illustrating the characteristics of the spawning sites collected during the field analyses are presented.

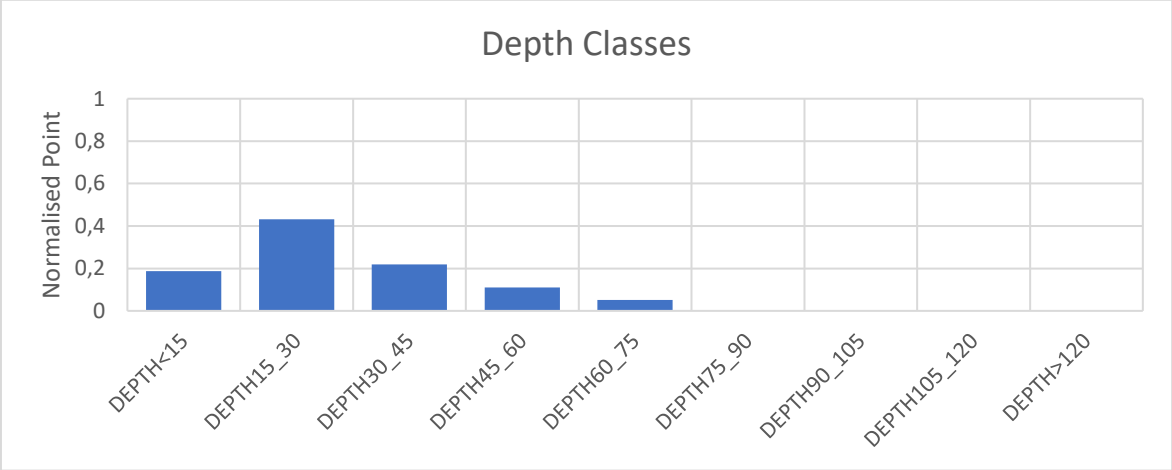

Figure 67: Spawning Area Depth Classes

Figure 67 shows the depth classes that emerged from the field analyses. The optimal depths for trout spawning seems to be in the range of 0 cm to 75 cm.

This result partially differs from the range obtained from the literature analysis conducted by Negro and Guglielmetto, as the range considered for the model conditions based on this study is between 15 cm and 90 cm.

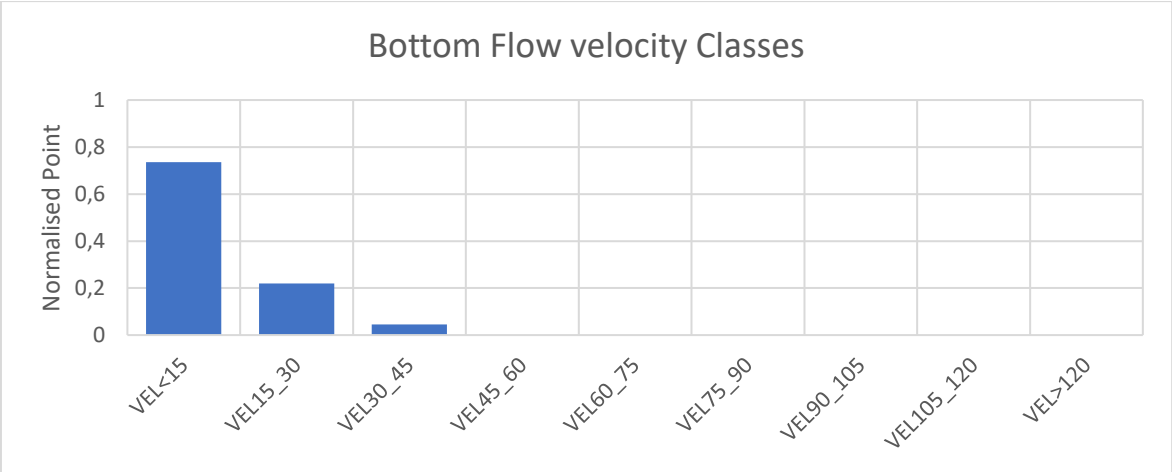

Figure 68: Spawning Area Bottom Flow Velocity Classes

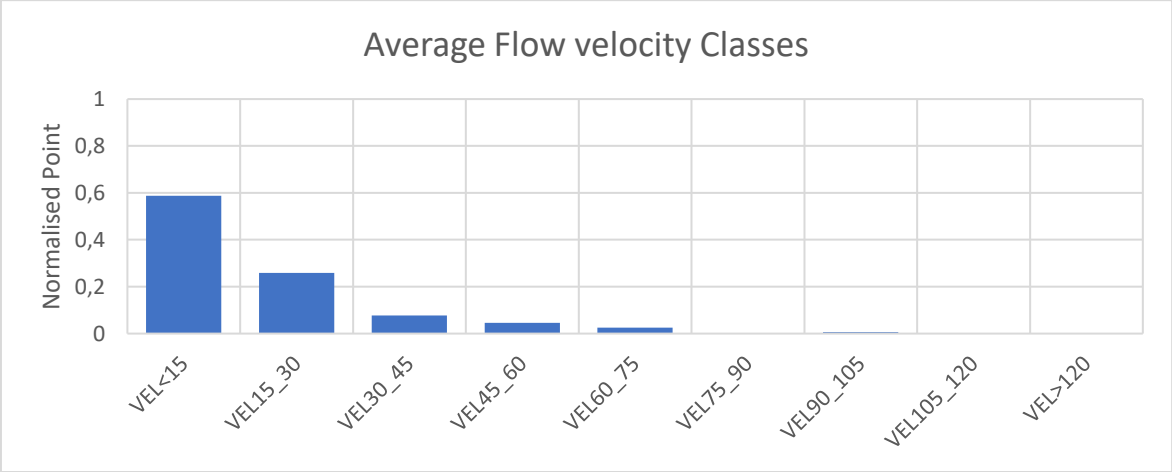

Figure 69: Spawning Area Average Flow Velocity Classes

From *Figures 68* and *69,* it is possible to observe the flow velocity classes that emerged from the field analyses, it seems that the optimal velocities for trout spawning are in the range of 0 cm/s to 75 cm/s.

This result partially differs from the range obtained from the literature analysis, as the range considered for the model conditions based on this study is between 15 cm/s and 75 cm/s.

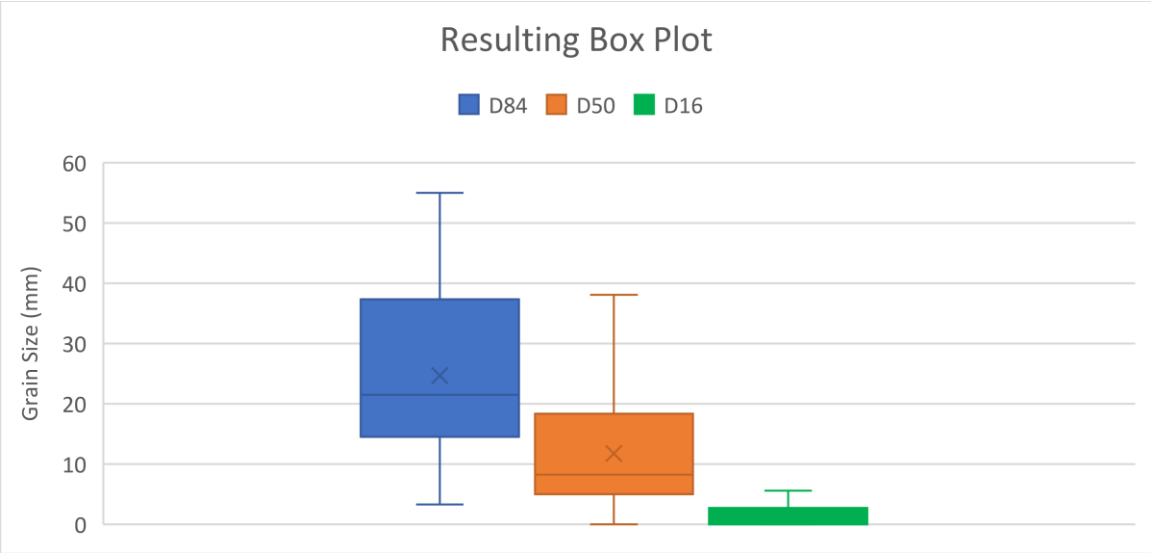

Figure 70: Spawning Area Box Plot Transition at 84%, 50%, and 16%

The box plot in *Figure 70* representing the distribution of the substrate shows that most of the grain size present in the spawning areas is distributed in a range between 15 mm and 38 mm. Consequently, most of the sediments present belong to the akal and microlithal classes, as confirmed by Negro's analysis.

3.5 Model Results

As cited in *Chapter 2.4.2 Model for Identifying Suitable Spawning Sites*, starting from the literature analysis conducted by Negro and Guglielmetto, an initial model was created, able to indicate suitable spawning areas.

Figure 71 shows the decision tree representing the conditional model based on the literature analysis for adult trout spawning:

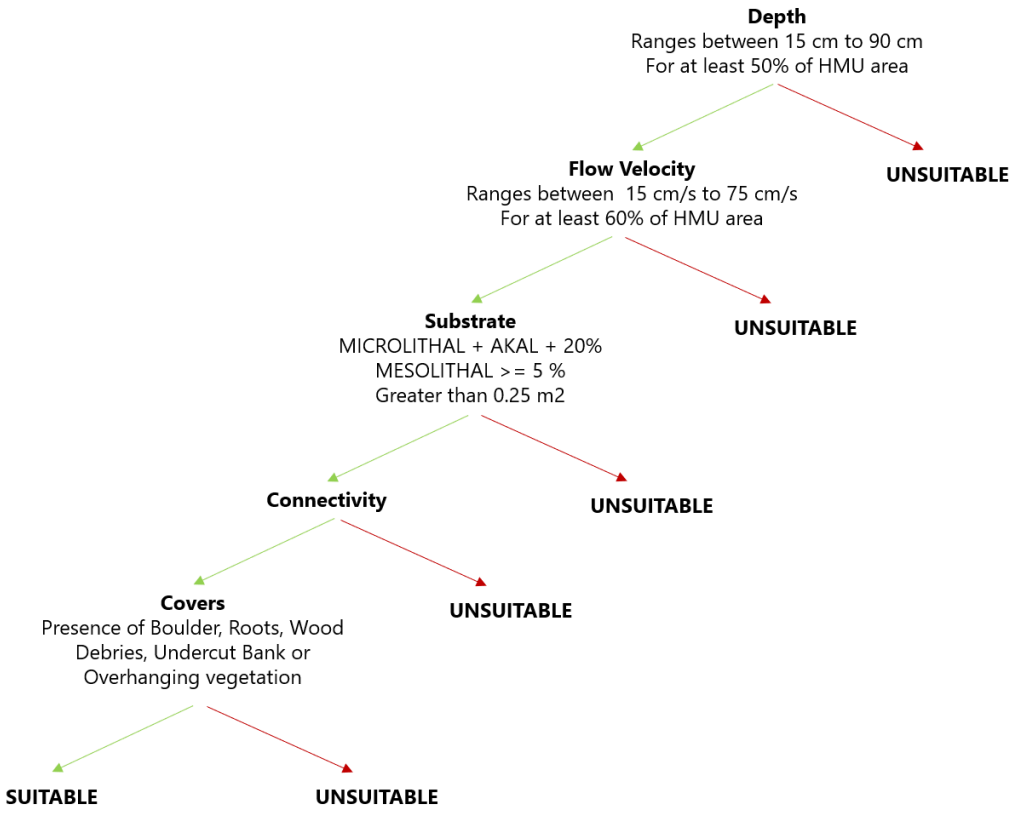

Figure 71: Decision Tree Representing the Conditional Model Based on Literature for Adult Trout Spawning

As observed in *Chapter 3.4, Spawning Areas Description*, some ranges obtained from the literature review partially differ from the ranges where trout spawning sites were found in the field. Therefore, it was decided to proceed with the creation of a second model, whose conditions were modified compared to the initial one, based on field observations.

Table 14 reports the ranges and conditions of the different models, and *Figure 72* shows the basic scheme of the modified model.

Table 14: Comparison of the Models

	Literature Model	Modified Model
Flow Velocity Range	15 to 75 cm/s	0 to 75 cm/s
Depth Range	15 cm to 90 cm	0 cm to 90 cm
Substrate	Microlithal + Akal + 0.2 Mesolithal	Microlithal + Akal + Mesolithal
Covers	Boulder, Roots, Wood Debris or Overhanging Vegetation	Boulder, Roots, Wood Debris or Overhanging Vegetation
Connectivity	Present	Present

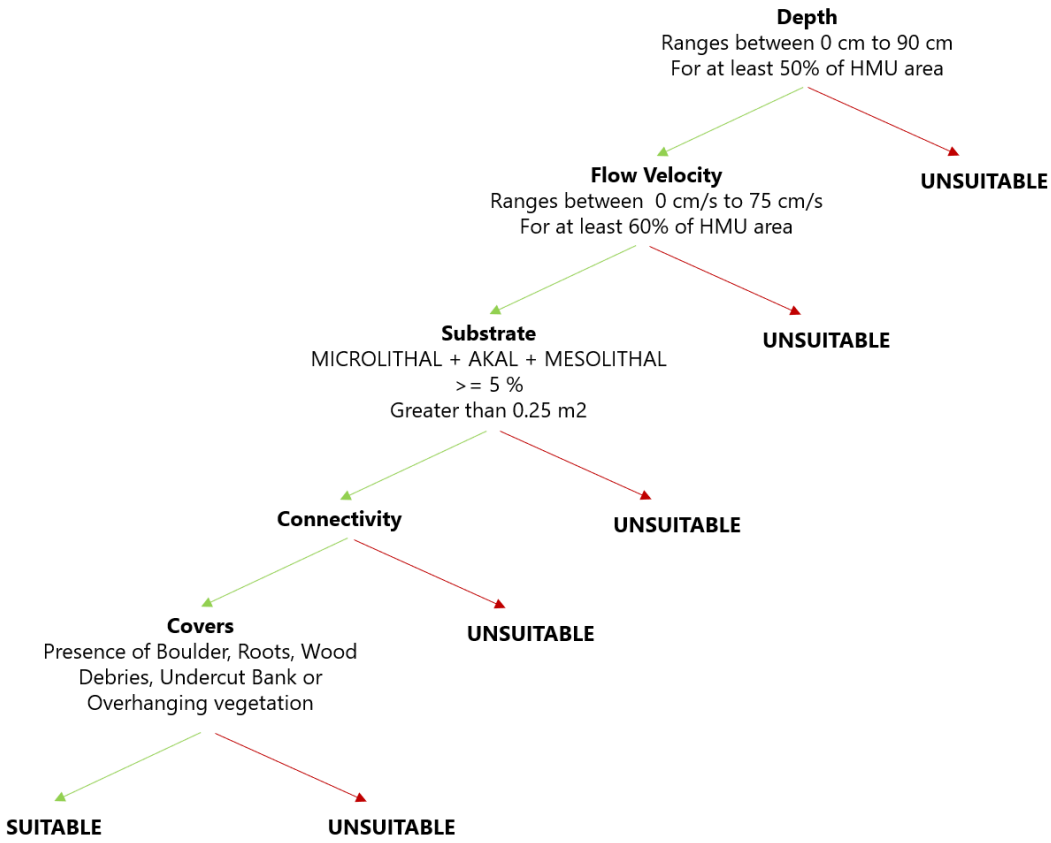

Figure 72: Decision Tree Representing the Conditional Modified Model for Adult Trout Spawning

To determine which of the two models was more effective in identifying areas suitable for trout spawning, it was decided to verify that the Hydro-Morphological Units (HMUs), where trout spawning sites were found during the field analysis conducted in December, were defined as suitable areas by both models.

The tables below show the results of this analysis for each river considered. The observed field result (HMUs suitable for spawning as indicated by the presence of spawning sites) is compared with the predicted results of the two models.

Table 15: Ayasse – Comparison between Observed and Predicted HMU

HMU	Observed	Predicted by Literature Model	Predicted by Modified Model
HMU 1	*Suitable*	*Suitable*	*Suitable*
HMU 2	*Suitable*	*No Suitable*	*Suitable*
HMU 3	*Suitable*	*No Suitable*	*Suitable*
HMU 4	*Suitable*	*No Suitable*	*Suitable*
HMU 5	*Suitable*	*No Suitable*	*Suitable*
HMU 6	*Suitable*	*Suitable*	*Suitable*
HMU 7	*Suitable*	*No Suitable*	*Suitable*
HMU 8	*Suitable*	*No Suitable*	*Suitable*
HMU 9	*Suitable*	*No Suitable*	*Suitable*

Table 16: Graines - Comparison between Observed and Predicted HMU

HMU	Observed	Predicted by Literature Model	Predicted by Modified Model
HMU 1	*Suitable*	*Suitable*	*Suitable*
HMU 2	*Suitable*	*No Suitable*	*Suitable*
HMU 3	*Suitable*	*Suitable*	*Suitable*
HMU 4	*Suitable*	*No Suitable*	*Suitable*
HMU 5	*Suitable*	*No Suitable*	*Suitable*

Table 17: Savara - Comparison between Observed and Predicted HMU

HMU	Observed	Predicted by Literature Model	Predicted by Modified Model
HMU 1	*Suitable*	*No Suitable*	*Suitable*
HMU 2	*Suitable*	*No Suitable*	*Suitable*
HMU 3	*Suitable*	*No Suitable*	*Suitable*
HMU 4	*Suitable*	*Suitable*	*Suitable*
HMU 5	*Suitable*	*No Suitable*	*Suitable*

From the tables, it is evident that the model whose conditions are derived solely from the literature analysis does not categorize all areas as suitable. On the other hand, the modified model, incorporating field analysis, correctly identifies all areas suitable for spawning.

However, it was deemed necessary to conduct an additional analysis to determine whether all the changes made were indispensable or whether only one or two of the range changes affected the model result.

The analysis revealed that the only factor that made a difference in this case was flow velocity.

This means that, by changing only the flow velocity range, the modified model identifies all units as suitable.

In *Figure 73* is reported the decision tree representing the conditions of the original model with just the flow velocity range modified.

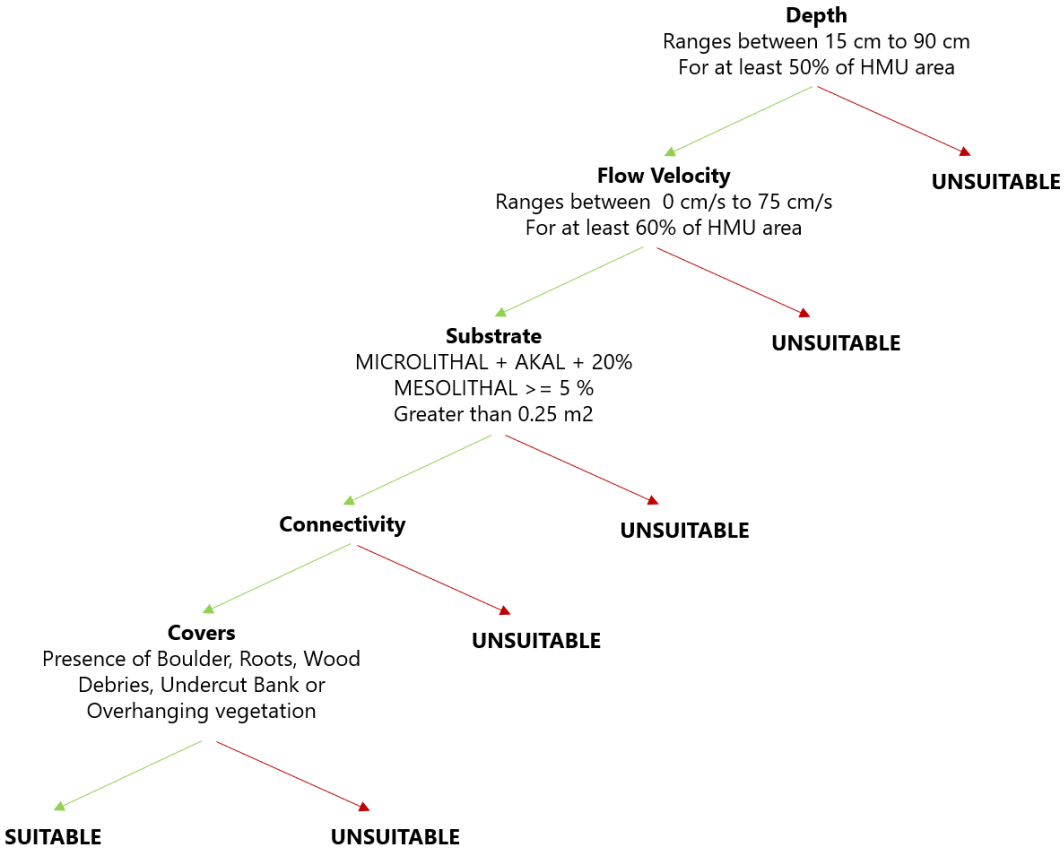

Figure 73: Decision Tree Representing the Second Conditional Modified Model for Adult Trout Spawning

3.6 Model Validation

The models have been validated not only with the data collected in the field during the month of December 2023, in which HMU units containing trout spawning sites were characterized, but also with the data acquired in February 2024, in which other HMU units were characterized without the presence of trout spawning sites.

This approach allowed to determine which model was most effective in identifying areas suitable for spawning.

In *Appendix B* are reported the results of the validation of the three models based on the data collected in the field in December and February:

- Model 1 → The model's conditions are based on the literature analysis conducted by PhD. Giovanni Negro.
- Model 2 → The flow velocity condition was modified by adding CV_15 class, identified in the field analyses.
- Model 3 → The conditions of flow velocity, depth, and substrate were modified by adding the classes identified in the field analyses.

The confusion matrix for each model, resulting from the validation of the data collected in the field, is presented for each river down below. Subsequently, overall accuracy, sensitivity, specificity, and True Skill Statistics are computed.

Ayasse:

Table 18: Ayasse - Confusion Matrix Model 1

		Observed	
Predicted by Model 1		**V**	**F**
	V	2	1
	F	7	6

Table 19: Ayasse - Confusion Matrix Model 2

		Observed	
		V	**F**
Predicted by Model 2	**V**	9	4
	F	0	3

Table 20: Ayasse - Confusion Matrix Model 3

		Observed	
		V	**F**
Predicted by Model 3	**V**	9	6
	F	0	1

Graines

Table 21: Graines - Confusion Matrix Model 1

		Observed	
		V	**F**
Predicted by Model 1	**V**	2	1
	F	3	14

Table 22: Graines - Confusion Matrix Model 2

		Observed	
		V	**F**
Predicted by Model 2	**V**	5	7
	F	0	8

Table 23: Graines - Confusion Matrix Model 3

		Observed	
		V	**F**
Predicted by Model 3	**V**	5	10
	F	0	5

Savara

Table 24: Savara - Confusion Matrix Model 1

		Observed	
		V	**F**
Predicted by Model 1	**V**	1	0
	F	4	5

Table 25: Savara - Confusion Matrix Model 2

		Observed	
		V	**F**
Predicted by Model 2	**V**	5	2
	F	0	3

Table 26: Savara - Confusion Matrix Model 3

		Observed	
		V	**F**
Predicted by Model 3	**V**	5	4
	F	0	1

Below are reported the overall confusion matrices for each model along with their respective statistical indices:

Table 27: Confusion Matrix Model 1

		Observed	
Predicted by Model 1		**V**	**F**
	V	5	2
	F	14	25

$$Overall\ Accuracy \rightarrow \frac{TP + TN}{P + N} = 0{,}65$$

$$Sensitivity \rightarrow \frac{TP}{TP + FN} = 0{,}26$$

$$Specificity \rightarrow \frac{TN}{TN + FN} = 0{,}93$$

$$TSS \rightarrow Sensitivity + Specificity - 1 = \ 0{,}19$$

$$Precision \rightarrow \frac{TP}{TP + FP} = 0{,}71$$

Where:

- TP represents true positives,
- TN represents true negatives,
- FP represents false positives,
- FN represents false negatives.

Table 28: Confusion Matrix Model 2

		Observed	
Predicted by Model 2		**V**	**F**
	V	19	13
	F	0	14

$$Overall\ Accuracy \rightarrow 0{,}72$$

$$Sensitivity \rightarrow 1$$

$$Specificity \rightarrow 0{,}52$$

$$TSS \rightarrow 0{,}52$$

$$Precision \rightarrow 0{,}59$$

Table 29: Confusion Matrix Model 3

		Observed	
Predicted by Model 3		**V**	**F**
	V	19	20
	F	0	7

$$Overall\ Accuracy \rightarrow 0{,}57$$

$$Sensitivity \rightarrow 1$$

$$Specificity \rightarrow 0{,}26$$

$$TSS \rightarrow 0{,}26$$

$$Precision \rightarrow 0{,}49$$

In the context of habitat modelling, evaluating the model's performance is of crucial importance. Two key metrics in this context are sensitivity and specificity. A thorough analysis of these metrics allows to understand the strengths and weaknesses of the model, guiding potential optimizations.

In this analysis, sensitivity plays a primary role. It represents the model's ability to correctly identify areas genuinely suitable for spawning. High sensitivity is fundamental to minimize the risk of excluding potentially suitable areas, ensuring their inclusion in the assessment.

On the contrary, specificity assumes secondary importance in this context. It measures the model's ability to correctly exclude unsuitable areas. While a certain degree of specificity is desirable, its low extent does not necessarily pose a problem. This is because the habitat may indeed be suitable, even if not currently utilized.

The primary goal of habitat modelling is to identify areas that potentially can be used for spawning. Consequently, focusing on sensitivity becomes crucial for the accurate identification of suitable zones, even if not necessarily utilized at the time of analysis.

Table 30: Comparison between Model 1, Model 2 and Model 3

	Model 1	Model 2	Model 3
Accuracy	*0,65*	*0,72*	*0,57*
Sensitivity	*0,26*	*1*	*1*
Specificity	*0,93*	*0,52*	*0,26*
TSS	*0,19*	*0,52*	*0,26*

The conducted analysis reveals that Model 2 is the most effective in identifying areas suitable for spawning. Indeed, Model 2 demonstrates higher accuracy and sensitivity compared to Model 1, despite the latter having higher specificity. However, as emphasized, sensitivity is a more crucial factor in this case. Additionally, Model 2 exhibits better accuracy and specificity than Model 3.

Chapter 4 - Discussion

As mentioned in *Chapter 3.6 Validation Model Results*, the model that best predicts suitable areas for trout spawning is Model 2, in which the flow velocity condition is modified by adding the CV_15 class identified in the field analyses. This modification contrasts with the initial model, which was solely based on literature analysis.

By integrating this model into the SimStream Web Software, it was possible to generate the so-called Habitat Flow Rating Curves, that illustrates the correlation between habitat and flow rate, using data collected in the years 2010, 2011, and 2012.

These curves are represented on the x-axis by the flow rate in m^3/s and on the y-axis by the channel percentile area.

There are two curves in each graph: one represents the wetted area, which should theoretically increase as the flow rate increases, as shown in the graphs below. The second curve indicates the area suitable for spawning, which should ideally increase as the flow rate increases and then stabilise or continue to increase.

Down below are reported the three Habitat Flow Rating Curves of the three rivers (*Figure 74, 75* and *76*).

Ayasse:

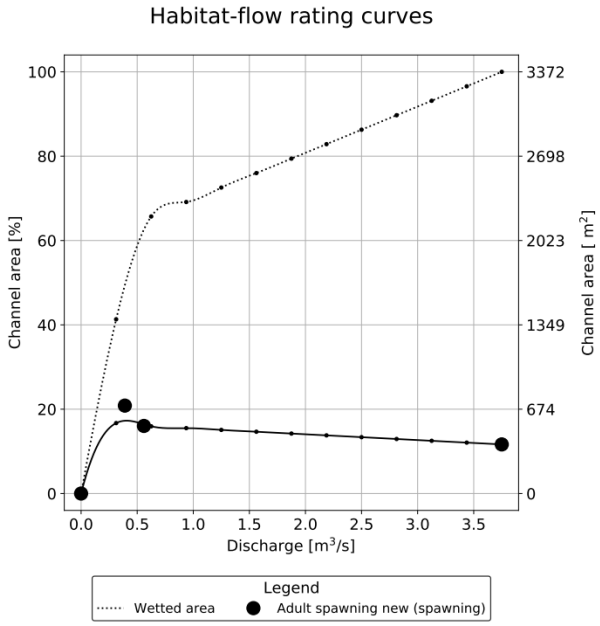

Figure 74: Ayasse - Habitat Flow Rating Curve

Graines:

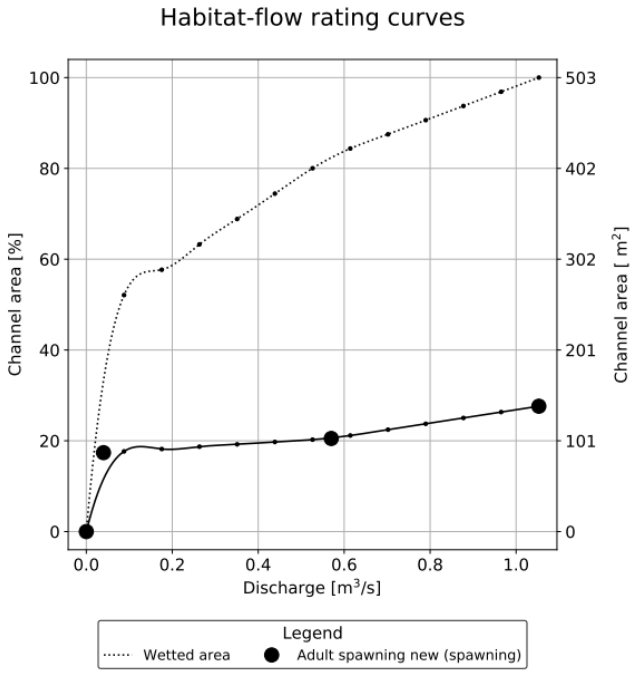

Figure 75: Graines - Habitat Flow Rating Curve

Savara:

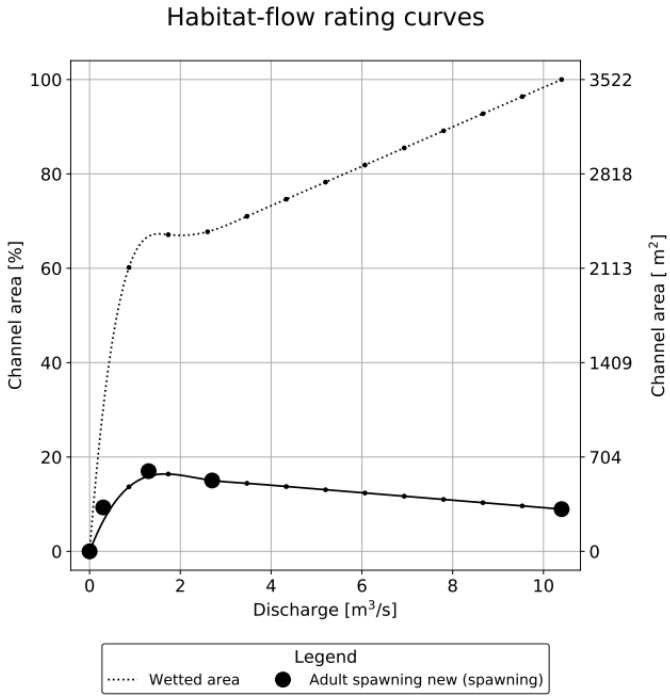

Figure 76: Savara - Habitat Flow Rating Curve

From the first two Habitat Flow Rating Curves (respectively, Ayasse and Graines rivers), a significant increase is observed with minimal discharge variations. Despite these curves follow the expected trends, the habitat increment may be excessive.

It is crucial to consider that the data used to generate these curves were collected in the periods 2010, 2011, and 2012, following procedures inconsistent with the MesoHABSIM methodology employed during the 2023 field analyses. Numerous hydromorphological units (HMUs), in fact, were not described with the collection of at least 15-20 points for each but often with a lower number.

Additionally, during the data consistency analysis reported in *Chapter 2.4.1 Data Consistency*, further discrepancies were identified. While not considered significant inconsistencies, these divergences can still impact the overall results.

Therefore, the curves are essential in the analysis but could be further refined by utilizing more recent data adhering to the techniques outlined in the MesoHABSIM methodology.

It is evident that, for each river, the Habitat Flow Rating Curve follows an expected pattern, regarding the rivers Ayasse and Savara, the trend is characterized by an initial increase, followed by a peak and subsequent decline of the curve. While the Graines river follows a slightly different trend, as the curve continues to rise even after the initial peak. This could be attributed to an increase in areas suitable for spawning, due to the growing presence of new wetted areas with rising discharge.

Both trends highlight that, at lower flow rates, an increase in water flow results in a more pronounced expansion of both wetted area and available habitat for spawning.

Conversely, at higher flow rates, the distinction in habitat becomes less pronounced. Specifically, the decrease in the curve for Ayasse and Savara rivers, as well as the rise in the curve for the Graines river, exhibit smoother transitions compared to the initial phase of growth.

In *Table 31*, the values of the minimum ecological flow are reported, representing the current flow rates released from the diversion of hydroelectric plants on these rivers.

Meanwhile, in *Table 32*, are reported the values of the discharge that should be released by the diversion in order to maximize the habitat used for spawning. This value is derived from the peak observed in the Habitat Flow Rating Curve.

Table 31: Minimum Ecological Flow for each River

Minimum Ecological Flow	
Ayasse	0.05 m^3/s
Graines	0.03 m^3/s
Savara	0.325 m^3/s

Table 32: Flow to Maximize the Habitat for each River

Flow to Maximize the Habitat	
Ayasse	0.31 m^3/s
Graines	0.18 m^3/s
Savara	1.73 m^3/s

Dividing the discharge to maximize habitat by the minimum ecological flow allows to determine by how much the discharge released from the diversion should be increased to maximize habitat during the spawning periods.

$$Ayasse \rightarrow \frac{0.31\ m^3/s}{0.05\ m^3/s} = 6.2$$

$$Graines \rightarrow \frac{0.18\ m^3/s}{0.03\ m^3/s} = 6$$

$$Savara \rightarrow \frac{1.73\ m^3/s}{0.325\ m^3/s} = 5.3$$

From the results, it can be observed that the minimum ecological flow is significantly lower than the value required to maximize habitat during spawning periods. In fact, the flow that should be released is 5-6 times higher than the current discharge.

Increasing the minimum ecological flow to maximize spawning habitat during low-flow periods results in a decrease in hydroelectric power production during these periods, as the water intake by the plant is reduced.

4.1 Further Development

The final model created through this analysis considers various features essential for characterizing areas suitable for spawning, such as flow velocity, depth, substrate, covers, and longitudinal connectivity.

A useful feature to describe spawning areas, but not considered by the model, is temperature. Indeed, if the model were employed to characterize spawning suitable areas using data collected outside the spawning period (November–January), it could potentially misidentify areas as suitable, given suboptimal temperature conditions for spawning.

Therefore, even if the conditions of flow velocity, depth, substrate, covers, and connectivity are satisfied, spawning might not occur due to the unsuitability of temperature.

Consequently, one way to optimize this model would be to incorporate a temperature range or a temporal range to better define the zones suitable for spawning.

In the literature analysis conducted by Negro and subsequently implemented by Guglielmetto, there are also temperature ranges that characterize the spawning periods of trout.

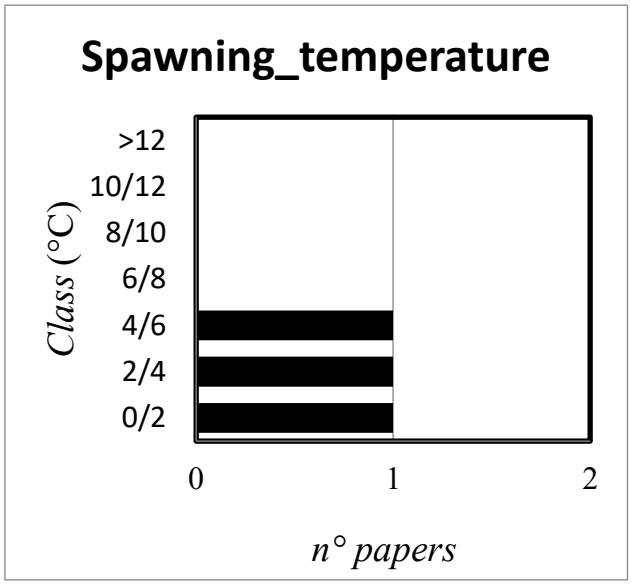

Figure 77: Marble Trout - Spawning Temperature Range

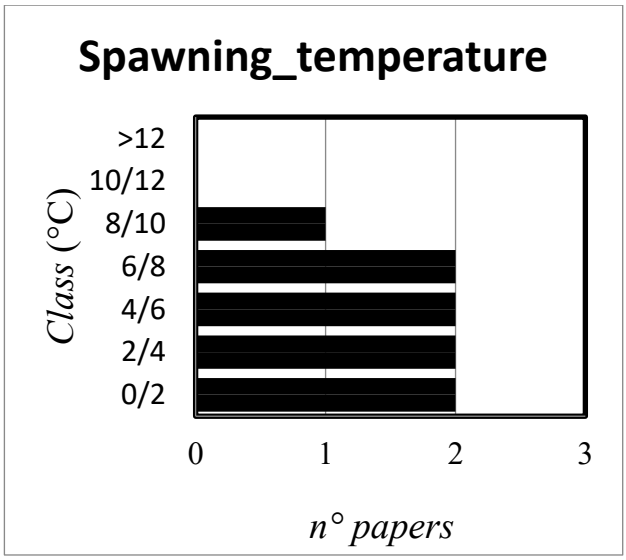

Figure 78: Brown Trout - Spawning Temperature Range

Furthermore, a model does not necessarily need to achieve absolute perfection. Its practical utility in various situations is more important than being flawless only in the limited cases in which it was validated and developed.

Therefore, it would be worthwhile to assess the model on additional mountain streams, and perhaps even on rivers and streams in plain areas.

This would help confirm its effectiveness in identifying suitable spawning areas across diverse environments. Such assessments could lead to refinements, optimizing the model for broader applications in this context.

4.2 Limits of the Research

The field data used to develop the Habitat-Flow Rating Curves were collected several years ago (2010, 2011, and 2012). This time gap creates a mismatch between the methodology employed for their collection and current practices.

In particular, the number of data points acquired to characterize a HMU unit is often significantly lower than what is typically expected in data collection using MesoHABSIM method. This disparity can lead to errors in defining areas suitable for spawning and, consequently, in the creation of the Habitat-Flow Rating curves.

Although the curves obtained describe the general trend of the habitat, it is possible that using more recently acquired data collected according with the MesoHABSIM methodology would yield more accurate curves.

Furthermore, the validation of the model depends on a limited and unbalanced sample, posing a challenge in assessing the model's effectiveness in excluding unsuitable areas and identifying suitable ones accurately.

Currently, the MesoHABSIM approach is based on Random Forest, a machine learning technique for predicting habitat suitability. By increasing the sample size of spawning site observations, it becomes feasible to construct a more extensive database. This, in turn, facilitates the creation of a statistical model that is smoother and more flexible in its approach. Consequently, the model would be better equipped to return more significant curves.

Chapter 5 - Conclusion

The materials, methods, and analysis presented in this study aim to experimentally establish a relationship between trout spawning habitat and flow rate.

The primary achievement of this research is the development of a model able to predict spawning habitat, and to generate the so-called Habitat-Flow Rating Curve, that illustrates the correlation between habitat and flow rate. This model relies on key features such as flow velocity, depth, substrate, covers, and longitudinal connectivity.

The significance of this outcome lies in providing a foundation for future research aimed at demonstrating that ecological flows can be set to enhance the habitat condition for trout spawning.

Further development can include water temperature, as a predictive variable, and the possibility of using machine learning techniques to build habitat suitability models.

It would be possible to increase the sample size building a larger database. Currently, the MesoHABSIM approach is already based on Random Forest, a machine learning technique that is used to predict habitat suitability.

The Habitat-Flow Rating Curves derived from the proposed conditional model suggest a significant increase in habitat in line with discharge, especially during low-flow periods, when trout spawning occurs.

Furthermore, it can be observed that the minimum ecological flow can play an important role to maximize habitat during spawning periods.

The present thesis constitutes an important baseline for further research investigating spawning habitat availability for trout in mountainous streams.

By demonstrating this potential, the approach can contribute to the development of sustainable hydropower, trying to maintain both spawning habitats and electricity production.

Ultimately, this study represents a significant step forward in understanding the interaction between bedload sediment transport and trout spawning habitat, offering valuable insights for fish conservation and sustainable management of sediment fluxes.

References

Allouche, O., Tsoar, A., & Kadmon, R. (2006). Assessing the accuracy of species distribution models: Prevalence, kappa and the true skill statistic (TSS). *Journal of Applied Ecology*, *43*(6), 1223–1232. https://doi.org/10.1111/j.1365-2664.2006.01214.x

Cody Corporation. (n.d.). *360R TRUPULSE RANGEFINDER*. Retrieved March 12, 2024, from https://lasersurveyingequipment.com.au/product/360r-trupulse-rangefinder/

Consorzio regionale per la tutela, l'incremento e l'esercizio della pesca in V. d'Aosta. (n.d.). *Torrente Ayasse*. Retrieved January 19, 2024, from https://www.pescavda.it/torrente-ayasse/

CVA. (n.d.-a). *Centrale di Chavonne*. Retrieved January 19, 2024, from https://cvaspa.it/centrale-di-chavonne

CVA. (n.d.-b). *Centrale di Isollaz*. Retrieved January 19, 2024, from https://cvaspa.it/centrale-di-isollaz

CVA. (n.d.-c). *Centrale Hone 2*. Retrieved January 19, 2024, from https://cvaspa.it/centrale-di-hone-2

CVA. (n.d.-d). *CVA - la nostra storia*.

Enel Green Power. (n.d.). *Tutti i vantaggi dell'energia idroelettrica*. Retrieved January 26, 2024, from https://www.enelgreenpower.com/it/learning-hub/energie-rinnovabili/energia-idroelettrica/vantaggi

Gloria Campilongo. (2021, April 7). *Analisi granulometrica per setacciatura dei terreni e Norme di riferimento*. GeoStru.

GSE. (2020). *FONTI RINNOVABILI IN ITALIA E IN EUROPA -2020-*.

GSE. (2021). *RAPPORTO STATISTICO 2021 ENERGIA DA FONTI RINNOVABILI IN ITALIA*.

Hoskin Scientific. (n.d.). *OTT MF pro – Water Flow Meter*. Retrieved March 12, 2024, from https://hoskin.ca/product/ott-mf-pro-water-flow-meter/

ISPRA. (2017a). *Manuale tecnico-operativo per la modellazione e la valutazione dell'integrità dell'habitat fluviale*.

ISPRA. (2017b). *Manuale tecnico-operativo per la modellazione e la valutazione dell'integrità dell'habitat fluviale*.

Laterza Enzo. (2021, July 29). *RICEVITORI GNSS: COME FUNZIONANO? QUALI I PRO E I CONTRO?* https://www.enzolaterza.it/gnss/ricevitori-gnss-come-funzionano-quali-i-pro-e-i-contro/

Lorenzo Tancioni e Michele Scardi. (2005). *I pesci come indicatori di qualità ambientale: indici biotici ed altri approcci*.

Magno, M. C., Bergamin, L., Pierfranceschi, G., Venti, F., & Romano, E. (n.d.). *Metodologie e strumentazioni per l'analisi granulometrica dei sedimenti*.

Marco Angelo Riva (Marple). (2013, July). *La pesca elettrica*.

Marco Fortunato. (2016). *Foto di Trota Fario*. https://www.juzaphoto.com/galleria.php?t=1972475

N. LEROY POFF AND JULIE K. H. ZIMMERMAN. (2010). *Ecological responses to altered flow regimes:a literature review to inform the science and managementof environmental flows*.

Negro, G., Fenoglio, S., Quaranta, E., Comoglio, C., Garzia, I., & Vezza, P. (2021). Habitat Preferences of Italian Freshwater Fish: A Systematic Review of Data Availability for Applications of the MesoHABSIM Model. In *Frontiers in Environmental Science* (Vol. 9). Frontiers Media S.A. https://doi.org/10.3389/fenvs.2021.634737

NESTLE. (n.d.). *GeoMax Zenith60*. Retrieved March 12, 2024, from https://g-nestle.de/en/GeoMax-Zenith60/29531000

Nikolai Friberg. (2011). Biomonitoring of Human Impacts in Freshwater Ecosystems: The Good, the Bad and the Ugly. *Advance in Ecological Research*.

Pesca Fiume. (n.d.). *Trota Marmolada*.

Protezione Civile - Provincia Autonoma di Trento. (n.d.). *Analisi Granulometrica - Geotecnica*.

Regione VdA. (n.d.). *Caratteristiche Generali Idro 5*. Retrieved January 19, 2024, from https://www.regione.vda.it/territorio/territorio/Piano_acque/documentazione/CaratteristicheGenerali/Pdf/Idro_5.pdf

Trasmanian Government. (2018, March 21). *River Survey*. https://www.ifs.tas.gov.au/news/2018/mar/21/river-surveys

User Manual. (2021). https://ftp.isprambiente.it

Zerunian, S., & De Ruosi, T. (n.d.). *Quaderni di Conservazione della Natura NUMERO 20 ISTITUTO NAZIONALE PER LA FAUNA SELVATICA "ALESSANDRO GHIGI" MINISTERO DELL'AMBIENTE E DELLA TUTELA DEL TERRITORIO Direzione per la Protezione della Natura*.

Appendix A

Granulometric Curve

Ayasse

Spawning sites A

Table 33: Ayasse - Granulometric Analysis Data Nests A

	[mm]	2	3,3	5,6	9,5	13,2	19	25,4	38,1	50	63	75	Total weight
1	[kg]	0,90	1,16	1,69	1,51	1,68	0,86	0,57	0,11	0,00	0,00	0,00	8,47
	%p/p	10,61	24,24	44,15	61,98	81,82	91,92	98,67	100,00	100,00	100,00	100,00	
2	[kg]	0,90	1,16	1,69	1,51	1,68	0,86	0,57	0,11	0,00	0,00	0,00	8,47
	[%p/p]	10,61	24,24	44,15	61,98	81,82	91,92	98,67	100,00	100,00	100,00	100,00	
3	[kg]	0,90	1,16	1,69	1,51	1,68	0,86	0,57	0,11	0,00	0,00	0,00	8,47
	[%p/p]	10,61	24,24	44,15	61,98	81,82	91,92	98,67	100,00	100,00	100,00	100,00	
4	[kg]	0,90	1,16	1,69	1,51	1,68	0,86	0,57	0,11	0,00	0,00	0,00	8,47
	[%p/p]	10,61	24,24	44,15	61,98	81,82	91,92	98,67	100,00	100,00	100,00	100,00	
5	[kg]	0,90	1,16	1,69	1,51	1,68	0,86	0,57	0,11	0,00	0,00	0,00	8,47
	[%p/p]	10,61	24,24	44,15	61,98	81,82	91,92	98,67	100,00	100,00	100,00	100,00	
6	[kg]	0,28	0,26	0,32	0,16	0,30	0,32	0,55	0,32	0,00	0,00	0,00	2,52
	[%p/p]	10,92	21,43	34,31	40,85	52,58	65,33	87,13	100,00	100,00	100,00	100,00	
7	[kg]	0,46	0,45	0,55	0,35	0,55	0,59	1,02	0,53	0,35	0,00	0,00	4,85
	[%p/p]	9,40	18,77	30,12	37,37	48,61	60,82	81,88	92,89	100,00	100,00	100,00	
8	[kg]	1,01	0,55	0,66	0,45	0,42	0,26	0,25	0,35	0,00	0,00	0,00	3,94
	[%p/p]	25,63	39,45	56,28	67,79	78,31	84,93	91,19	100,00	100,00	100,00	100,00	
9	[kg]	0,27	0,18	0,27	0,13	0,59	0,49	0,74	0,54	0,00	0,00	0,00	3,21
	[%p/p]	8,32	14,07	22,42	26,59	45,04	60,17	83,30	100,00	100,00	100,00	100,00	
10	[kg]	0,18	0,11	0,13	0,09	0,11	0,08	0,25	0,55	0,28	0,00	0,00	1,78
	[%p/p]	10,15	16,10	23,38	28,39	34,82	39,15	53,40	84,37	100,00	100,00	100,00	
11	[kg]	0,77	0,27	0,31	0,23	0,31	0,26	0,16	0,19	0,00	0,00	0,00	2,50
	[%p/p]	30,65	41,60	53,87	63,08	75,32	85,81	92,23	100,00	100,00	100,00	100,00	
12	[kg]	0,73	0,53	0,44	0,24	0,31	0,40	0,37	0,78	0,00	0,00	0,73	4,53
	[%p/p]	16,14	27,88	37,58	42,76	49,62	58,53	66,70	83,89	83,89	83,89	100,00	

Spawning sites B

Table 34: Ayasse - Granulometric Analysis Data Nests B

	[mm]	2	3,3	5,6	9,5	13,2	19	25,4	38,1	50	63	75	Total weight
1	[kg]	0,87	0,67	0,68	0,38	0,47	0,63	0,66	0,00	0,42	0,00	0,00	4,80
	[%p/p]	18,16	32,06	46,30	54,29	64,08	77,31	91,15	91,15	100,00	100,00	100,00	
2	[kg]	1,42	1,22	1,03	0,54	0,47	0,15	0,09	0,00	0,00	0,00	0,00	4,93
	[%p/p]	28,77	53,61	74,46	85,52	95,01	98,14	99,98	99,98	99,98	99,98	99,98	
3	[kg]	0,28	0,45	0,52	0,22	0,21	0,25	0,20	0,17	0,00	0,00	0,00	2,29
	[%p/p]	12,23	32,12	54,69	64,30	73,31	84,03	92,56	100,00	100,00	100,00	100,00	
4	[kg]	0,26	0,14	0,13	0,14	0,10	0,07	0,10	0,25	0,34	0,00	0,00	1,52
	[%p/p]	16,80	25,86	34,50	43,76	50,61	54,93	61,48	77,76	100,00	100,00	100,00	
5	[kg]	0,09	0,09	0,15	0,21	0,48	0,31	0,95	0,62	0,63	0,00	0,00	3,53
	[%p/p]	2,47	4,89	9,26	15,13	28,74	37,56	64,56	82,22	100,00	100,00	100,00	
6	[kg]	0,33	0,22	0,25	0,23	0,41	0,31	0,88	0,92	0,28	0,00	0,00	3,82
	[%p/p]	8,64	14,28	20,77	26,80	37,43	45,50	68,51	92,56	100,00	100,00	100,00	
7	[kg]	1,00	0,42	0,37	0,30	0,34	0,41	0,63	0,45	0,18	0,00	0,00	4,09
	[%p/p]	24,34	34,67	43,83	51,04	59,30	69,23	84,58	95,60	100,00	100,00	100,00	
8	[kg]	0,15	0,13	0,22	0,12	0,20	0,14	0,34	0,38	0,00	0,00	0,00	1,69
	[%p/p]	8,60	16,37	29,57	36,83	48,87	57,21	77,31	100,00	100,00	100,00	100,00	
9	[kg]	0,65	0,45	0,74	0,62	0,54	0,15	0,06	0,13	0,00	0,00	0,00	3,35
	[%p/p]	19,35	32,91	54,94	73,34	89,46	94,08	95,99	100,00	100,00	100,00	100,00	
10	[kg]	0,35	0,19	0,23	0,16	0,31	0,27	0,25	0,44	1,29	0,00	0,00	3,48
	[%p/p]	10,03	15,42	21,95	26,41	35,33	43,11	50,32	62,93	100,00	100,00	100,00	
11	[kg]	0,36	0,25	0,33	0,25	0,20	0,40	0,75	0,75	0,40	0,00	0,00	3,70
	[%p/p]	9,84	16,51	25,45	32,33	37,82	48,54	68,77	89,09	100,00	100,00	100,00	
12	[kg]	0,31	0,23	0,27	0,16	0,23	0,37	0,56	0,54	0,58	0,00	0,00	3,24
	[%p/p]	9,66	16,69	25,13	30,02	37,00	48,30	65,51	82,23	100,00	100,00	100,00	

Graines

Table 35: Graines - Granulometric Analysis Data

	[mm]	2	3,3	5,6	9,5	13,2	19	25,4	38,1	50	63	75	Total weight
1	[kg]	0,05	0,02	0,02	0,07	0,11	0,16	0,36	1,01	0,32	0,63	0,00	2,74
	[%p/p]	1,75	2,48	3,37	5,74	9,66	15,49	28,74	65,65	77,13	99,93	99,93	
2	[kg]	1,07	0,18	0,29	0,30	0,57	0,31	0,30	0,00	0,00	0,00	0,00	3,03
	[%p/p]	35,45	41,23	50,78	60,84	79,72	90,04	100,00	100,00	100,00	100,00	100,00	
3	[kg]	0,35	0,15	0,18	0,14	0,19	0,29	0,25	0,07	0,14	0,00	0,00	1,75
	[%p/p]	19,74	28,15	38,66	46,41	57,11	73,82	87,95	92,13	100,00	100,00	100,00	
4	[kg]	0,56	0,06	0,07	0,05	0,08	0,16	0,16	0,12	0,00	0,00	0,00	1,26
	[%p/p]	44,66	49,40	54,86	59,04	65,10	78,21	90,80	100,00	100,00	100,00	100,00	
5	[kg]	1,49	0,58	0,64	0,37	0,38	0,30	0,14	0,00	0,00	0,00	0,00	3,89
	[%p/p]	38,23	53,24	69,64	79,11	88,78	96,37	100,00	100,00	100,00	100,00	100,00	

Savara

Table 36: Savara - Granulometric Analysis Data

	[mm]	2	3,3	5,6	9,5	13,2	19	25,4	38,1	50	63	75	Total weight
1	[kg]	0,33	0,13	0,17	0,16	0,22	0,22	0,34	0,38	1,42	0,47	0,00	3,84
	[%p/p]	8,65	12,10	16,46	20,61	26,26	32,07	40,86	50,86	87,70	100,00	100,00	
2	[kg]	1,42	0,79	1,14	0,97	1,32	1,03	1,35	0,59	0,00	0,00	0,00	8,62
	[%p/p]	16,53	25,68	38,94	50,20	65,47	77,47	93,18	100,00	100,00	100,00	100,00	
3	[kg]	1,01	0,60	1,05	0,96	1,10	0,75	0,24	0,00	0,00	0,00	0,00	5,72
	[%p/p]	17,70	28,24	46,65	63,42	82,71	95,74	100,00	100,00	100,00	100,00	100,00	
4	[kg]	2,31	0,90	1,09	0,84	0,72	0,35	0,14	0,00	0,00	0,00	0,00	6,36
	[%p/p]	36,40	50,61	67,69	80,88	92,26	97,80	100,00	100,00	100,00	100,00	100,00	
5	[kg]	1,10	0,10	0,10	0,05	0,02	0,02	0,00	0,00	0,00	0,00	0,00	1,38
	[%p/p]	79,47	86,53	93,66	97,07	98,70	100,00	100,00	100,00	100,00	100,00	100,00	
6	[kg]	4,10	1,79	1,88	1,07	0,65	0,13	0,26	0,00	0,00	0,00	0,00	9,87
	[%p/p]	41,48	59,66	78,71	89,57	96,11	97,38	100,00	100,00	100,00	100,00	100,00	
7	[kg]	0,79	0,28	0,43	0,36	0,67	0,68	2,44	1,45	1,25	1,82	0,00	10,48
	[%p/p]	7,49	10,19	14,25	17,69	24,08	30,58	53,83	67,63	79,51	96,88	96,88	

Appendix B

Validation Result

Ayasse

Model 1:

Table 37: Ayasse – Comparison between Observed and Predicted HMU Model 1

	Observed	Predicted	Error Rate	Sensitivity		Specificity		TSS
HMU 1	***Suitable***	*Suitable*	0	1	0	0	0	0,08
HMU 2	***Suitable***	*No Suitable*	1	0	1	0	0	
HMU 3	***Suitable***	*No Suitable*	1	0	1	0	0	
HMU 4	***Suitable***	*No Suitable*	1	0	1	0	0	
HMU 5	***Suitable***	*No Suitable*	1	0	1	0	0	
HMU 6	***Suitable***	*Suitable*	0	1	0	0	0	
HMU 7	***Suitable***	*No Suitable*	1	0	1	0	0	
HMU 8	***Suitable***	*No Suitable*	1	0	1	0	0	
HMU 9	***Suitable***	*No Suitable*	1	0	1	0	0	
HMU 10	***No Suitable***	*No Suitable*	0	0	0	1	0	
HMU 11	***No Suitable***	*Suitable*	1	0	0	0	1	
HMU 12	***No Suitable***	*No Suitable*	0	0	0	1	0	
HMU 13	***No Suitable***	*No Suitable*	0	0	0	1	0	
HMU 14	***No Suitable***	*No Suitable*	0	0	0	1	0	
HMU 15	***No Suitable***	*No Suitable*	0	0	0	1	0	
HMU 16	***No Suitable***	*No Suitable*	0	0	0	1	0	
		Total Error	0,5	**a**	**c**	**d**	**b**	
		Total Score	0,5	0,22		0,86		
			Accuracy	***Sensitivity***		***Specificity***		

Model 2:

Table 38: Ayasse – Comparison between Observed and Predicted HMU Model 2

	Observed	Predicted	Error Rate	Sensitivity		Specificity		TSS
HMU 1	***Suitable***	*Suitable*	0	1	0	0	0	0,43
HMU 2	***Suitable***	*Suitable*	0	1	0	0	0	
HMU 3	***Suitable***	*Suitable*	0	1	0	0	0	
HMU 4	***Suitable***	*Suitable*	0	1	0	0	0	
HMU 5	***Suitable***	*Suitable*	0	1	0	0	0	
HMU 6	***Suitable***	*Suitable*	0	1	0	0	0	
HMU 7	***Suitable***	*Suitable*	0	1	0	0	0	
HMU 8	***Suitable***	*Suitable*	0	1	0	0	0	
HMU 9	***Suitable***	*Suitable*	0	1	0	0	0	
HMU 10	***No Suitable***	*No suitable*	0	0	0	1	0	
HMU 11	***No Suitable***	*Suitable*	1	0	0	0	1	
HMU 12	***No Suitable***	*Suitable*	1	0	0	0	1	
HMU 13	***No Suitable***	*No suitable*	0	0	0	1	0	
HMU 14	***No Suitable***	*No suitable*	0	0	0	1	0	
HMU 15	***No Suitable***	*Suitable*	1	0	0	0	1	
HMU 16	***No Suitable***	*Suitable*	1	0	0	0	1	
		Total Error	0,25	**a**	**c**	**d**	**b**	
		Total Score	0,75	1		0,43		
			Accuracy	***Sensitivity***		***Specificity***		

Model 3:

Table 39: Ayasse – Comparison between Observed and Predicted HMU Model 3

	Observed	Predicted	Error Rate	Sensitivity		Specificity		TSS
HMU 1	***Suitable***	*Suitable*	0	1	0	0	0	0,14
HMU 2	***Suitable***	*Suitable*	0	1	0	0	0	
HMU 3	***Suitable***	*Suitable*	0	1	0	0	0	
HMU 4	***Suitable***	*Suitable*	0	1	0	0	0	
HMU 5	***Suitable***	*Suitable*	0	1	0	0	0	
HMU 6	***Suitable***	*Suitable*	0	1	0	0	0	
HMU 7	***Suitable***	*Suitable*	0	1	0	0	0	
HMU 8	***Suitable***	*Suitable*	0	1	0	0	0	
HMU 9	***Suitable***	*Suitable*	0	1	0	0	0	
HMU 10	***No Suitable***	*Suitable*	1	0	0	0	1	
HMU 11	***No Suitable***	*Suitable*	1	0	0	0	1	
HMU 12	***No Suitable***	*Suitable*	1	0	0	0	1	
HMU 13	***No Suitable***	*No suitable*	0	0	0	1	0	
HMU 14	***No Suitable***	*Suitable*	1	0	0	0	1	
HMU 15	***No Suitable***	*Suitable*	1	0	0	0	1	
HMU 16	***No Suitable***	*Suitable*	1	0	0	0	1	
		Total Error	0,375	**a**	**c**	**d**	**b**	
		Total Score	0,63	1		0,14		
			Accuracy	***Sensitivity***		***Specificity***		

Graines

Model 1:

Table 40: Graines – Comparison between Observed and Predicted HMU Model 1

	Observed	Predicted	Error Rate	Sensitivity		Specificity		TSS
HMU 1	***Suitable***	*Suitable*	0	1	0	0	0	
HMU 2	***Suitable***	*No suitable*	1	0	1	0	0	
HMU 3	***Suitable***	*Suitable*	0	1	0	0	0	
HMU 4	***Suitable***	*No suitable*	1	0	1	0	0	
HMU 5	***Suitable***	*No suitable*	1	0	1	0	0	
HMU 6	***No Suitable***	*No suitable*	0	0	0	1	0	
HMU 7	***No Suitable***	*No suitable*	0	0	0	1	0	
HMU 8	***No Suitable***	*No suitable*	0	0	0	1	0	
HMU 9	***No Suitable***	*No suitable*	0	0	0	1	0	
HMU 10	***No Suitable***	*No suitable*	0	0	0	1	0	
HMU 11	***No Suitable***	*No suitable*	0	0	0	1	0	0,33
HMU 12	***No Suitable***	*No suitable*	0	0	0	1	0	
HMU 13	***No Suitable***	*Suitable*	1	0	0	0	1	
HMU 14	***No Suitable***	*No suitable*	0	0	0	1	0	
HMU 15	***No Suitable***	*No suitable*	0	0	0	1	0	
HMU 16	***No Suitable***	*No suitable*	0	0	0	1	0	
HMU 17	***No Suitable***	*No suitable*	0	0	0	1	0	
HMU 18	***No Suitable***	*No suitable*	0	0	0	1	0	
HMU 19	***No Suitable***	*No suitable*	0	0	0	1	0	
HMU 20	***No Suitable***	*No suitable*	0	0	0	1	0	
		Total Error	0,2	a	c	d	b	
		Total Score	0,8	0,4		0,93		
			Accuracy	***Sensitivity***		***Specificity***		

Model 2:

Table 41: Graines – Comparison between Observed and Predicted HMU Model 2

	Observed	Predicted	Error Rate	Sensitivity		Specificity		TSS
HMU 1	***Suitable***	*Suitable*	0	1	0	0	0	0,53
HMU 2	***Suitable***	*Suitable*	0	1	0	0	0	
HMU 3	***Suitable***	*Suitable*	0	1	0	0	0	
HMU 4	***Suitable***	*Suitable*	0	1	0	0	0	
HMU 5	***Suitable***	*Suitable*	0	1	0	0	0	
HMU 6	***No Suitable***	*No Suitable*	0	0	0	1	0	
HMU 7	***No Suitable***	*No Suitable*	0	0	0	1	0	
HMU 8	***No Suitable***	*Suitable*	1	0	0	0	1	
HMU 9	***No Suitable***	*No Suitable*	0	0	0	1	0	
HMU 10	***No Suitable***	*No Suitable*	0	0	0	1	0	
HMU 11	***No Suitable***	*Suitable*	1	0	0	0	1	
HMU 12	***No Suitable***	*No Suitable*	0	0	0	1	0	
HMU 13	***No Suitable***	*Suitable*	1	0	0	0	1	
HMU 14	***No Suitable***	*Suitable*	1	0	0	0	1	
HMU 15	***No Suitable***	*No Suitable*	0	0	0	1	0	
HMU 16	***No Suitable***	*Suitable*	1	0	0	0	1	
HMU 17	***No Suitable***	*No Suitable*	0	0	0	1	0	
HMU 18	***No Suitable***	*Suitable*	1	0	0	0	1	
HMU 19	***No Suitable***	*Suitable*	1	0	0	0	1	
HMU 20	***No Suitable***	*No Suitable*	0	0	0	1	0	
		Total Error	0,35	a	c	d	b	
		Total Score	0,65	1		0,53		
			Accuracy	***Sensitivity***		***Specificity***		

Model 3:

Table 42: Graines – Comparison between Observed and Predicted HMU Model 3

	Observed	Predicted	Error Rate	Sensitivity		Specificity		TSS
HMU 1	***Suitable***	*Suitable*	0	1	0	0	0	0,33
HMU 2	***Suitable***	*Suitable*	0	1	0	0	0	
HMU 3	***Suitable***	*Suitable*	0	1	0	0	0	
HMU 4	***Suitable***	*Suitable*	0	1	0	0	0	
HMU 5	***Suitable***	*Suitable*	0	1	0	0	0	
HMU 6	***No Suitable***	*Suitable*	1	0	0	0	1	
HMU 7	***No Suitable***	*Suitable*	1	0	0	0	1	
HMU 8	***No Suitable***	*Suitable*	1	0	0	0	1	
HMU 9	***No Suitable***	*No Suitable*	0	0	0	1	0	
HMU 10	***No Suitable***	*Suitable*	1	0	0	0	1	
HMU 11	***No Suitable***	*Suitable*	1	0	0	0	1	
HMU 12	***No Suitable***	*No Suitable*	0	0	0	1	0	
HMU 13	***No Suitable***	*Suitable*	1	0	0	0	1	
HMU 14	***No Suitable***	*Suitable*	1	0	0	0	1	
HMU 15	***No Suitable***	*No Suitable*	0	0	0	1	0	
HMU 16	***No Suitable***	*Suitable*	1	0	0	0	1	
HMU 17	***No Suitable***	*No Suitable*	0	0	0	1	0	
HMU 18	***No Suitable***	*Suitable*	1	0	0	0	1	
HMU 19	***No Suitable***	*Suitable*	1	0	0	0	1	
HMU 20	***No Suitable***	*No Suitable*	0	0	0	1	0	
		Total Error	0,5	a	c	d	b	
		Total Score	0,5	1		0,33		
			Accuracy	***Sensitivity***		***Specificity***		

Savara

Model 1:

Table 43: Savara – Comparison between Observed and Predicted HMU Model 1

	Observed	Predicted	Error Rate	Sensitivity		Specificity		TSS
HMU 1	***Suitable***	*No Suitable*	1	0	1	0	0	0,2
HMU 2	***Suitable***	*No Suitable*	1	0	1	0	0	
HMU 3	***Suitable***	*No Suitable*	1	0	1	0	0	
HMU 4	***Suitable***	*Suitable*	0	1	0	0	0	
HMU 5	***Suitable***	*No Suitable*	1	0	1	0	0	
HMU 6	***No Suitable***	*No Suitable*	0	0	0	1	0	
HMU 7	***No Suitable***	*No Suitable*	0	0	0	1	0	
HMU 8	***No Suitable***	*No Suitable*	0	0	0	1	0	
HMU 9	***No Suitable***	*No Suitable*	0	0	0	1	0	
HMU 10	***No Suitable***	*No Suitable*	0	0	0	1	0	
		Total Error	0,4	**a**	**c**	**d**	**b**	
		Total Score	0,6	0,2		1		
			Accuracy	***Sensitivity***		***Specificity***		

Model 2:

Table 44: Savara – Comparison between Observed and Predicted HMU Model 2

	Observed	Predicted	Error Rate	Sensitivity		Specificity		TSS
HMU 1	***Suitable***	*Suitable*	0	1	0	0	0	0,6
HMU 2	***Suitable***	*Suitable*	0	1	0	0	0	
HMU 3	***Suitable***	*Suitable*	0	1	0	0	0	
HMU 4	***Suitable***	*Suitable*	0	1	0	0	0	
HMU 5	***Suitable***	*Suitable*	0	1	0	0	0	
HMU 6	***No Suitable***	*No Suitable*	0	0	0	1	0	
HMU 7	***No Suitable***	*No Suitable*	0	0	0	1	0	
HMU 8	***No Suitable***	*No Suitable*	0	0	0	1	0	

HMU 9	***No Suitable***	*Suitable*	1	0	0	0	1	
HMU 10	***No Suitable***	*Suitable*	1	0	0	0	1	
		Total Error	0,2	**a**	**c**	**d**	**b**	
		Total Score	0,8	1		0,6		
			Accuracy	***Sensitivity***		***Specificity***		

Model 3:

Table 45: Savara – Comparison between Observed and Predicted HMU Model 3

	Observed	Predicted	Error Rate	Sensitivity		Specificity		TSS
HMU 1	***Suitable***	*Suitable*	0	1	0	0	0	0,2
HMU 2	***Suitable***	*Suitable*	0	1	0	0	0	
HMU 3	***Suitable***	*Suitable*	0	1	0	0	0	
HMU 4	***Suitable***	*Suitable*	0	1	0	0	0	
HMU 5	***Suitable***	*Suitable*	0	1	0	0	0	
HMU 6	***No Suitable***	*Suitable*	1	0	0	0	1	
HMU 7	***No Suitable***	*Suitable*	1	0	0	0	1	
HMU 8	***No Suitable***	*No Suitable*	0	0	0	1	0	
HMU 9	***No Suitable***	*Suitable*	1	0	0	0	1	
HMU 10	***No Suitable***	*Suitable*	1	0	0	0	1	
		Total Error	0,4	**a**	**c**	**d**	**b**	
		Total Score	0,6	1		0,2		
			Accuracy	***Sensitivity***		***Specificity***		